Copyright Warning & Restrictions

The copyright law of the United States (Title 17, United States Code) governs the making of photocopies or other reproductions of copyrighted material.

Under certain conditions specified in the law, libraries and archives are authorized to furnish a photocopy or other reproduction. One of these specified conditions is that the photocopy or reproduction is not to be "used for any purpose other than private study, scholarship, or research." If a, user makes a request for, or later uses, a photocopy or reproduction for purposes in excess of "fair use" that user may be liable for copyright infringement,

This institution reserves the right to refuse to accept a copying order if, in its judgment, fulfillment of the order would involve violation of copyright law.

Please Note: The author retains the copyright while the New Jersey Institute of Technology reserves the right to distribute this thesis or dissertation

Printing note: If you do not wish to print this page, then select "Pages from: first page # to: last page #" on the print dialog screen

ABSTRACT

FLAME DYNAMICS IN UNSTEADY STRAINED FLOWS

by
Zili Huang

In this dissertation, the response of a premixed flame to time-dependent strained flow fields is investigated. Because of the potential application to turbulent combustion modeling, the main focus is on the particular case of a flame in stagnation point flow with an imposed oscillatory strain rate. The flame is modeled as a hydrodynamic discontinuity separating burned from unburned gasses. To complete the formulation of the problem, conditions relating the fluid variables across the flame front are needed, as is a flame speed equation that determines the evolution of the discontinuity. These conditions are derived through asymptotic analysis of the flame structure.

In the first part of this dissertation, an existing hydrodynamic model is employed to assess flame response to oscillating stagnation point flow. The model is valid for near-equidiffusional conditions, i.e. for near-unity Lewis numbers. Under these conditions, the flame speed varies linearly with strain. Unlike previous theoretical investigations, the present formulation places no restrictions on the amplitude of the oscillations, and we account for the full interaction between the flame and the flow. Solutions are constructed by a combination of asymptotic and numerical methods. Results regarding flame response are in agreement with previous experiments and studies. We also obtain the following results as a consequence of the underlying time-periodic flow: (a) the mean flame position is shifted upstream from the steady state location, (b) a region of reverse flow appears immediately ahead of the flame front during part of each cycle, and (c) there is a maximum

amplitude of oscillation beyond which the flame fails to exist. These results are most pronounced at high frequencies and agree with the asymptotic solution constructed in that regime.

In the second part of this dissertation, a new model is derived which exhibits a nonlinear dependence of flame speed on strain. The model is valid for arbitrary Lewis number, and unlike previous models, it allows for an unsteady flame structure. Asymptotic methods are used to construct solutions across the narrow flame zone (and reaction zone), and asymptotic matching then yields the nonlinear flame speed equation. The new model is then employed to investigate flame response to unsteady strained flows. Our results predict that the flame becomes most sentive to fluctuations in the flow as steady state extinction conditions are approached. Also, at high frequency the flame response is the same, regardless of the mixture properties. These results are in good agreement with experiments.

FLAME DYNAMICS IN UNSTEADY STRAINED FLOWS

by
Zili Huang

A Dissertation
Submitted to the Faculty of
New Jersey Institute of Technology
in Partial Fulfillment of the Requirements for the Degree of
Doctor of Philosophy

Department of Mathematics

May 1999

APPROVAL PAGE

FLAME DYNAMICS IN UNSTEADY STRAINED FLOWS

Zili Huang

John K. Bechtold, Ph.D., Dissertation Advisor — Date
Associate Professor, Department of Mathematics,
New Jersey Institute of Technology, Newark NJ

Moshe Matalon, Ph.D., Committee Member — Date
Professor, Department of Applied Mathematics,
Northwestern University, Evanston IL

Demetrius Papageorgiou, Ph.D., Committee Member — Date
Associate Professor, Department of Mathematics,
New Jersey Institute of Technology, Newark NJ

Michael Booty, Ph.D., Committee Member — Date
Associate Professor, Department of Mathematics,
New Jersey Institute of Technology, Newark NJ

Jonathan Luke, Ph.D., Committee Member — Date
Associate Professor, Department of Mathematics,
New Jersey Institute of Technology, Newark NJ

BIOGRAPHICAL SKETCH

Author: Zili Huang

Degree: Doctor of Philosophy

Date: May 1999

Undergraduate and Graduate Education:

- Doctor of Philosophy in Mathematical Sciences,
  New Jersey Institute of Technology, Newark, NJ, 1999
- Master of Science in Applied Mathematics,
  New Jersey Institute of Technology, Newark, NJ, 1995
- Master of Science in Numerical Analysis,
  The Second Research Academy of The Ministry of Aero-Space Industry,
  Beijing, P. R. China, 1990
- Bachelor of Science in Computational Mathematics,
  Sichuan University, Cheng Du, Sichuan, P. R. China, 1987

Major: Applied Mathematics

Publications:

Zili Huang, John K. Bechtold and Moshe Matalon, "Weakly Stretched Premixed Flames in Oscillating Flows", *Combustion Theory and Modelling*, **2** (1998) 115-133.

Zili Huang, John K. Bechtold and Moshe Matalon, "A Premixed Flame in Oscillating Stagnation Point Flow: Hydrodynamic Effects", *ESCI Fall Technical Meeting*, October 27-29, 1997. Hartford, Connecticut.

Zili Huang and Degui Liu, "Waveform Relaxation Method for Stiff Large System", *Computer Engineering and Design* (ISSN 1000-7024), Vol **78** (1994) 55-64.

Zili Huang and Degui Liu, "Parallel Block Implicit Runge-Kutta Methods for Solving Initial Value Problem of ODEs", *Systems Engineering and Electronics* (ISSN 1001-506X), Vol **15** (1993) 62-67.

Zili Huang, "A Class of Parallel Block Implicit Methods", *Systems Engineering and Electronics* (ISSN 1001-506X), Vol **14** (1992) 40-44.

Zili Huang and Degui Liu, "The A-Stability Analysis for a Class of Parallel Implicit Runge-Kutta Methods", *Systems Engineering and Electronics* (ISSN 1001-506X), Vol **13** (1991) 25-30.

To my parents and Lily

ACKNOWLEDGMENT

I would like to express my most sincere gratitude and appreciation to Professor John K. Bechtold, who has provided me with a lot of knowledge and encouragement throughout this research. I have been greatly influenced by his organized and disciplined style of research. He really made a big difference in my life and I will never forget him for the great person he is.

My special thanks goes to Professor Demetrius Papageorgiou and Professor Moshe Matalon. I can not thank them enough for their great impact toward the completion of my work and their endless encouragement. They were always willing to offer me their timely help whenever I needed it, so words are inadequate to express my gratitude to them.

A debt of gratitude is owed to Professor Michael Booty and Professor Jonathan Luke for serving as members of my dissertation committee and for their comments. This work would not have been possible otherwise.

I would like to express my deepest appreciation to my family for their continuing support, encouragement and love. Without them, I would not be where I am today. They have contributed to this dissertation in more ways than they know, and for that and many other things, I thank them.

I would like to thank all my friends for their invaluable support and help throughout those years of my study.

I would like to extend my gratitude to all the faculty, staff and my fellow graduate students in the Department of Mathematics of New Jersey Institute of Technology for their help, encouragement and friendship.

TABLE OF CONTENTS

Chapter **Page**

LIST OF FIGURES

Figure Page

CHAPTER 1

INTRODUCTION

1.1 Motivation and Objective

Combustion phenomena are interesting and complicated physiochemical processes, in which thermodynamics, fluid mechanics, chemical kinetics, and transport processes take place. As such, the equations governing even the simplest practical combustion system are extremely difficult to solve because they possess many nonlinearties, including Arrhenius Reaction Rate terms. No analytical solutions exist, and the equations are beyond the scope of even the most sophisiticated computational techniques. An understanding of these complicated processes must begin with careful mathematical modeling followed by analysis and interpretation of solutions. This approach has successfully explained many aspects of combustion, thus far, and will continue to play an important role in combustion research in the future. This dissertation is concerned with modeling of flames in unsteady, nonuniform flows.

One important topic of much active research is turbulent combustion modeling. Its importance is due to the fact that turbulent reacting flows occur in most practical combustion systems including rocket engines, gas turbine combustors, and internal combustion engines. A number of theoretical approaches have been taken in order to better understand turbulent combustion. This understanding is vital to give insight into such topics as emissions control, efficiency, etc. One successful modeling approach considers the reaction-sheet regime of turbulence, in which the flame structure remains intact while propagating through a turbulent flow field. The evolution of the flame front depends on local flow conditions. An important characteristic of turbulent flow is that it is unsteady and strained. Since flame propagation can be highly influenced by the presence of both unsteady and strained flows, a

detailed description of flame propagation in these conditions can lead to a better understanding of turbulent combustion and can also effectively guide future studies and experiments.

The present study investigates these issues of premixed flame propagation. There are two main projects: 1) employ a simplified model to analyze flame dynamics in a simple unsteady strained flow, and 2) to derive new model of flame propagation which allows for unsteady flame structures and captures the flame extinctions.

1.2 Overview of Problems

Many combustion phenomena are characterized as having localized regions where solutions change rapidly due to wide disparities in spatial and temporal scales. Asymptotic methods are therefore an effective tool to analyze such systems by exploiting different scales.

One particular limit that has led to huge advances in combustion science is the limit of large activation energy. Reaction usually proceeds according to an Arrhenius law, which exhibits an exponential dependence on temperature. In most practical combustion systems, the activation energy is quite large and as a result, chemistry is confined to a very narrow zone. Asymptotic methods can formally be used to resolve these reaction zones, effectively replacing the nonlinear reaction rate term by jump conditions relating all relevant variables across the reaction zone.

This technique was used by soviet scientists in the 1940's, but its largest impact as a singular perturbation technique to advance combustion theory come after the work by Bush and Fendell(1970), see also the review by Williams(1971) in the Annual Review of Fluid Mechanics. These ideas have led to significant theoretical advances in all areas of combustion science. In particular, it has allowed for the formal derivation

of reduced models of premixed flame propagation. Two classes of models that are of particular interest are Diffusional-Thermal Models and Hydrodynamic Models.

The essense of diffusional thermal models suppose that the transport equations are decoupled from the fluid dynamic equations. Thus one specifies a flow field and solves for the temperature and reactant concentration. This approximation takes the effect of flow field on the flame into account, but ignores the effect of the flame on the flow field. This is formally true only when thermal expansion is weak, and for this reason, these models are commonly refered to as constant density models. Matkowsky and Sivashinsky(1979) gave a consistent mathematical derivation of this model by using matched asymptotics. The resulting model has since been used extensively to study a wide variety of flame dynamics, such as extinction and instabilities.

The second class of models, and that are of interest in this dissertation, are commonly referred to as hydrodynamic models, which describe flames whose diffusion thickness is much smaller than a typical length scale associated with the outer bulk flow, for example, the radius of curvature of the flame front. As such, the flame is treated as a moving "surface" of density discontinuity separating burned from unburned gasses. The flow on either side is governed by the incompressible Navier-Stokes equations, although the density is different on either side. This model was first proposed by Landau(1944), in his study of the stability of a planar flame propagating in a tube. To relate the fluid variables on either side, he imposed the Rankine-Hugoniot relations, expressing conservation of mass and momentum across the flame and also assumed a constant flame speed, i.e. he assumed that the surface propagates at a constant speed relative to the incoming flow. However, contrary to experimental observations, Landau's model predicted that a plane flame is unconditionally unstable due to thermal expansion of the gas. It was believed that stable

flame must be result of stablizing influence of flame structure. In order to improve on Landau's model, Markstein(1951) assumed that the propagation velocity of the flame relative to the gas was a function of the curvature of the flame front. Thus he assumed a linear relation between flame speed and curvature and he introduced a phenomenological constant μ to account for this. He showed that the flame is stable under perturbations of sufficiently short wavelength when $\mu > 0$.

More recently, conditions relating fluid variables and flame speed equations have been rationally derived using matched asymptotics. Those works exploit the dual limit of high activation energy and thin flames. Models have been developed for Near-Equidiffusional Flames(NEFs) Matalon and Matkowsky(1982), as well as Slowly Varying Flames(SVFs) Sivashinsky(1976); Buckmaster(1977).

The NEF models are appropriate to describe flames in mixtures with near unity Lewis number, which is defined as the ratio of thermal to mass diffusivities. Such models predict a linear dependence of flame speed on stretch. These models explicitly contain those expressions and thus they are free of phenomenological parameters. Clavin and Williams(1982), also analyzed the flame structure and its interaction with the fluid flow to derive the flame speed equation and jump conditions for fluid variables across the flame front. Matalon and Matkowsky(1982) took flame structure into account and derived an equation for the propagation of the flame surface and jump conditions for fluid variables across the front for NEFs. Bechtold and Matalon(1998) later extended this model by including near-stoichiometric effects as well as variable transport properties, and their results are valid for arbitrary flame shapes in general fluid flows.

SVF models are essentially hydrodynamic models which allow for arbitrary Lewis number. They are derived for a distinguished limit relating flame thickness and inverse activation energy. These models exhibit a nonlinear dependence of flame

speed on stretch, and lead to predictions of various nonlinear phenomena, including extinction. Sivashinsky(1976) considered flames that are slowly varying in both space and time and derived an equation relating the shape of flame front to hydrodynamic flow. And for a weakly perturbed stationary plane flame front, Sivashinsky's equation gives a Markstein type dependence. Buckmaster(1977) considered distinguished limit perturbations of the classical one-dimensional deflagration wave in the limit of large activation energy in order to investigate unsteady effects, three-dimensional effects, and the effects of heat losses and area changes on slowly varying laminar flames.

Both of these classes of models have been used to study flame response to various flow conditions. One particular geometry often used is the flame in a stagnation point flow. This is motivated in part by the reaction sheet regime of turbulent combustion for which this geometry serves as the prototype for a laminar flamelet.

There are a number of studies that have considered steady stagnation point flow. Libby and Williams(1982) used a diffusional-thermal model to study flame response to straining caused by turbulent fluctuations. They concluded that, for moderate and lower strain rates, there are reaction surfaces that maintain a diffusive-reactive balance. But for high strain rates, there is an extinction regime in which there is a reaction zone having a diffusive-convective-reaction balance. Wu and Law(1984) experimentally studied the effects of stretch on the determination of the laminar flame speed. Their results demonstrate that preferential diffusion can cause the flame temperature and mass burning rate to either increase or decrease, depending on the mixture effective Lewis number and whether the flame is positively or negatively stretched. Eteng, Ludford and Matalon(1986) adopted the stagnation point flow configration to examine issues such as the flow displacement and extinction characteristics of steady strained flames. In their study, they used an

NEF Hydrodynamic model and the strain rate was assumed to be moderate rather than large, so that the flame stands clear of the viscous boundary layer near the wall. They constructed complete solutions for flow field, which explicitly described the displacement effect due to thermal expansion. Kim and Matalon(1988) later used a SVF model to study flame extinction.

More recently, it has been recognized that unsteady effects may have a significant influence on strained flames. This has led to a number of investigations of flame in unsteady strained flows. Saitoh and Otsuka(1976) were the first to experimentally examine the response of counterflow flames to small amplitude sinusoidal variations in the imposed flow field. They also carried out a numerical simulation to support their observation. Their results suggested that the amplitude of the flame response decreases as the frequency of imposed oscillation is increased to high values, and the phase lag between the flame and the imposed flow becomes nearly 90° out of phase for NEFs.

Later on, Stahl and Warnatz(1991), and Egolfopoulos(1994) numerically investigated the influence of unsteadiness on the structure and dynamics of counterflowing premixed laminar strained flames. The unsteady conservation equations of mass, momentum, energy and species were solved along the stagnation streamline of the counterflow by using detailed description of chemistry and variable transport properties. Their results demonstrate that the flame response is quasi-steady at low imposed frequency, while at high frequency it fails to respond to the imposed velocity oscillations. Petrov and Ghoniem(1995) revisited the validity of the traditional assumption that the flame response to strain is instantaneous by examining the time-dependent response of a premixed laminar flame when subjected to either a sudden change in strain or a periodic strain. They also investigated Lewis number effects in their study. They found that at low frequency oscillations, the phase shift

between the strain and the burning velocity is close to 0 for $Le < 1$ and near 90° for $Le \geq 1$. At high frequency oscillating strains, and over the entire range of Lewis number and flame temperature, the phase shift is of order of 140°.

Most recently, Im, Bechtold and Law(1996) studied the response of counterflow premixed flames to oscillating strain rates by using both twin and single flame counterflow configrations. Their emphasis was to examine the response of the reaction sheet and burning rate to time varying strain rates, and attention was focused on near-extinction conditions so that the time scale of the imposed unsteadiness was comparable to that of diffusive transport. The Lewis number was shown to play an important role in the flame response, especially for flames near extinction. Their results also demonstrate that extinction can be delayed when the strain rate oscillates about the static extinction point. Thus the laminar flamelet regime of turbulent combustion may be broader than predicted by steady analyses. The results of all above mentioned studies agree qualitatively with the experimental observations reported by Saitoh and Otsuka(1976).

All of the unsteady theoretical studies employed diffusional-thermal models that are appropriate for high strain rates when the flame lies in the viscous boundary layer near the stagnation plane. In this dissertation, those analyses are extended by considering weakly strained flow so that the flame resides outside the viscous layer. Thus hydrodynamic models are appropriate to describe the flame-flow interactions. Solutions to the model problems are constructed using a combination of asymptotic and numerical methods. Focus is on nonlinear flame response, including extinction. An outline of the contents of this dissertation is as follows.

In chapter 2, I introduce the full system of governing equations for premixed flame propagation in a gaseous combustible mixture. Appropriate scales are identified and nondimensionalization is discussed.

In chapter 3, I will use the NEF model derived by Bechtold and Matalon(1998) to investigate the flame response to the stagnation point flow with time-dependent strain rate. Both time-periodic and impulsively-changed strain rates are considered. I use a combination of numerical and asymptotic techniques to construct complete solutions to the governing equations which include the flame response to the imposed unsteadiness as well as the displacement of the incident flow due to the thermal expansion. I also use the same NEF flame model to investigate how the mass and thermal diffusivities as well as the viscosity affect the flame response to incoming flow.

In chapter 4, I use asymptotic techniques to derive a flame speed equation for SVFs in general flow field in which all the transport coefficients are temperature dependent. Similar to previous studies, the flame structure is quasi-one-dimensional along the coordinate attached to the flame front but unsteady effects are retained in the structure. This is in contrast to previous studies, which considered quasi-steady structures. The new model is used to assess the influence of fast-time oscillation on extinction.

Finally, in chapter 5, I summarize the results and suggest extensions of this work for future research.

CHAPTER 2

BASIC EQUATIONS FOR HYDRODYNAMIC FLAME MODEL

2.1 The Model

The equations to describe premixed flame propagation in general flow field involve the coupling of Navier-Stokes equations for fluid dynamics to the transport equations of combustion. For a single reactant mixture, the mass, momentum, species and energy conservative equations governing flow field and chemical reaction are given by

$$\hat{p} = \hat{\rho}\hat{T}\hat{R}^{\circ} \tag{2.1}$$

$$\hat{\rho}_{\hat{t}} + \hat{\nabla}\cdot(\hat{\rho}\hat{\mathbf{V}}) = 0 \tag{2.2}$$

$$\hat{\rho}\left(\hat{\mathbf{V}}_{\hat{t}} + (\hat{\mathbf{V}}\cdot\hat{\nabla})\hat{\mathbf{V}}\right) = -\hat{\nabla}\hat{p} + \hat{\nabla}\cdot\hat{\sigma}_{ij} \tag{2.3}$$

$$\hat{\rho}\left(\hat{Y}_{\hat{t}} + (\hat{\mathbf{V}}\cdot\hat{\nabla})\hat{Y}\right) = -\hat{\Omega} + \hat{\nabla}\cdot(\hat{\rho}\hat{\mathcal{D}}\hat{\nabla}\hat{Y}) \tag{2.4}$$

$$\hat{\rho}\hat{C}_p\left(\hat{T}_{\hat{t}} + (\hat{\mathbf{V}}\cdot\hat{\nabla})\hat{T}\right) = \hat{Q}\hat{\Omega} + \hat{\nabla}\cdot(\hat{\lambda}\hat{\nabla}\hat{T}) + \frac{\hat{D}\hat{p}}{\hat{D}\hat{t}} + \hat{\mu}\hat{\Phi} \tag{2.5}$$

together with the boundary conditions

$$\hat{T}(-\infty) = \hat{T}_{-\infty} \qquad \hat{Y}(-\infty) = \hat{Y}_{-\infty} \qquad x \to -\infty \tag{2.6}$$

$$\hat{T}(\infty) = \hat{T}_{\infty} \qquad \hat{Y}(\infty) = 0 \qquad x \to \infty \tag{2.7}$$

where $\hat{p}$ is pressure; $\hat{\rho}$ is the mixtures gas density; $\hat{R}^{\circ}$ is the universal gas constant; $\hat{C}_p$ is the specific heat at constant pressure; $\hat{\mathcal{D}}$ is the diffusion coefficient of the deficent reactant; $\hat{\lambda}$ is the thermal diffusivity of the gas; $\hat{Q}$ is the heat release of per unit mass of reactant; $\hat{Y}$ is the mass fraction of the deficient reactant in the mixtured gas; $\hat{T}$ is temperature; $\hat{\Phi}$ is the dissipation function; $\hat{\mathbf{V}}$ is velocity field; and $\hat{\sigma}_{ij}$ is stress tensor, given by

$$\hat{\sigma}_{ij} = 2\hat{\mu}\left(\hat{d}_{ij} - \frac{1}{3}\hat{\nabla}\cdot\hat{\mathbf{V}}\right) \qquad \hat{d}_{ij} = \frac{1}{2}\left(\frac{\partial\hat{u}_i}{\partial\hat{x}_j} + \frac{\partial\hat{u}_j}{\partial\hat{x}_i}\right) \tag{2.8}$$

The reaction rate term $\hat{\Omega}$ has the form

$$\hat{\Omega} = \Lambda \hat{\rho} \hat{Y} \exp\Big(- \hat{E}/(\hat{R}^{\circ}\hat{T}) \Big) \tag{2.9}$$

where Λ is the preexponential factor and $\hat{E}$ is the activation energy of the reaction. Note that the reaction rate term $\hat{\Omega}$ depends exponentially on temperature $\hat{T}$, and this kind of nonlinearity greatly increases the difficulty of these problems.

This system serves as the starting point to describe a wide range of combustion problems.

2.2 Nondimensionalization

To begin, we nondimensionalize all variables with respect to their values in the fresh cold mixture, thus we can introduce nondimensional variables as follows:

$$\hat{T} = \hat{T}_{-\infty} \cdot T \qquad \hat{Y} = \hat{Y}_{-\infty} \cdot Y$$

$$\hat{\rho} = \hat{\rho}_{-\infty} \cdot \rho \qquad \hat{\mathbf{x}} = L \cdot \mathbf{x}$$

$$\hat{\mathbf{V}} = S_f^{\circ} \cdot \mathbf{V} \qquad \hat{t} = \frac{L}{S_f^{\circ}} \cdot t$$

$$\hat{\lambda} = \hat{\lambda}_{-\infty} \cdot \lambda \qquad \hat{\mu} = \hat{\mu}_{-\infty} \cdot \mu$$

where L is a typical length scale of hydrodynamic flow, and S_f° is the adiabatic flame speed, i.e. the velocity of an adiabatic plane flame through the given mixture. Since the velocity of flame propagation is much slower than that of sound propagation, the Mach number M_a ($M_a = S_f^{\circ}(\hat{\rho}_{-\infty}/\hat{p}_{-\infty})^{\frac{1}{2}} \ll 1$) is small. The above equations can then be expanded in the small parameter M_a. Therefore the nondimensionalized pressure P is then expanded as $P \sim 1 + M_a^2 p + \cdots$, which implies $\nabla P = O(M_a^2) \sim 0$. This means the process is nearly isobaric. Then in terms of the nondimensional quantities, the leading order terms in Mach number M_a expansion are

$$\rho T = 1 \tag{2.10}$$

$$\rho_t + \nabla \cdot (\rho \mathbf{V}) = 0 \tag{2.11}$$

$$\rho\Big(\mathbf{V}_t + (\mathbf{V} \cdot \nabla)\mathbf{V}\Big) = -\nabla p + \delta Pr \nabla \cdot \sigma_{ij} \tag{2.12}$$

$$\rho\Big(T_t + (\mathbf{V} \cdot \nabla)T\Big) = \delta q \Omega + \delta \nabla \cdot (\lambda \nabla T) \tag{2.13}$$

$$\rho\Big(Y_t + (\mathbf{V} \cdot \nabla)Y\Big) = -\delta \Omega + \frac{\delta}{Le} \nabla \cdot (\lambda \nabla Y) \tag{2.14}$$

where

$$\sigma_{ij} = 2\lambda \left(d_{ij} - \frac{1}{3} \nabla \cdot \mathbf{V} \right) \qquad d_{ij} = \frac{1}{2} \left(\frac{\partial u_i}{\partial x_j} + \frac{\partial u_j}{\partial x_i} \right) \tag{2.15}$$

$$Le = \frac{\hat{\lambda}_{-\infty}}{\hat{\mathcal{D}} \hat{C}_p \hat{\rho}_{-\infty}} \qquad Pr = \frac{\hat{C}_p \hat{\mu}_{-\infty}}{\hat{\lambda}_{-\infty}} \tag{2.16}$$

$$\delta = \frac{\hat{\lambda}_{-\infty}}{L S_f^{\circ} \hat{C}_p \hat{\rho}_{-\infty}} \qquad q = \frac{\hat{Q} \hat{Y}_{-\infty}}{\hat{C}_p \hat{T}_{-\infty}} \tag{2.17}$$

and both $\hat{C}_p$ and $\hat{\mathcal{D}}$ are assumed to be constant. The Lewis number Le is the ratio of heat to mass diffusivities; the Prandtl number Pr is the ratio of viscous to thermal effects; $\delta (\ll 1)$ is the ratio of the thickness of transport zone to the typical hydrodynamic length scale; q is the total heat of reaction per unit mass of reactant consumption made dimensionless by $\hat{C}_p \hat{T}_{-\infty}$. Finally, the reaction rate Ω takes the form

$$\Omega = \Lambda \delta^{-2} \rho Y \exp(-E/T) \tag{2.18}$$

where $E \gg 1$ is the dimensionless activation energy. The preexponential factor Λ is such that the nondimensional flame speed of a plane adiabatic flame is unity.

We are concerned with the development of hydrodynamic models, for which the flame thickness is relatively small compared with the typical hydrodynamic length scale i.e. $\delta \ll 1$. It follows from the above equations that all physiochemical processes are confined to a very thin region, called flame zone. Also, in the limit $E \gg 1$, reaction is confined to a thinner region, of $O(\delta E^{-1})$ within the flame. In figure 2.1, a schematic illustration of a thin flame is shown.

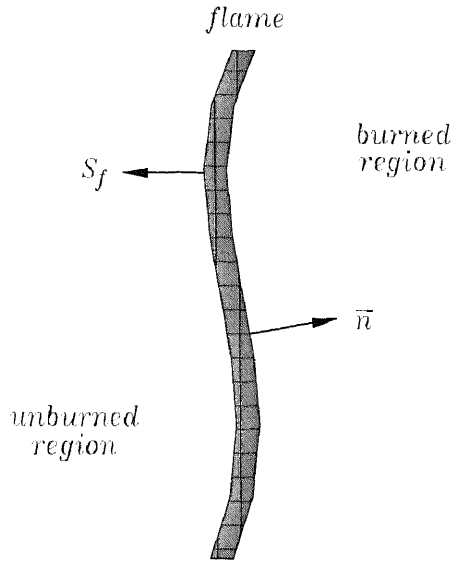

Figure 2.1 Flame as surface separating burned from unburned gas

Outside the flame zone, the shaded region in sketch, the flow field is that of an incompressible and inviscid flow, although the density is lower on the burned side as compared to unburned side.

In Landau's original model, he considered the flame to be a surface on either side of which the transport variables T, ρ, Y remain constant. Thus he essentially set $\delta = 0$, in which case the above equations reduce to

$$\nabla \cdot \mathbf{V} = 0 \tag{2.19}$$

$$\rho\left(\frac{\partial \mathbf{V}}{\partial t} + \mathbf{V} \cdot \nabla \mathbf{v}\right) = -\nabla p \tag{2.20}$$

with

$$T^{-1} = \rho = \begin{cases} 1 & \text{unburned region} \\ (1+q)^{-1} & \text{burned region} \end{cases}$$

$$Y = \begin{cases} 1 & \text{unburned region} \\ 0 & \text{burned region} \end{cases}$$

Integrating the above equations across flame "surface" at $x = f(y,z,t)$, gives Rankine-Hugoniot relations for mass and momentum conservation, i.e.

$$\Big[\rho(\mathbf{V}\cdot\mathbf{n}-\nu_n)\Big] = 0 \tag{2.21}$$

$$\Big[\mathbf{V}\times\mathbf{n}\Big] = 0 \tag{2.22}$$

$$\Big[p+\rho\mathbf{V}\cdot\mathbf{n}(\mathbf{V}\cdot\mathbf{n}-\nu_n)\Big] = 0 \tag{2.23}$$

where the brackets $[\cdot]$ are used to denote jumps across the surface. For convenience, we express the flame surface mathematically as

$$F(\mathbf{X},t) = x - f(y,z,t) \tag{2.24}$$

such that the unit normal pointing toward the burned gasses is

$$\mathbf{n} = \frac{\nabla F}{\mid \nabla F \mid} \quad , \tag{2.25}$$

and the propagation speed of the front relative to a fixed frame of reference is

$$\nu_n = -\frac{F_t}{\mid \nabla F \mid} \quad . \tag{2.26}$$

In order to complete his formulation, Landau further assumed that the flame speed, i.e. the speed of the flame relative to the local flow velocity, remained constant and equal to the laminar flame speed S_f°, and is therefore nondimensionalized to unity, i.e.

$$\mathbf{V}\cdot\mathbf{n}-\nu_n = 1 \quad . \tag{2.27}$$

This model predicts that a plane flame is unconditionally unstable, contrary to experimental observations. This can be attributed to the fact that Landau's analysis ignores the flame structure effects. However, as recently demonstrated, cf. Matalon and Matkowsky(1982), Pelce and Clavin(1982), Bechtold and Matalon(1998) these effects can be incorporated by analyzing the flame structure with asymptotic

methods. In particular, these new models exhibit an explicit dependence of flame speed on both strain rate and curvature, as well as the diffusional thermal parameters.

In the chapter to follow, I employ these models to study flame response to unsteady nonuniform flow.

CHAPTER 3

THE RESPONSE OF NEAR EQUIDIFFUSIONAL FLAMES TO UNSTEADY STAGNATION POINT FLOW

3.1 Problem Description

Premixed flame propagation can be highly influenced by the presence of unsteady strained flow. In this chapter, I will use a NEF model derived by Bechtold and Matalon(1998) to study how the premixed flame responds to an unsteady strained flow. The geometry under consideration is sketched on figure 3.1 below.

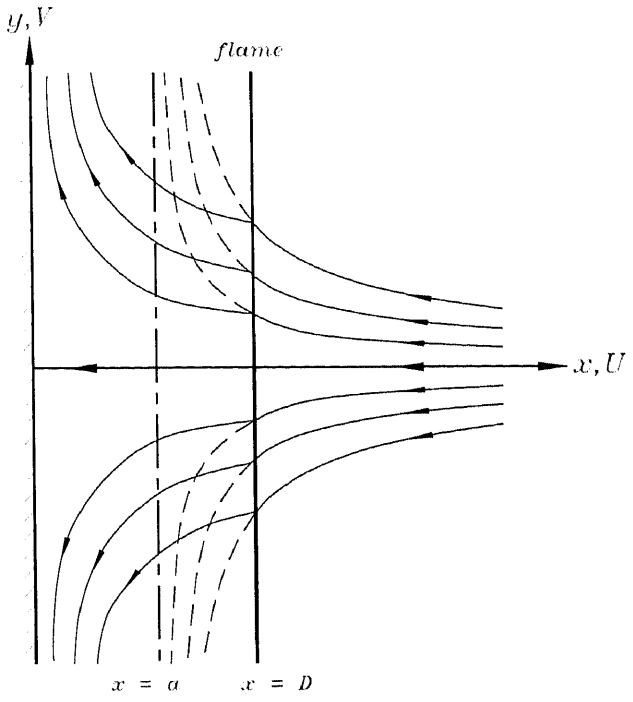

Figure 3.1 Flame in unsteady stagnation point flow

I restrict attention to a flat flame in a two-dimensional or axisymmetric stagnation point flow as illustrated in the figure. Experiments confirm that this is indeed a stable configration. The velocity field is $\mathbf{V} = (U, V)$, where U and V correspond to the axial and transverse (or radial) components of the velocity. The location of the stagnation plane and of the flame front are denoted by $x = 0$

and $x = D$, respectively. It is anticipated the flame remains flat, but its location changes continuously in time as a result of temporal variations in the flow field, i.e. $D = D(t)$.

The flame surface, which separates the gas into burned and unburned regions, can be described mathematically as

$$F(\mathbf{X}, t) = D(t) - x \tag{3.1}$$

such that $F > 0$ corresponds to the burned region. Outside the flame zone, the density ρ and temperature T remain constant, and in particular, we have

$$T^{-1} = \rho = \begin{cases} 1 & x > D(t) \\ 1/\sigma & x < D(t) \end{cases}$$

where $\sigma = 1 + q = \rho_u/\rho_b$ is the unburned to burned density ratio, or the thermal expansion coefficient.

Although the model has been derived for arbitrary λ, we assume that λ and T are linearly related, i.e. $\lambda = T$, so that the governing equations (2.10)–(2.15) outside flame zone, can be written as

$$\nabla \cdot \mathbf{V} = 0 \tag{3.2}$$

$$\rho\left(\frac{\partial \mathbf{V}}{\partial t} + (\mathbf{V} \cdot \nabla)\mathbf{V}\right) = -\nabla p + \frac{\delta Pr}{\rho}\nabla^2 \mathbf{V} \,. \tag{3.3}$$

The relations, relating the fluids variables across the flame surface, and the normalized flame speed equation derived by Bechtold and Matalon(1998), can be expressed in coordinate-free form as

$$-\nu_n + \mathbf{V} \cdot \mathbf{n} \,|_{x=D^+} = 1 - \delta\alpha\kappa \tag{3.4}$$

$$\Big[\rho(\mathbf{V} \cdot \mathbf{n} - \nu_n)\Big] = \delta q \kappa \tag{3.5}$$

$$\Big[\mathbf{V} \times \mathbf{n}\Big] = \delta\Big\{ -(1+q)(Pr+1)\Big[\nabla \times \mathbf{V}\Big] + qPr\mathbf{n} \times \tau^- \cdot \mathbf{n}\Big\} \tag{3.6}$$

$$\Big[p+\rho\mathbf{V}\cdot\mathbf{n}(\mathbf{V}\cdot\mathbf{n}-\nu_n)\Big]=\delta\Big\{q\nu_n\kappa+(1+q)\Big[\mathbf{n}\cdot\nabla p\Big] \\ -q\Big(2+\frac{3}{2}q\Big)\nabla\cdot\mathbf{n}+Pr\Big(-q^2\nabla\cdot\mathbf{n}+q\mathbf{n}\cdot\tau^-\cdot\mathbf{n}\Big)\Big\}\,, \tag{3.7}$$

where $[\phi]=\phi(x=D^+)-\phi(x=D^-)$ denotes the jump in the variable ϕ across the flame. Also κ is the flame stretch, given by

$$\kappa=\nu_n\nabla\cdot\mathbf{n}-\mathbf{n}\cdot\nabla\times(\mathbf{V}\times\mathbf{n})\,|_{x=D+} \tag{3.8}$$

and for the geometry under investigation, $\mathbf{n}$ and ν_n take the form

$$\mathbf{n}=(-1,0,0) \qquad\qquad \nu_n=-D'(t)\ .$$

The parameter α is commonly referred as to the Markstein number and is given by

$$\alpha=1+q+\frac{1}{2}q\ell_c\ , \tag{3.9}$$

and τ is the stress tensor whose component are given by $2d_{ij}$ as shown in (2.15). In addition to the above conditions, I require that the normal component of velocity vanish at the wall, i.e. $U(0,t)=0$. It should also be noted that a viscous boundary layer exists near the wall that causes transverse velocity, V, to vanish there as well.

3.2 Analysis

The imposed flow at $x=\infty$ resembles the flow against a wall in the absence of vorticity, and is characterized by a time-dependent strain rate $\mu(t)$. Since the flow ahead of the flame, for $x>D(t)$, remains potential flow, it is given by

$$\mathbf{V}=(U,V)=\mu(t)\Big(-(\nu+1)(x-a)\,,\ y\Big)\,, \tag{3.10}$$

with $a=a(t)\neq 0$ and, where ν is a geometric factor that takes the value $\nu=0$ for the two-dimensional case and $\nu=1$ for the axisymmetric case. The velocity field described by (3.10) can effectively express the flow against a virtual body

at $x = a(t)$, standing in front of the actual one; that is, the flame displaces the incoming stream away from the body a distance a (see figure 3.1), which remains to be determined during the course of the analysis. This displacement is a direct consequence of thermal expansion which causes a deflection of the streamlines upon crossing the flame front. It should be pointed out that this effect is in addition to the viscous boundary layer displacement and, in fact, is more pronounced than the latter persisting as it does when the viscosity goes to zero. However, it does not persist when $\sigma \to 1$ and indeed, a tends to zero in this limit. The pressure in the unburned gas is obtained from Bernoulli's equation as

$$p = p^{vs} - \frac{1}{2}\mu^2\Big((\nu+1)^2(x-a)^2 + y^2\Big) + \frac{1}{2}\mu_t\Big(-y^2 + (\nu+1)(x-a)^2\Big) - a_t\mu(\nu+1)(x-a) \ , \tag{3.11}$$

where p^{vs} is the pressure at the virtual stagnation point, i.e. at the location $(a, 0)$. The equation for the flame speed equation (3.4), provides a relation between the flame position $D(t)$, and the flow displacement $a(t)$, namely

$$D_t + \mu(\nu+1)(D-a) = 1 - \delta\alpha\kappa \ . \tag{3.12}$$

Thus, the problem thus reduces to solving equations (3.2) and (3.3) for the flow field in the burned region $0 < x < D$, subject to the conditions (3.4)–(3.7).

In the burned region, vorticity is produced along flame surface, so it is convenient to introduce the vorticity $\varpi = \partial V/\partial x - \partial U/\partial y$, that satisfies

$$\frac{\partial}{\partial t}\left(\frac{\varpi}{y^\nu}\right) + U\frac{\partial}{\partial x}\left(\frac{\varpi}{y^\nu}\right) + V\frac{\partial}{\partial y}\left(\frac{\varpi}{y^\nu}\right) = \frac{\delta Pr}{\rho^2 y^\nu}\left\{\frac{\partial^2\varpi}{\partial x^2} + \frac{\partial}{\partial y}\left(\frac{1}{y^\nu}\frac{\partial(y^\nu\varpi)}{\partial y}\right)\right\} \ , \tag{3.13}$$

which is obtained by taking the curl of the momentum equation (3.3). The amount of vorticity produced at the flame is determined by integrating the y-component of the momentum equation (see Appendix A), which yields

$$\varpi^+ = -y\left(\frac{q}{1+q}(\mu_t + \mu^2) + \delta f(t)\right) \ ,$$

where

$$f(t) = \frac{q}{1+q}\Big((\nu+1)(\alpha-q)(\mu\mu_t+\mu^3) - (Pr+1)(\mu_{tt}+4\mu\mu_t+2\mu^3) \\ - Pr\left(\mu_{tt}+2\mu\mu_t+(1-\nu)(\mu\mu_t+\mu^3)\right)\Big) \ . \tag{3.14}$$

In terms of the stream function $\Psi(x,y,t)$, defined by the relations

$$U = \frac{1}{y^\nu}\frac{\partial\Psi}{\partial y} \qquad\qquad V = -\frac{1}{y^\nu}\frac{\partial\Psi}{\partial x} \ , \tag{3.15}$$

the vorticity ϖ takes the form

$$\varpi = -\left\{\frac{1}{y^\nu}\frac{\partial^2\Psi}{\partial x^2} + \frac{\partial}{\partial y}\left(\frac{1}{y^\nu}\frac{\partial\Psi}{\partial y}\right)\right\} \ . \tag{3.16}$$

The vorticity condition suggests that we look for solutions of the form $\Psi(x,y,t) = y^{\nu+1}H(x,t)$, which when inserted into (3.13) yields

$$H_{xxt} + (\nu+1)HH_{xxx} + (\nu-1)H_xH_{xx} = \frac{\delta Pr}{\rho^2}H_{xxxx} \ , \tag{3.17}$$

and above nonlinear PDE is to be solved under those conditions, which come from (3.4)–(3.7) (see Appendix A)

$$H(0,t) = 0 \tag{3.18}$$

$$H(D^-,t) = \frac{D_t}{\nu+1} - \frac{1+q}{\nu+1} + \delta(1+q)(\alpha-q)\mu \tag{3.19}$$

$$H_x(D^-,t) = -\mu - \delta q(Pr+1)(\mu_t+\mu^2) \tag{3.20}$$

$$H_{xx}(D^-,t) = \frac{q}{1+q}(\mu_t+\mu^2) + \delta f(t) \tag{3.21}$$

$$H_{xxx}(D^-,t) = \frac{q}{(1+q)^2}\Big(\mu_{tt}+2\mu\mu_t+(1-\nu)(\mu\mu_t+\mu^3)\Big) \ , \tag{3.22}$$

where

$$f(t) = \frac{q}{1+q}\Big((\nu+1)(\alpha-q)(\mu\mu_t+\mu^3) - (Pr+1)(\mu_{tt}+4\mu\mu_t+2\mu^3) \\ - Pr\left(\mu_{tt}+2\mu\mu_t+(1-\nu)(\mu\mu_t+\mu^3)\right)\Big) \ . \tag{3.23}$$

We integrate (3.17) once, and also make following transformation

$$z = x - D(t) \qquad H(x,t) = \frac{D_t}{\nu+1} + G(z,t) \tag{3.24}$$

$$\partial_x \to \partial_z \qquad \partial_t \to \partial_t - D_t \partial_z \ , \tag{3.25}$$

so that the problem becomes

$$G_{zt} + (\nu+1)GG_{zz} - G_z^2 = -(1+q)(\mu_t + \mu^2) + \delta Pr(1+q)^2 G_{zzz} \tag{3.26}$$

$$G(0,t) = -\frac{1+q}{\nu+1} + \delta\mu(1+q)(\alpha - q) \tag{3.27}$$

$$G_z(0,t) = -\mu - \delta q(Pr+1)(\mu_t + \mu^2) \tag{3.28}$$

$$G_{zz}(0,t) = \frac{q}{1+q}(\mu_t + \mu^2) + \delta f(t) \tag{3.29}$$

$$D_t = -(\nu+1)G(-D,t) \tag{3.30}$$

$$D_t + (\nu+1)(D-a)\mu = 1 - \delta(\nu+1)\alpha\mu \ . \tag{3.31}$$

The advantage of this formulation is that the boundary conditions at the flame are now independent of D and are applied at the fixed position $z = 0$. We can therefore solve first for $G(z,t)$ and then use (3.30), namely

$$D_t = -(\nu+1)G(-D,t) \tag{3.32}$$

to determine the flame location. Finally, the flow displacement $a(t)$ is obtained from (3.31). At this point, entire problem is reduced to solve (3.26)–(3.31) for the stream function in the burned region.

3.3 Hydrodynamic Effects with Time Periodic Strain Rate

The system (3.26)–(3.31) can be solved in terms of a power series expansion in δ, i.e.

$$G \sim G_0 + \delta G_1 + \delta^2 G_2 + \cdots \ .$$

At leading order, we have

$$G_{0zt} + (\nu+1)G_0 G_{0zz} - G_{0z}^2 = -\sigma(\mu_t + \mu^2) \tag{3.33}$$

$$G_0(0,t) = -\frac{\sigma}{\nu+1} \qquad D_{0t} = -(\nu+1)G_0(-D_0,t) \tag{3.34}$$

$$G_{0z}(0,t) = -\mu \qquad D_{0t} + (\nu+1)(D_0 - a_0)\mu = 1\ . \tag{3.35}$$

For a constant strain rate, $\mu = constant$, the system (3.33)–(3.35) possesses an exact solution given by Eteng, Ludford and Matalon(1986); these results are quoted here for completeness. For the two-dimensional case ($\nu = 0$), the solution and flame location are given by

$$G_0(z) = -\sqrt{\frac{\sigma-1}{\sigma}}\sin\left(\frac{\mu\sqrt{\sigma-1}}{\sigma}(z+D_0)\right) \tag{3.36}$$

$$D_0 = \frac{\sigma}{\mu\sqrt{\sigma-1}}\arctan\left(\sqrt{\sigma-1}\right)\ . \tag{3.37}$$

For the axisymmetric case ($\nu = 1$), the solution and flame location are given by

$$G_0(z) = \frac{1}{2}\frac{\sigma-1}{\sigma}\mu^2 z^2 - \mu z - \frac{\sigma}{2} \qquad D_0 = \frac{\sigma}{\mu(1+\sqrt{\sigma})} \tag{3.38}$$

respectively. The displacement a_0 follows from the relation (3.35). The results indicate that an increase in strain rate will result in a shift in the flame standoff distance towards the wall and a reduction in the distance between the flame and the virtual stagnation plane.

In general, the system (3.33)–(3.35) must be solved numerically, although asymptotic solutions can be constructed in limiting parameter regimes. For this purpose, it is convenient to introduce the new dependent variable $\phi(z,t)$, given by

$$G_0(z,t) = -\frac{\sigma}{\nu+1} + \int_0^z \phi(\eta,t)\,d\eta\ , \tag{3.39}$$

such that equation (3.33) takes the form

$$\phi_t + (\nu+1)G_0\phi_z - \phi^2 = -\sigma(\mu_t + \mu^2)\ . \tag{3.40}$$

This first order quasi-linear hyperbolic partial differential equation can be solved by using the method of characteristics, cf. Smith(1978). The characteristic curves are determined from the equation

$$\frac{d\,z}{d\,t} = (\nu + 1)G_0(z,t) \ , \tag{3.41}$$

and along each of these curves, ϕ satisfies the Ricatti equation

$$\phi_t - \phi^2 = -\sigma(\mu_t + \mu^2) \ . \tag{3.42}$$

By comparing equation (3.34) with (3.41), one notes that the wall position, $z = -D$, in addition of being a streamline is also a characteristic curve. A predictor-corrector method is used to solve (3.41) and (3.42), and at each time step the integral in (3.39) is evaluated by using the trapezoid rule.

Because of the potential application to turbulent combustion modelling, we first solve the above system for an imposed time periodic strain rate; particularly we consider

$$\mu(t) = \bar{\mu}\Big(1 + A\sin(\omega t)\Big) \ , \tag{3.43}$$

with A the normalized amplitude and ω the frequency. We consider $\mid A \mid < 1$, so that the imposed flow at $x = \infty$ is always moving towards the wall, but otherwise place no restriction on the magnitude of A. The mean value $\bar{\mu}$ can be readily scaled out of the problem so that, without loss generality, we set $\bar{\mu} = 1$. Our interest here is to trace the evolution of the flame after it is set in motion, and so the boundary data are sufficient to determine $G_0(z,t)$. The flame location is then found by integrating (3.34), with the flame assumed to reside at its steady state (corresponding to $\mu = 1$) initially. In the calculations reported below, we have fixed $\sigma = 6$. Only results for the axisymmetric ($\nu = 1$) case are reported; results for the two-dimensional configuration exhibit similar behaviour.

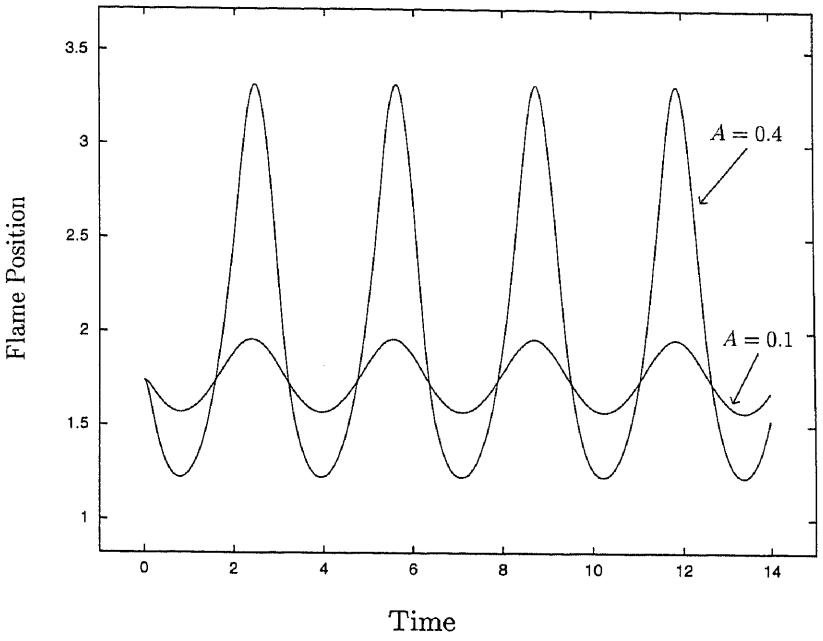

Figure 3.2 Flame position versus time for two different values of the imposed amplitude $A = 0.1$ and $A = 0.4$, with $\omega = 2$ and $\sigma = 6$

In figures 3.2 and 3.3, we plot the flame position D, and the displacement a as functions of time for fixed frequency $\omega = 2$ and two different values of the amplitude of the imposed oscillation A. As expected, for small values of A the flame and displacement are seen to respond sinusoidally about their steady states. For larger values of A, the nonlinear effects become apparent as illustrated by the curves for $A = 0.4$. In particular, the response remains periodic (this result is also readily seen in the phase plane diagrams of both flame position $D(t)$ and the flow displacement $a(t)$), but the sinusoidal character of the curves is lost. The mean position of the flame over one period is now further away from the wall when compared to the steady state location (3.38). Note that the peaks of the curves are much sharper than the troughs indicating a more rapid motion when the flame resides further upstream. This results from the fact that, in an upstream location, the flame experiences a large relative change in normal gas velocity over a short time interval. The nonlinear effects are more apparent in the curves showing the variation of the displacement

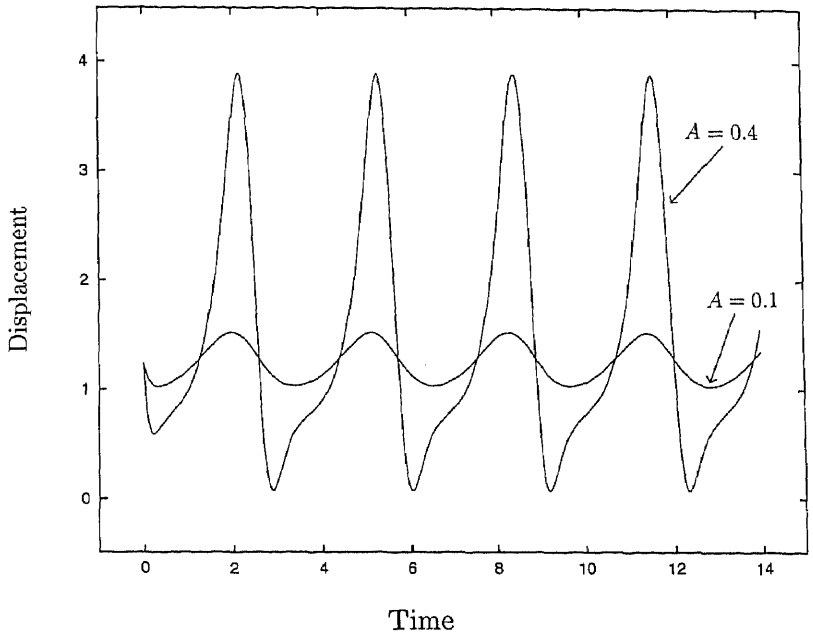

Figure 3.3 Flow displacement versus time for two different values of the imposed amplitude $A = 0.1$ and $A = 0.4$, with $\omega = 2$ and $\sigma = 6$

$a(t)$ in time, and also in the phase planes of both flame position $D(t)$ and the flow displacement $a(t)$.

We next investigate how the flame response is affected by the frequency of imposed oscillations. As previously discovered, both experimentally and theoretically, cf. Saitoh and Otsuka(1976) and Im, Bechtold and Law(1996), the flame exhibits a phase lag with the imposed fluctuations. Our results confirm this phenomenon and, furthermore, identify a phase lag in the flow displacement. In figure 3.4, the phase lag is plotted as a function of frequency for fixed amplitude $A = 0.1$. For $\omega \ll 1$ both the flame and displacement respond almost instantaneously to the fluctuating flow field and are effectively in phase. The phase lag in the flame's response is seen to increase monotonically with ω and at high frequencies the flame is nearly 90° out of phase. On the other hand, the phase lag between the displacement and imposed flow is non-monotonic. For modest values of ω they are

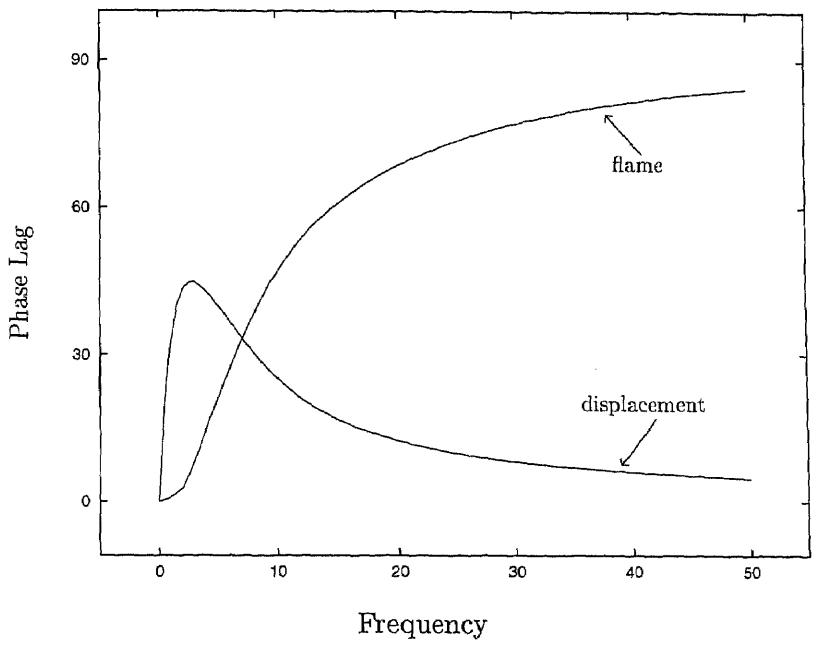

Figure 3.4 Phase lag of flame and of flow displacement relative to the incoming flow as a function of frequency with $A = 0.1$ and $\sigma = 6$

clearly out of phase, but at high frequencies they again become in phase with one another.

In figures 3.5 and 3.6, we plot the flame position and flow displacement as functions of time for two frequencies, $\omega = 2$ and $\omega = 20$ with $A = 0.1$. There are several interesting features of these figures that are further elucidated in later figures. We first note from figure 3.5 that the amplitude of oscillations of the flame is smaller for the higher frequency. This trend was observed by Saitoh and Otsuka(1976) and has been predicted in previous studies as well. However, the amplitude of the displacement fluctuations is seen to be larger at the higher frequency. In figure 3.7 we have plotted these amplitudes, which we define as the difference between successive maximum and minimum locations over one period, as functions of frequency. The amplitude of the flame is seen to be non-monotonic. At low frequencies the flame responds almost instantaneously to the slow fluctuations in the flow and its amplitude

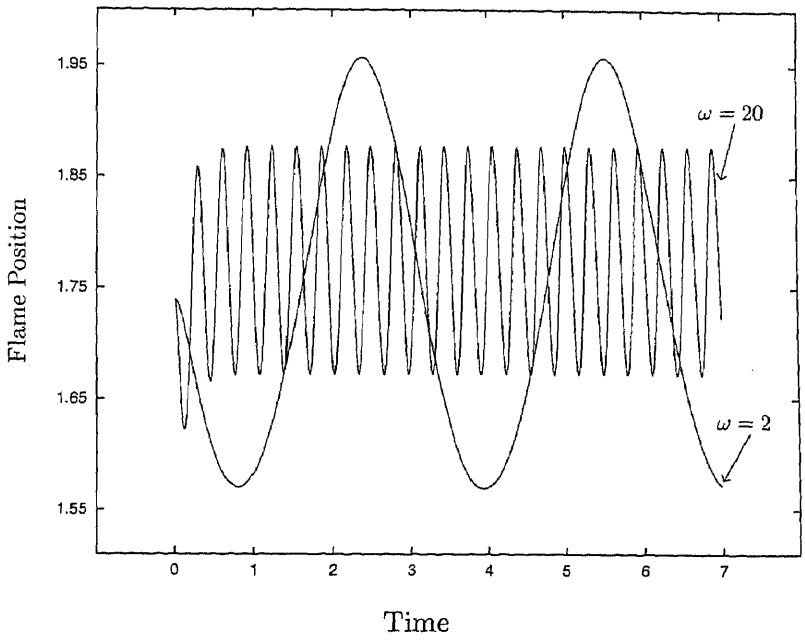

Figure 3.5 Flame position versus time for two different values of frequency $\omega = 2$ and $\omega = 20$, with $A = 0.1$ and $\sigma = 6$

is approximately $\{2A/(1-A^2)\}\{\sigma/(1+\sqrt{\sigma})\}$, also obtained from (3.38) with $\mu = 1 + A\sin(\omega t)$. As the frequency is increased, the amplitude first increases, reaches a maximum near $\omega \sim 4.5$, and then decreases approaching zero as $\omega \to \infty$. In contrast, the amplitude of the fluctuations in the flow displacement increases monotonically with ω and asymptotes to a finite value. At high frequencies the flame is unable to respond to the rapid oscillations in the flow and appears to be confined to a single location. Due to the varying strain rate of the flow impinging on the flame there is a continual change in the divergence of the streamlines so that the flow displacement $a(t)$, oscillates with a finite amplitude.

The negligible response of the flame at high frequencies as compared to the pronounced displacement effect suggests the possibility that the magnitude of the flow displacement may temporarily exceed the flame standoff distance. This is illustrated in figures 3.8 to 3.11, where we have plotted both $D(t)$ and $a(t)$ for four

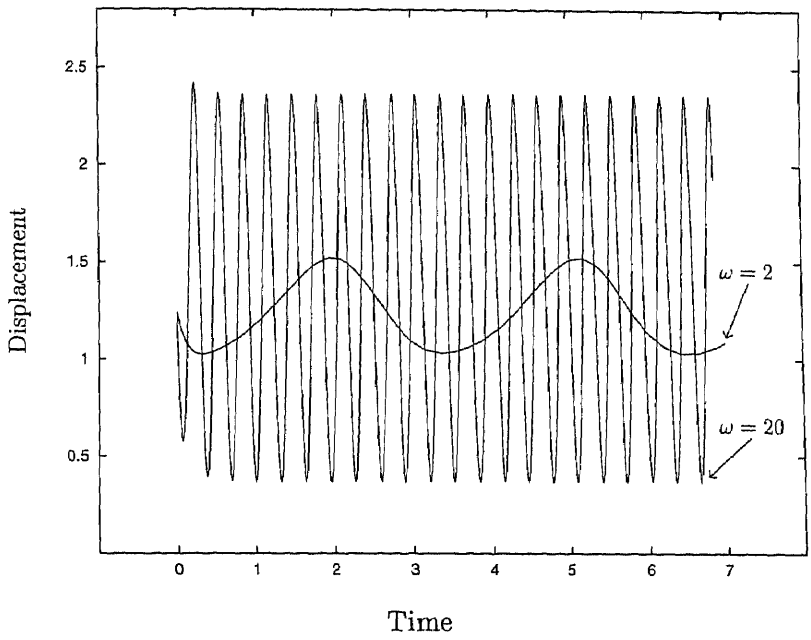

Figure 3.6 Flow displacement versus time for two different values of frequency $\omega = 2$ and $\omega = 20$, with $A = 0.1$ and $\sigma = 6$

different values of ω with $A = 0.1$. Even for the modest value of $\omega = 6$ (figure 3.10), there exists a portion of each cycle where the magnitude of the displacement exceeds the flame standoff distance. During these time intervals, the fluctuating flame causes a flow reversal immediately ahead of the flame. This results in the formation of a temporary stagnation plane slightly upstream of the flame. A sketch of the streamlines at four different times within one cycle (figure 3.12 to 3.16) illustrates this phenomenon. Note that at higher frequency, the temporary stagnation plane is located further upstream. Finally, we remark that the flame always moves upstream during the time interval that a reverse flow exists. Another trend that we observe from figure 3.5 is that, at higher frequency, the mean flame location is shifted slightly upstream from the steady position (which is the position shown at $t = 0$ in the figure). In figure 3.17 we plot the flame position for a large value of $A = 0.3$ and a very large value of ω, i.e. $\omega = 100$. The dashed line in the figure denotes the mean position that is determined asymptotically in the limit $\omega \to \infty$ and will be discussed

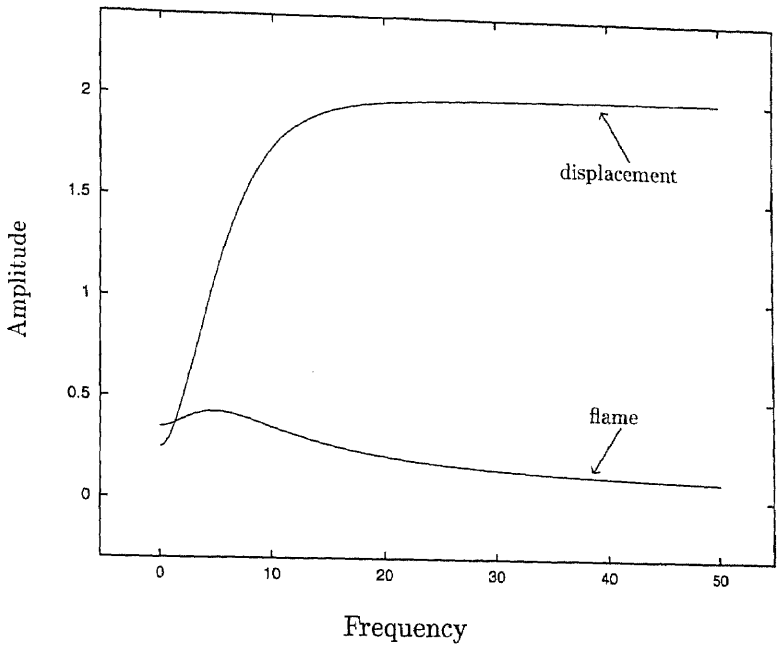

Figure 3.7 The amplitude of the fluctuations of the flame and of the flow displacement as functions of frequency with $A = 0.1$ and $\sigma = 6$

shortly. The shift is a consequence of nonlinear interactions between flame and flow that results in a decrease in the mean value of the normal velocity component ahead of the flame. This, in turn, causes the flame to position itself (on average) further upstream in order to achieve a balance with the incoming flow. The mean value of normal velocity component for the two limiting cases $\omega \to 0$ and $\omega \to \infty$ is plotted in figure 3.18.

Plots of the phase planes of both flame position D and flow displacement a, give further evidences to support the results reported thus far. In figures 3.19 and 3.20, we plot these phase planes for $\sigma = 6$, $A = 0.1$ and $\omega = 2$. For small amplitude and moderate ω, both flame and flow displacement are seen to evolve rapidly to a periodic solution about steady state values. In figures 3.21 and 3.22, we increased the values of imposed amplitude and frequency to $A = 0.4$ and $\omega = 50$, respectively. The flame position and flow displacement again evolve to a periodic state, although

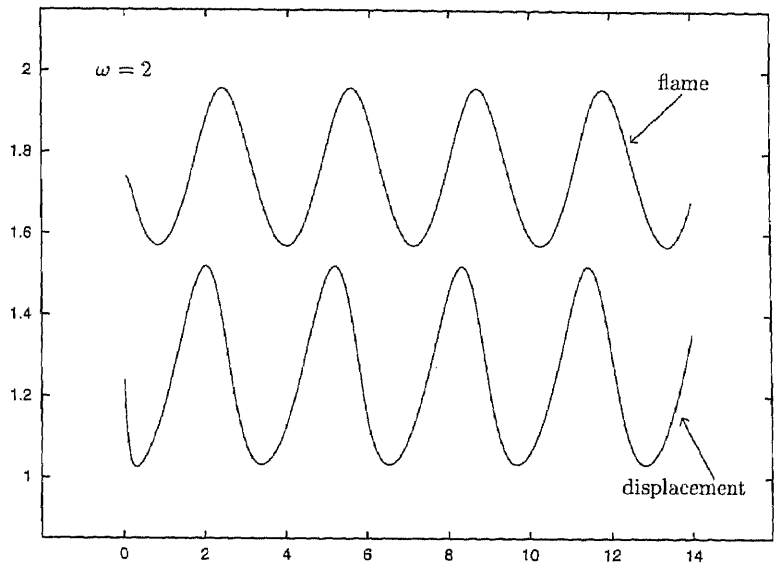

Figure 3.8 Flow displacement and flame position versus time for frequency $\omega = 2$, showing their relative positions; with $A = 0.1$ and $\sigma = 6$

the initial transient is much longer at higher frequencies and larger amplitude. These figures also clearly demonstrate the shift in the mean flame position from the steady state value ($D_s \sim 1.75$ in figure 3.21).

We emphasize that our analysis places no restrictions on the amplitude of the imposed oscillations A. However, our computations indicate that, for sufficiently large ω, a maximum value of A exists beyond which convergence is not attained and solutions fail to exist. This is consistent with the high frequency asymptotic solution that we now discuss.

3.4 The High Frequency Limit

Many of the interesting results reported in the previous section are most pronounced at high frequency. We have therefore treated this limit in more detail with our primary objective being the determination of the mean flame position. To this end

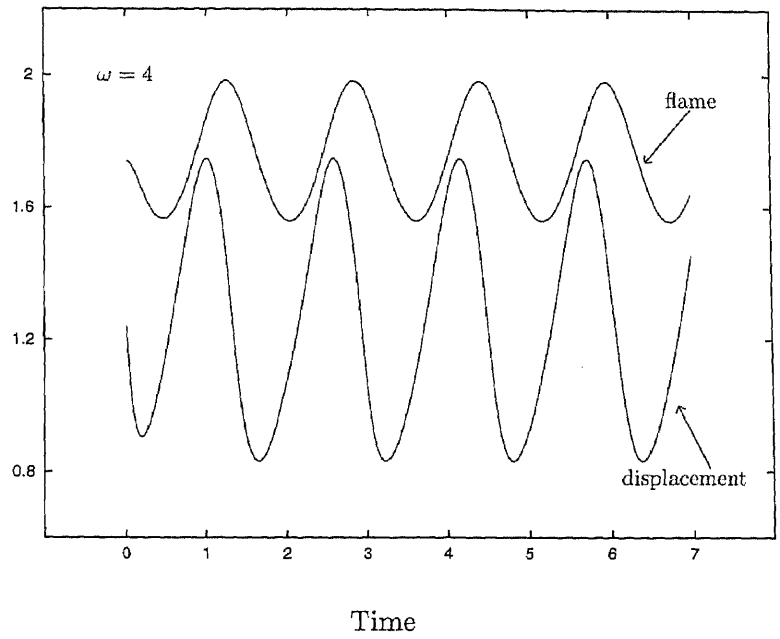

Figure 3.9 Flow displacement and flame position versus time for frequency $\omega = 4$, showing their relative positions; with $A = 0.1$ and $\sigma = 6$

we introduce the more natural time, $\tau = \omega t$, and spatial, $\zeta = \omega z$, scales into the system (3.33)–(3.35) which, for $\nu = 1$, takes the form

$$\omega^2\Big(G_{\zeta\tau} + 2GG_{\zeta\zeta} - G_\zeta^2\Big) = -\sigma A\omega\cos(\tau) - \sigma\Big(1 + A\sin(\tau)\Big)^2 \tag{3.44}$$

$$G(0,\tau) = -\frac{\sigma}{2} \qquad \omega G_\zeta(0,\tau) = -1 - A\sin(\tau)\ . \tag{3.45}$$

We are interested in the time-periodic response of the system to periodic forcing terms that result after the initial transient has faded away. The system (3.44) and (3.45) now has the form of an initial value problem in ζ. The asymptotic limit, for large ω, necessitates the introduction of the multi-scale expansion

$$G(\zeta,z,\tau) = G^{(0)}(\zeta,z,\tau) + \frac{1}{\omega}G^{(1)}(\zeta,z,\tau) + \frac{1}{\omega^2}G^{(2)}(\zeta,z,\tau) + \cdots\ , \tag{3.46}$$

with ζ, z being the fast and slow scales, respectively. Replacing ∂_ζ in equations (3.44) and (3.45) with $\partial_\zeta + \omega^{-1}\partial_z$ and collecting terms of like powers of ω^{-1}, we obtain a series of problems that are then solved recursively.

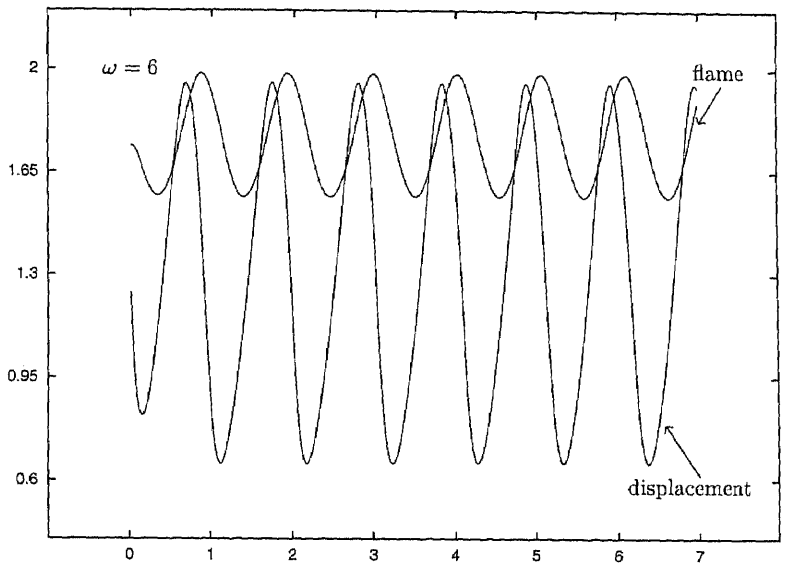

Figure 3.10 Flow displacement and flame position versus time for frequency $\omega = 6$, showing their relative positions; with $A = 0.1$ and $\sigma = 6$

To leading order we have

$$G^{(0)}_{\zeta\tau} + 2G^{(0)}G^{(0)}_{\zeta\zeta} - \left(G^{(0)}_{\zeta}\right)^2 = 0 \tag{3.47}$$

$$G^{(0)}(0,0,\tau) = -\frac{\sigma}{2} \qquad G^{(0)}_{\zeta}(0,0,\tau) = 0 \tag{3.48}$$

whose solution

$$G^{(0)}(\zeta, z, \tau) = \varphi(z) \tag{3.49}$$

must satisfy $\varphi(0) = -\sigma/2$, but is otherwise arbitrary.

At the next order we have

$$G^{(1)}_{\zeta\tau} + 2\varphi G^{(1)}_{\zeta\zeta} = -\sigma A\cos(\tau) \tag{3.50}$$

$$G^{(1)}(0,0,\tau) = 0 \qquad G^{(1)}_{\zeta}(0,0,\tau) = -1 - A\sin(\tau) - \varphi_z(0)\ , \tag{3.51}$$

and, while seeking solutions of form

$$G^{(1)} = f^{(1)} + h^{(1)}\sin(\tau) + g^{(1)}\cos(\tau)\ , \tag{3.52}$$

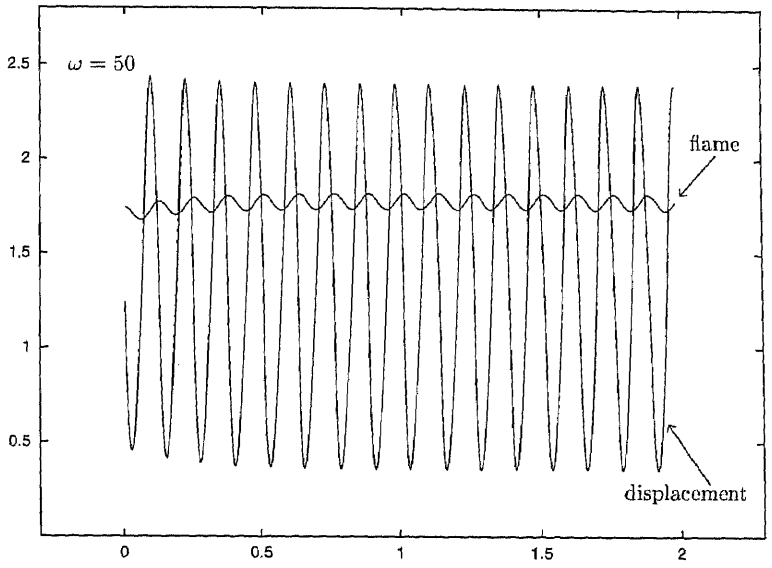

Figure 3.11 Flow displacement and flame position versus time for frequency $\omega = 50$, showing their relative positions; with $A = 0.1$ and $\sigma = 6$

we find that $f^{(1)}$, $h^{(1)}$ and $g^{(1)}$ must satisfy

$$f^{(1)}_{\zeta\zeta} = 0 \qquad h^{(1)}_{\zeta} + 2\varphi g^{(1)}_{\zeta\zeta} = -\sigma A \qquad -g^{(1)}_{\zeta} + 2\varphi h^{(1)}_{\zeta\zeta} = 0\ . \tag{3.53}$$

The general solution is

$$f^{(1)} = a_1(z)\zeta + a_2(z) \tag{3.54}$$

$$h^{(1)} = c_1(z) + c_2(z)\cos\left(\frac{\zeta}{2\varphi}\right) + c_3(z)\sin\left(\frac{\zeta}{2\varphi}\right) - \sigma A\zeta \tag{3.55}$$

$$g^{(1)} = 2\varphi h^{(1)}_{\zeta} + c_4(z)\ , \tag{3.56}$$

where the term $a_1(z)\zeta$ in $f^{(1)}$ contributes to solution $G(\zeta, z, \tau)$ a term that can, without loss of generality, be absorbed into the unknown function $\varphi(z)$. We thus set $a_1(z) \equiv 0$. The boundary condition (3.51) provides conditions for the remaining unknown functions, a_2 and c_i $i = 1, 2, 3, 4$, namely

$$a_2(0) = 0 \qquad c_1(0) = c_2(0) = 0 \tag{3.57}$$

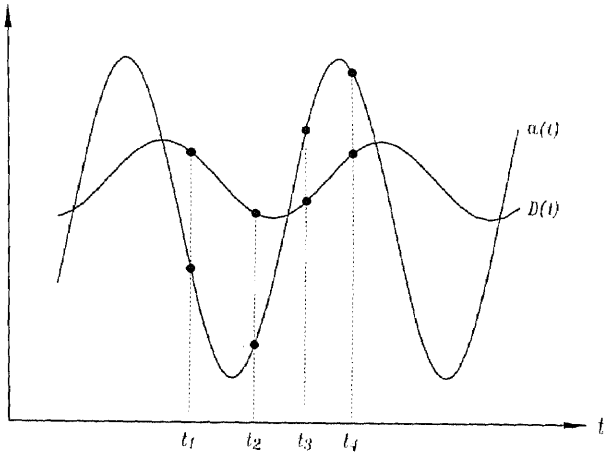

Figure 3.12 The relative position of flame position and flow displacement at four different times during one period

$$c_3(0) = -A\sigma(\sigma - 1) \qquad c_4(0) = -\sigma A \ , \tag{3.58}$$

together with the requirement $\varphi_z(0) = -1$. We note that the function $\varphi(z)$ remains undetermined at this stage so that one must proceed to the next order.

At $O(\omega^{-2})$ the problem becomes

$$\begin{aligned} G^{(2)}_{\zeta\tau} + 2\varphi G^{(2)}_{\zeta\zeta} = &-2G^{(1)}G^{(1)}_{\zeta\zeta} + \left(G^{(1)}_{\zeta}\right)^2 - G^{(1)}_{z\tau} - 4\varphi G^{(1)}_{\zeta z} + 2_z G^{(1)}_{\zeta} \\ &- 2\varphi\varphi_{zz} + \left(\varphi_z\right)^2 - \sigma\left(1 + \frac{1}{2}A^2 + 2A\sin(\tau) - \frac{1}{2}A^2\cos(2\tau)\right) \end{aligned} \tag{3.59}$$

$$G^{(2)}(0,0,\tau) = 0 \qquad G^{(2)}_{\zeta}(0,0,\tau) = -G^{(1)}_{z}(0,0,\tau) \ , \tag{3.60}$$

and the dependence on τ suggests seeking solutions of the form

$$G^{(2)} = f^{(2)} + h^{(2)}_1 \sin(\tau) + h^{(2)}_2 \sin(2\tau) + g^{(2)}_1 \cos(\tau) + g^{(2)}_2 \cos(2\tau)$$

which, upon inserting into (3.59) provides equations for the determination of the functions $f^{(2)}$, $h^{(2)}_1$, $h^{(2)}_2$, $g^{(2)}_1$, $g^{(2)}_2$ that depend only on ζ and z. Although solutions for all these variables can readily be constructed we need only consider the equations

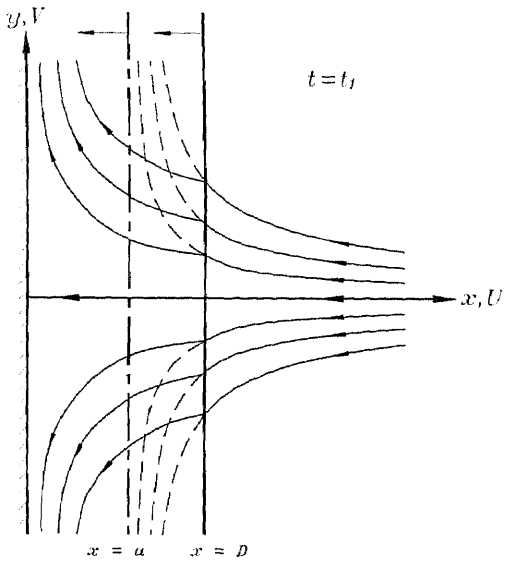

Figure 3.13 Schematic showing the streamlines at time $t = t_1$. The arrows extending from the surfaces $x = a$ and $x = D$ indicate their direction of motion at the given time

for $f^{(2)}$, $h_1^{(2)}$, and $g_1^{(2)}$ to obtain the desired solvability condition for $\varphi(z)$. These equations are

$$2\varphi f_{\zeta\zeta}^{(2)} = -2\varphi\varphi_{\zeta\zeta} + \left(\varphi_z\right)^2 - \sigma\left(1 + \frac{1}{2}A^2\right) - g_1^{(1)}g_{1\zeta\zeta}^{(1)} + \frac{1}{2}\left(g_{1\zeta}^{(1)}\right)^2 - h_1^{(1)}h_{1\zeta\zeta}^{(1)} + \frac{1}{2}\left(h_{1\zeta}^{(1)}\right)^2 \tag{3.61}$$

$$h_{1\zeta}^{(2)} + 2\varphi g_{1\zeta\zeta}^{(2)} = -2a_2 g_{1\zeta\zeta}^{(1)} - h_{1z}^{(1)} - 4\varphi g_{1\zeta z}^{(1)} + 2\varphi_z g_{1\zeta}^{(1)} \tag{3.62}$$

$$-g_{1\zeta}^{(2)} + 2\varphi g_{1\zeta\zeta}^{(2)} = -2a_2 h_{1\zeta\zeta}^{(1)} + g_{1z}^{(1)} - 4\varphi h_{1\zeta z}^{(1)} + 2\varphi_z h_{1\zeta}^{(1)} - 2A\sigma\ . \tag{3.63}$$

After some manipulation the system can be reduced to two equations for $f^{(2)}$ and $h_1^{(2)}$. Particular solutions of these equations are of the form

$$2\varphi f^{(2)} = \frac{1}{2}\left(-2\varphi\varphi_{zz} + \left(\varphi_z\right)^2 - \sigma\left(1 + \frac{1}{2}A^2\right) + \frac{1}{2}\sigma^2A^2 + \frac{3}{8\varphi^2}\left(c_2^2 + c_3^2\right)\right)\zeta^2 + \left(c_2c_4 - c_1c_3 - 4\sigma Ac_2\varphi\right)\sin\left(\frac{\zeta}{2\varphi}\right) - \left(c_3c_4 + c_1c_2 - 4\sigma Ac_3\varphi\right)\cos\left(\frac{\zeta}{2\varphi}\right) + \sigma Ac_3\left\{\frac{\zeta}{2\varphi}\cos\left(\frac{\zeta}{2\varphi}\right) - \sin\left(\frac{\zeta}{2\varphi}\right)\right\} - \sigma Ac_2\left\{\frac{\zeta}{2\varphi}\sin\left(\frac{\zeta}{2\varphi}\right) + \cos\left(\frac{\zeta}{2\varphi}\right)\right\}$$

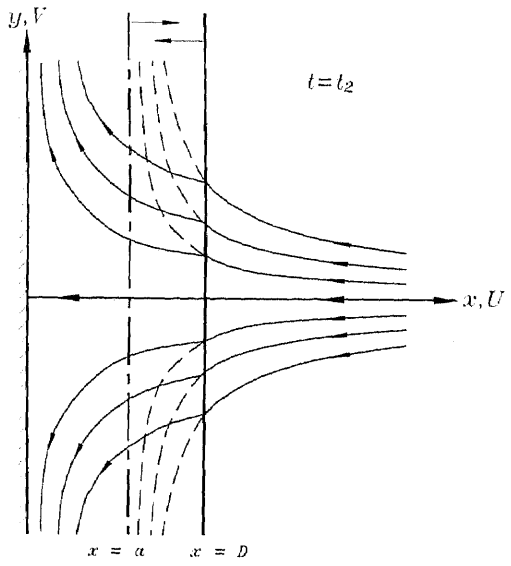

Figure 3.14 Schematic showing the streamlines at time $t = t_2$. The arrows extending from the surfaces $x = a$ and $x = D$ indicate their direction of motion at the given time

and

$$h_1^{(2)} = -\zeta c_{1z} + \left\{ \frac{c_3\varphi_z}{4\varphi^2}\zeta^2 - \left(c_{2z} - \frac{2c_2\varphi_z}{\varphi} + \frac{c_3 a_2}{2\varphi^2} \right) \zeta \right\} \cos\left(\frac{\zeta}{2\varphi}\right) - \left\{ \frac{c_2\varphi_z}{4\varphi^2}\zeta^2 + \left(c_{3z} - \frac{2c_3\varphi_z}{\varphi} - \frac{c_2 a_2}{2\varphi^2} \right) \zeta \right\} \sin\left(\frac{\zeta}{2\varphi}\right) .$$

In a similar way as before, we note that there are terms proportional to ζ, ζ^2, $\zeta\cos(\zeta/2\varphi)$ and $\zeta\sin(\zeta/2\varphi)$ that provide contributions which are already accounted for in previous terms of the expansion for $G(\zeta, z, \tau)$. Thus, without loss of generality, we set

$$c_{1z} = 0 \tag{3.64}$$

$$-2\varphi\varphi_{zz} + \left(\varphi_z\right)^2 - \sigma\left(1 + \frac{1}{2}A^2\right) + \frac{1}{2}\sigma^2 A^2 + \frac{3}{8\varphi^2}\left(c_2^2 + c_3^2\right) = 0 \tag{3.65}$$

$$-c_{2z} + \frac{2c_2\varphi_z}{\varphi} - \frac{a_2 c_3}{2\varphi^2} = 0 \tag{3.66}$$

$$-c_{3z} + \frac{2c_3\varphi_z}{\varphi} + \frac{a_2 c_2}{2\varphi^2} = 0 \, . \tag{3.67}$$

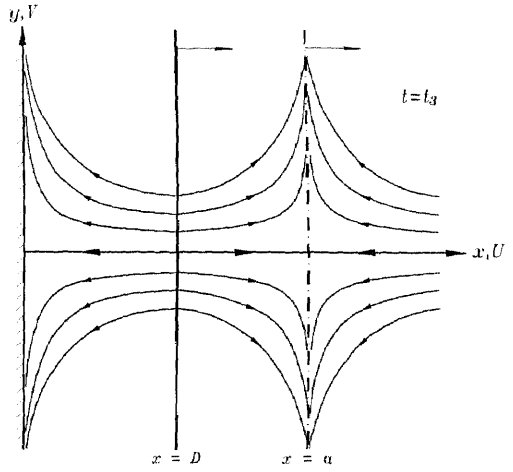

Figure 3.15 Schematic showing the streamlines at time $t = t_3$. The arrows extending from the surfaces $x = a$ and $x = D$ indicate their direction of motion at the given time. Note the appearance of the reversal flow at times t_3 and t_4

the first equation, together with the condition that $c_1(0) = 0$, yields that $c_1 \equiv 0$. Multiplying the last two by c_3 and c_2, respectively, and adding the results yields an equation for the quantity $c_2^2 + c_3^2$. When solved subject to the conditions (3.57) and (3.58), one finds

$$c_2^2 + c_3^2 = \frac{16A^2(1-\sigma)^2}{\sigma^2}\varphi^4 \,, \tag{3.68}$$

and the remaining equation now provides the needed solvability condition for φ, namely

$$-2\varphi\varphi_{zz} + \left(\varphi_z\right)^2 - \sigma\left(1 + \frac{1}{2}A^2\right) + \frac{1}{2}\sigma^2A^2 + \alpha^2\varphi^2 = 0 \,, \tag{3.69}$$

where $\alpha^2 = 6A^2(\sigma-1)^2/\sigma^2$. This nonlinear equation must be solved subject to the conditions

$$\varphi(0) = -\frac{\sigma}{2} \qquad\qquad \varphi_z(0) = -1 \tag{3.70}$$

obtained previously. Differentiating once we find that the nontrivial solutions of this equation are governed by the linear third-order equation

$$\varphi_{zzz} - \alpha^2\varphi_z = 0 \,, \tag{3.71}$$

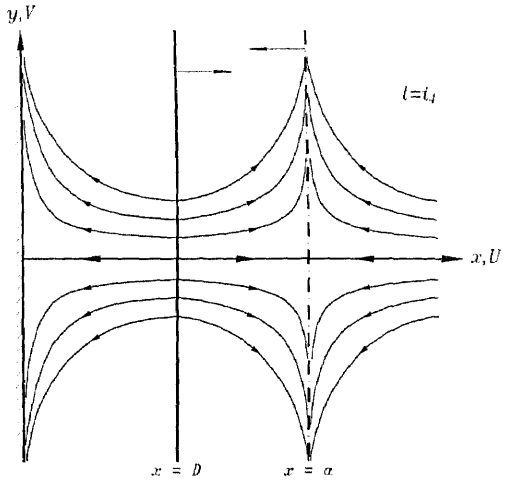

Figure 3.16 Schematic showing the streamlines at time $t = t_4$. The arrows extending from the surfaces $x = a$ and $x = D$ indicate their direction of motion at the given time. Note the appearance of the reversal flow at times t_3 and t_4

whose solution is

$$\varphi = \frac{1}{2\alpha^2}\left((\chi-\alpha)\exp(\alpha z) + (\chi+\alpha)\exp(-\alpha z) - \left(\sigma\alpha^2 + a\chi\right)\right) \tag{3.72}$$

with

$$\chi = \left(1 - \frac{1}{2}A^2(4\sigma - 3)\right)\frac{\sigma - 1}{\sigma}\,, \tag{3.73}$$

and the coefficients, c_i, can also be uniquely determined by going to higher orders in the perturbation scheme, but we shall not carry out these details.

In summary, an approximation to the solution of (3.33)–(3.35), valid for large ω, is of the form

$$\begin{aligned} G \sim \sigma A z\sin(\omega t) + \varphi(z) + \frac{1}{\omega}\Big\{ & c_4(z)\cos(\omega t) - 2\sigma A\varphi(z)\cos(\omega t) \\ & + a_2(z) - c_2(z)\sin\left(\frac{\omega z}{2\varphi} - \omega t\right) + c_3(z)\cos\left(\frac{\omega z}{2\varphi} - \omega t\right)\Big\} + \cdots\,, \end{aligned} \tag{3.74}$$

which indicates that the temporal fluctuations induce rapid spatial oscillations in the burned region and that the period of these oscillations varies slowly, but an $O(\omega^{-1})$

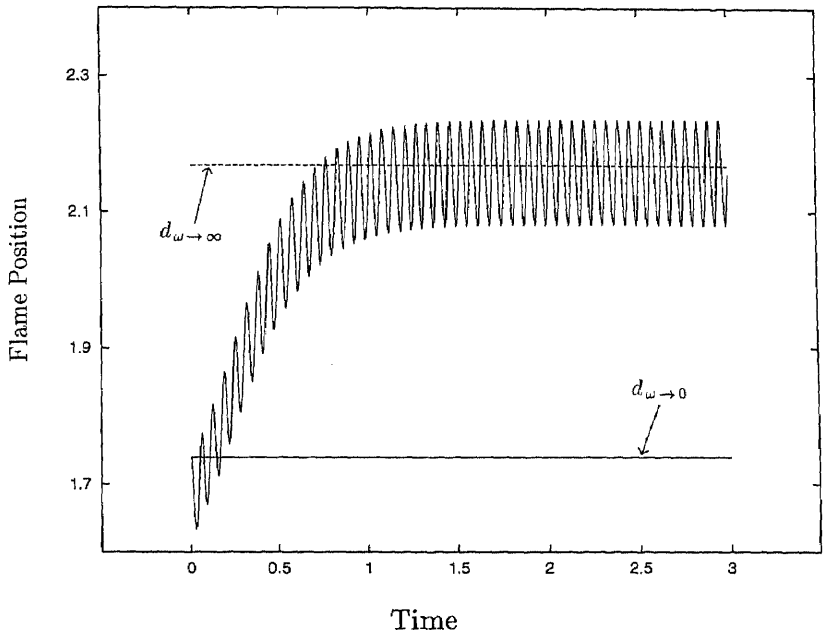

Figure 3.17 Flame position versus time for high frequency $\omega = 100$; calculated for $A = 0.3$ and $\sigma = 6$. The broken line denotes the mean flame position determined asymptotically in the limit $\omega \to \infty$; the solid straight line represents the steady state solution ($\omega = 0$)

amount. This result agrees extremely well with the numerical calculations discussed in the previous section when ω is taken sufficiently large.

Turning to equation (3.34), we introduce the expansion

$$D_0 = D^{(0)} + \frac{1}{\omega} D^{(1)} + \frac{1}{\omega^2} D^{(2)} + \cdots \ , \tag{3.75}$$

and at leading order we immediately find that $D^{(0)} = \bar{D} = \textit{constant}$, which is the mean position about which the flame fluctuates. At $O(\omega^{-1})$ we find that $D^{(1)}$ is governed by the equation

$$D^{(1)}_{\tau} = -2\varphi\left(-\bar{D}\right) \ , \tag{3.76}$$

and for the solution $D^{(1)}(\tau)$ to remain bounded in time, we must set $\varphi\left(-\bar{D}\right) = 0$. Hence

$$\bar{D} = \frac{\sigma(\sigma-1)^{-1}}{\sqrt{6}A} \ln\left\{ \frac{2 + (2\sigma-3)A^2 \pm 2A\sqrt{3\sigma\left(2-(\sigma-1)A^2\right)}}{\left(\sqrt{2}+A(2\sqrt{\sigma}+\sqrt{3})\right)\left(\sqrt{2}-A(2\sqrt{\sigma}-\sqrt{3})\right)} \right\} \ , \tag{3.77}$$

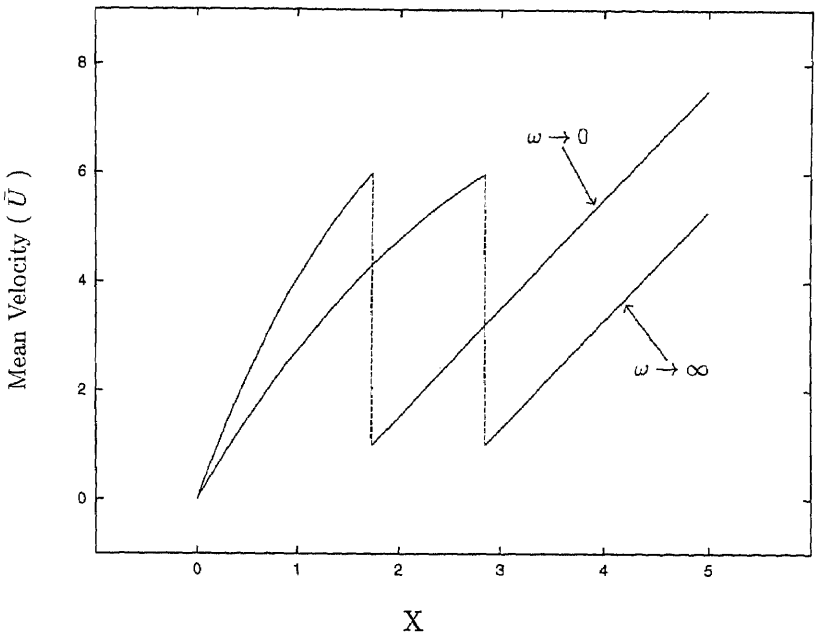

Figure 3.18 The mean axial velocity for two limiting cases $\omega \to 0$ and ∞

which consists of two branches corresponding to the $\pm$ signs in the numerator of the expression contained in the logarithm. The physically meaningful solution is the branch associated with + sign. For $A \ll 1$, the solution is

$$\bar{D} \sim \frac{\sigma}{1+\sqrt{\sigma}} \left\{ 1 + \left(3\sigma + 7 + \left(3 + \frac{2}{\sigma} \right) \left(1 + \sqrt{\sigma} \right) \right) \frac{A^2}{4} \right\} + \cdots , \tag{3.78}$$

which approaches the steady-state value (3.38) in the limit $A \to 0$, as it should. This expression also suggests that for $A \neq 0$ the mean flame position, on the average, exceeds the steady value; the flame locates itself further upstream and its mean position increases with increasing A. This trend remains valid for finite amplitude oscillations as seen in figure 3.23. The figure illustrates the dependence of the mean position $\bar{D}$ as a function of the amplitude A, based on the numerical evalution of equation (3.77). We note that the flame position $\bar{D} \to \infty$ as $A \to A_{bl}$, where

$$A_{bl} = \frac{\sqrt{2}}{2\sqrt{\sigma} - \sqrt{3}} \tag{3.79}$$

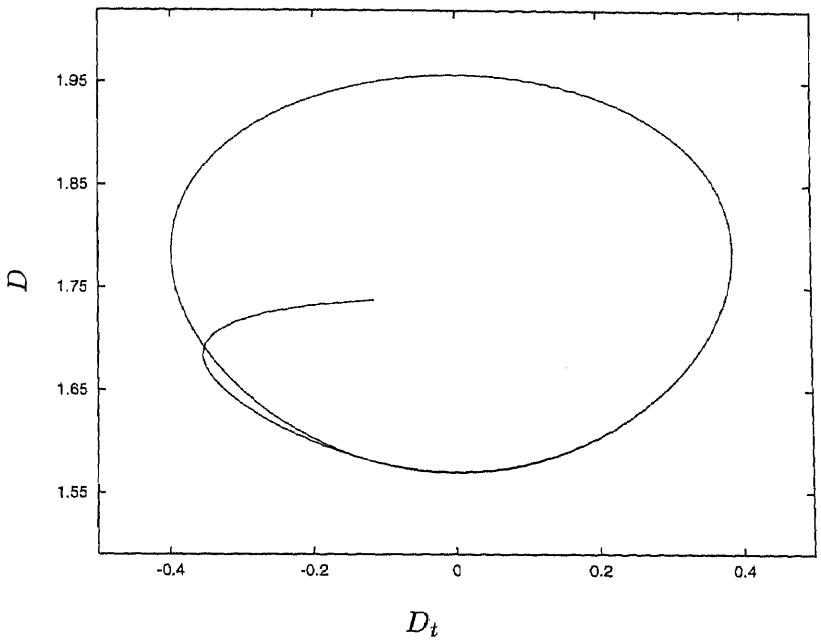

Figure 3.19 Phase plane of flame position D for the values of imposed amplitude $A = 0.1$ and imposed frequency $\omega = 2$, with $\sigma = 6$

is the value of A for which the denominator in the logarithm term on the right hand side of equation (3.77) vanishes. At high frequency the flame can no longer respond to the rapid oscillations in the flow field and, consequently, its does not fluctuate too much from its mean position. When the amplitude, A, becomes sufficiently large, the variations in the flow field become too extreme for the flame to withstand, and the flame is blown off to infinity. The non-existence of time-periodic solutions for $A > A_{bl}$ is also consistent with the numerical results reported earlier. For $\sigma = 6$, for example, $A_{bl} \simeq 0.446$ and indeed, the calculations carried out for the moderate frequency $\omega = 2$ and reported in figure 3.23 for $A = 0.1$ and 0.4, break down for $0.4 < A < 0.446$. For comparison with the numerical results obtained with $\omega = 100$ we have marked in figure 3.17 (broken curve) the mean position as calculated from (3.78). Also marked in this figure (full curve) is the position of the flame corresponding to a constant strain rate based on equation (3.38). Finally, we point out that the numerical solutions for

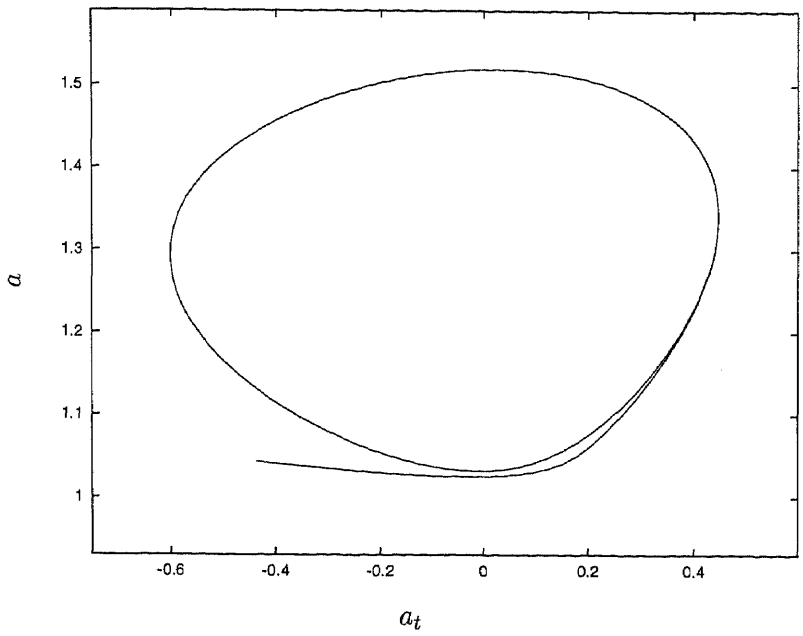

Figure 3.20 Phase plane of flow displacement a for the values of imposed amplitude $A = 0.1$ and imposed frequency $\omega = 2$, with $\sigma = 6$

given initial conditions show that the transient behaviour for $A > A_{bl}$ is one in which the flame oscillates a finite number of times before blow off.

3.5 The Constant-Density Approximation

We remark that our analysis fully accounts for the coupling between the flame and the underlying flow field. These effects are sometimes ignored in theoretical studies by assuming a constant-density flow. While such an assumption may compromise reality, the simplification is often adopted in order to gain insights and the approach has been successful in explaining a variety of flame phenomena. The present study, however, clearly demonstrates a situation for which the strong coupling between the flame and the hydrodynamics may result in qualitatively different predictions in flame behaviour. To illustrate this point further, we compare our results to those obtained when the effect of the flame on the flow is neglected. This is achieved by

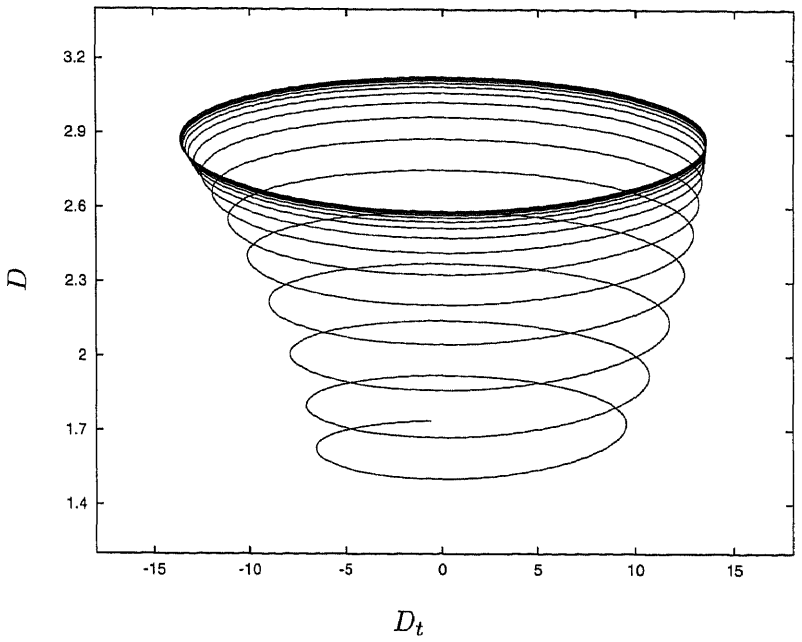

Figure 3.21 Phase plane of flame positiona D for the values of imposed amplitude $A = 0.4$ and imposed frequency $\omega = 50$, with $\sigma = 6$

setting $a = 0$, which is a direct consequence of taking the limit $\sigma \to 1$. It is easy to see that the flame speed equation (3.35) then uniquely determins D as

$$D = \frac{1}{2}\exp\left(-2t + \frac{2A}{\omega}\cos(\omega t)\right)\exp\left(-\frac{2A}{\omega}\right) + \exp\left(-2t + \frac{2A}{\omega}\cos(\omega t)\right)\int_0^t \exp\left(2s - \frac{2A}{\omega}\cos(\omega s)\right) ds \qquad (3.80)$$

and, in contrast to our previous results, is independent of the flow downstream. In figure 3.24 we show the flame location as determined from both, the constant-density model (3.80) and the 'exact' solutions obtained previously. Although the general shape of the response curves is similar in both cases, the mean flame location for the constant-density model is predicted to lie much closer to the wall. The phase lag is qualitatively the same, increasing monotonically with ω to 90° in agreement with the solution shown in figure 3.4. However, as shown in figure 3.25, the constant-density model predicts a monotonic decrease of flame amplitude with frequency, in contrast to the exact solution displayed in figure 3.7.

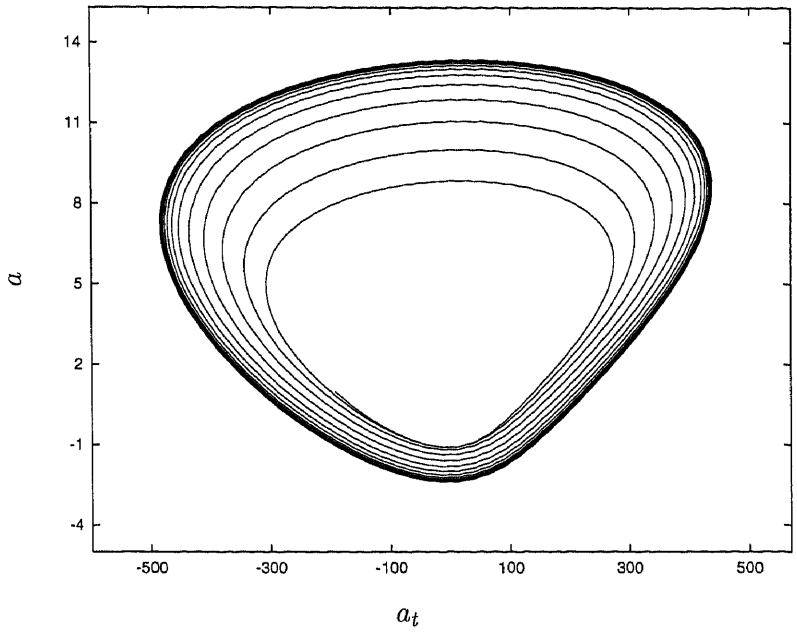

Figure 3.22 Phase plane of flow displacement a for the values of imposed amplitude $A = 0.4$ and imposed frequency $\omega = 50$, with $\sigma = 6$

Another difference is that the shift in the mean flame position that was observed at high frequencies does not persist when the constant-density simplification is invoked. This is illustrated in figure 3.26 where the flame location as given by equation (3.80) is plotted for $\omega = 100$. After an initial transient, the flame is seen to relax into oscillatory motion about the steady state solution $D = 1/2$. furthermore, the solution given by (3.80) exists for all values of imposed amplitude, A. Thus, when ignoring the effect of the flame on the underlying flow, blow off is not predicted. Finally, when the flow ahead of the flame remains potential it is clear that the appearance of a stagnation plane ahead of the flame and consequently the region of reverse flow, is not predicted.

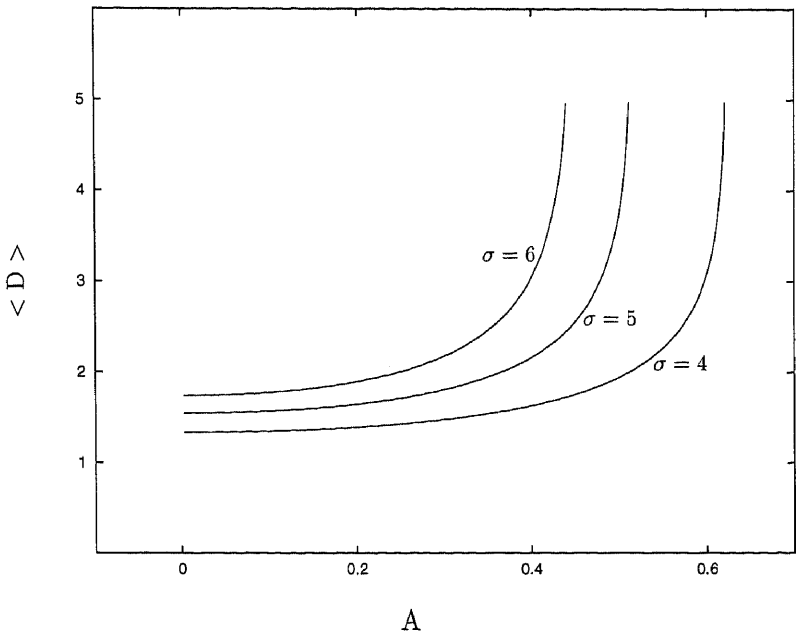

Figure 3.23 Mean flame position as a function of the amplitude A, for high frequency oscillations; plotted for several values of σ

3.6 Hydrodynamic Effects with Impulsive Strain Rate

To test the validity of the traditional assumption that the flame response to strain is instantaneous, Petrov and Ghoniem(1995) examined the time-dependent response of a premixed laminar flame when subjected to a sudden change in strain and a periodic strain. Their numerical study provides evidence that the flame response time strongly depends on the Lewis number and the flame temperature.

In this section, we employ our model to study how flame responds to a sudden change in strain rate from one constant value to another, and we construct an analytical expression for the evolution of flame front. Under a stepwise increase in strain rate, the leading order system to be investigated follows from (3.33)–(3.35) as

$$G_{zt} + (\nu + 1)GG_{zz} - G_z^2 = -\sigma\mu^2 \tag{3.81}$$

$$G(0,t) = -\frac{\sigma}{\nu+1} \qquad G_z(0,t) = -\mu \tag{3.82}$$

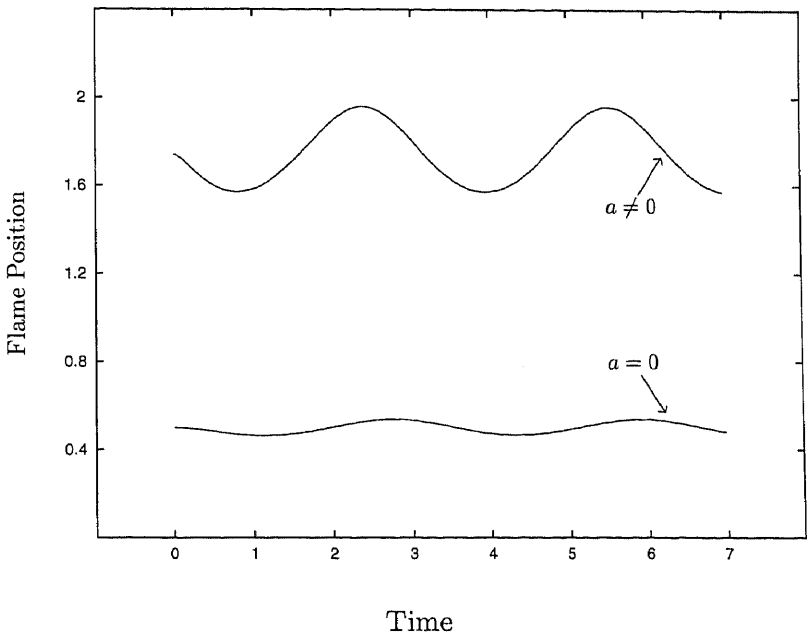

Figure 3.24 Comparison of flame position versus time for the constant density model (bottom curve) and the exact solution (top curve); calculated for $A = 0.1$ and $\omega = 2$. The top curve is determined numerically by solving (3.34) with $\sigma = 6$

$$D_t = -(\nu + 1)G(-D, t) \ , \tag{3.83}$$

where

$$\mu = \begin{cases} \mu_1 & t < t_c \\ \mu_2 & t > t_c \end{cases} \ .$$

We introduce the new variable ϕ as

$$\phi(z,t) = G_z(z,t) \qquad G(z,t) = -\frac{\sigma}{\nu+1} + \int_0^z \phi(\eta, t)\, d\eta \ , \tag{3.84}$$

so that equations (3.81)–(3.82) take the form

$$\phi_t + (\nu + 1)G\phi_z = \phi^2 - \sigma\mu \qquad \phi(0,t) = -\mu \ . \tag{3.85}$$

Equation (3.85) is a first order quasi-linear hyperbolic PDE, and the method of characteristics can be used to solve it. That is, ϕ satisfies the Ricatti Equation

$$\frac{d\phi}{dt} = \phi^2 - \sigma\mu^2 \qquad \phi(t_0) = -\mu \tag{3.86}$$

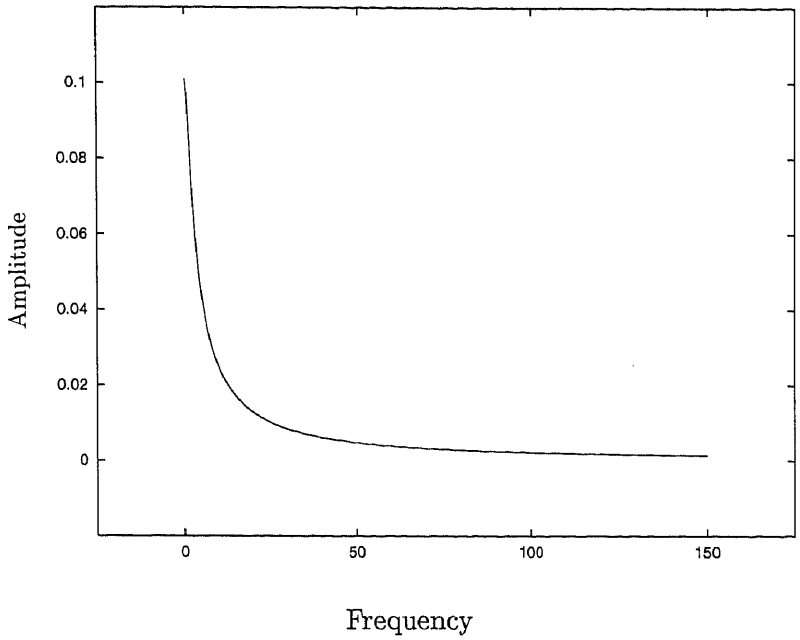

Figure 3.25 The amplitude of the fluctuations of the flame versus frequency for a constant density model

and the characteristic curves are

$$\frac{dz}{dt} = -\sigma + (\nu + 1)\int_0^z \phi(\eta, t)\, d\eta \qquad z(t_0) = 0 \ . \tag{3.87}$$

We only consider characteristic curves that initially start from the time axis, see the schematic diagram in figure 3.27. We use the notation that the ith characteristic curve intersects the time axis ($z = 0$) at t_0^i. Also note that, at time $t = t_c$, there is a sudden change in strain rate, therefore all the characteristic curves starting at $t_0 < t_c$, will experience a deflection at time $t = t_c$, while those curves starting at $t_0 > t_c$ would not.

Along characteristic curves, (3.86) is a Ricatti type equation, which can be solved exactly by introducing the following transformation

$$\phi = -\frac{S_t}{S} \qquad \phi_t = -\frac{S_{tt}}{S} + \frac{S_t^2}{S^2} \ , \tag{3.88}$$

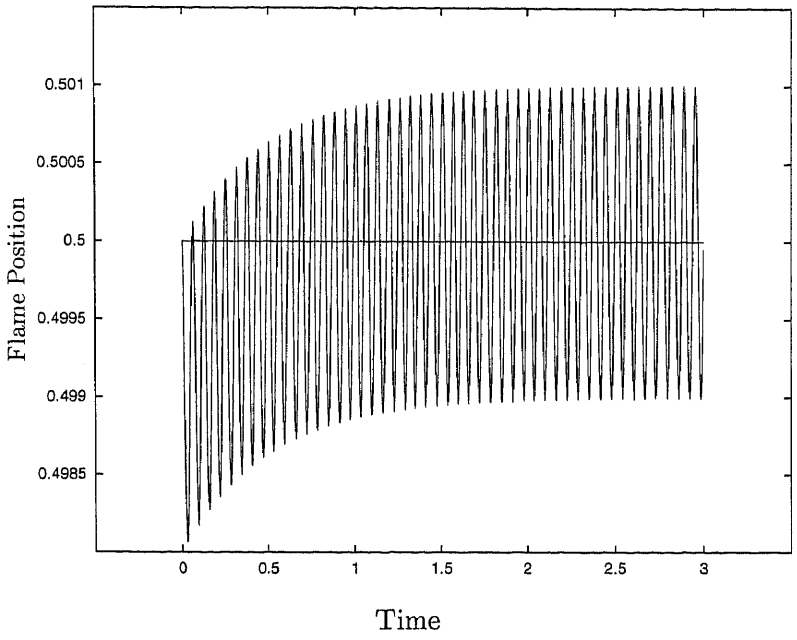

Figure 3.26 Flame position versus time for a constant density model

which reduces (3.86) to

$$S_{tt} = b^2 S \qquad b = \mu\sqrt{\sigma}\ . \tag{3.89}$$

Solutions are

$$S(t) = c\exp(bt) + d\exp(-bt) \qquad \phi(t) = -\frac{bc\exp(bt) - bd\exp(-bt)}{c\exp(bt) + d\exp(-bt)}\ , \tag{3.90}$$

where c and d are integration constants. The solution will take one of the following three forms:

$$\phi(t,t_0) = \begin{cases} \phi_1(t,t_0) & t_0 < t_c \text{ and } t < t_c \\ \phi_2(t,t_0) & t_0 < t_c \text{ and } t > t_c \\ \phi_3(t,t_0) & t_0 > t_c \text{ and } t > t_c \end{cases}$$

ϕ_1 and ϕ_3 are readily found by imposing the initial conditions

$$\phi_1(t_0,t_0) = \mu_1 \qquad \phi_3(t_0,t_0) = \mu_2\ .$$

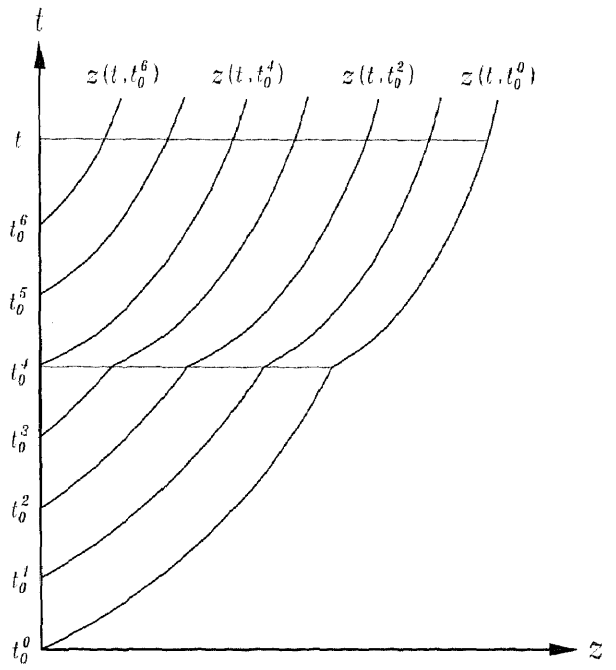

Figure 3.27 The evolution of characteristic curves experience a sudden change in strain rate at time $t = t_c$

To determine ϕ_2, however, we must impose the condition that ϕ_1 and ϕ_2 are continuous at $t = t_c$, i.e.

$$\phi_1(t_c, t_0) = \phi_2(t_c, t_0) \ .$$

Upon imposing conditions, solutions are found to be

$$\phi_1(t, t_0) = -\frac{b_1(b_1+\mu_1)\exp\Big(b_1(t-t_0)\Big) - b_1(b_1-\mu_1)\exp\Big(-b_1(t-t_0)\Big)}{(b_1+\mu_1)\exp\Big(b_1(t-t_0)\Big) + (b_1-\mu_1)\exp\Big(-b_1(t-t_0)\Big)} \tag{3.91}$$

$$\phi_2(t, t_0) = -\frac{b_2(M+m)\exp\Big(b_2(t-t_c)\Big) - b_2(M-m)\exp\Big(-b_2(t-t_c)\Big)}{(M+m)\exp\Big(b_2(t-t_c)\Big) + (M-m)\exp\Big(-b_2(t-t_c)\Big)} \tag{3.92}$$

$$\phi_3(t, t_0) = -\frac{b_2(b_2+\mu_2)\exp\Big(b_2(t-t_0)\Big) - b_2(b_2-\mu_2)\exp\Big(-b_2(t-t_0)\Big)}{(b_2+\mu_2)\exp\Big(b_2(t-t_0)\Big) + (b_2-\mu_2)\exp\Big(-b_2(t-t_0)\Big)} \tag{3.93}$$

where

$$b_1 = \mu_1\sqrt{\sigma} \qquad\qquad b_2 = \mu_2\sqrt{\sigma}$$

$$m = b_1 \left\{ (b_1 + \mu_1) \exp\Big(b_1(t_c - t_0)\Big) - (b_1 - \mu_1) \exp\Big(- b_1(t_c - t_0)\Big) \right\} \tag{3.94}$$

$$M = b_2 \left\{ (b_1 + \mu_1) \exp\Big(b_1(t_c - t_0)\Big) + (b_1 - \mu_1) \exp\Big(- b_1(t_c - t_0)\Big) \right\} . \tag{3.95}$$

To determine the characteristic curves, we now turn to the integral expression in (3.87). Thus we first look at figure 3.27, which describes the evolution of each characteristic curve starting from time axis. Each curve starts at different initial time t_0^i, $i = 0, 1, 2, 3, \cdots$. We can trace the evolution of a characteristic curve, for example, the one starting at t_0^0, and we observe that at time t, that curve is at a location $z(t, t_0^0)$. Within the integration of

$$\int_0^z \phi(\eta, t)\, d\eta \, , \tag{3.96}$$

the independent variable η goes from 0 to z, i.e. $\Big(0, z(t, t_0)\Big)$, while $d\eta = \Big(\eta_{t_0}(t, t_0)\Big) dt_0$. This is because t is fixed and only t_0 can vary. Thus we can interchange the integral limits in (3.87). As η varies from 0 to z, t_0 goes from t_0^0 to t, and therefore, the system (3.87) can be rewritten into

$$\frac{dz}{dt} = -\sigma + (\nu + 1) \int_t^{t_0} \phi(s, t) \eta_s(s, t)\, ds \qquad z(t_0, t_0) = 0 \, . \tag{3.97}$$

We differentiate (3.97) with respect to t_0, to get

$$z_{tt_0} = (\nu + 1) \phi(t, t_0) z_{t_0} \qquad z(t_0, t_0) = 0 \, , \tag{3.98}$$

and integration of (3.98) with respect to t yields an expression for z_{t_0}. Also we note that in (3.87), when $z \to 0^-$, then system (3.87) has local behavior as

$$\frac{dz}{dt} = -\sigma + (\nu + 1) \int_0^{0^-} \phi(\eta, t)\, d\eta \qquad z(t_0) = 0 \, , \tag{3.99}$$

therefore (3.99) can be expressed locally by

$$\frac{dz}{dt} = -\sigma \, , \quad z = \sigma(t_0 - t) \, , \qquad z_{t_0}(t_0) = \sigma \tag{3.100}$$

and the latter condition, $z_{t_0}(t_0) = \sigma$ will be needed when integrating (3.98). Thus the solution for z_{t_0} corresponding to each of the three cases can be given by

for $t_0 < t_c$ and $t < t_c$:

$$z_{t_0} = \frac{(2b_1)^{\nu+1}\sigma}{\Big\{(b_1+\mu_1)\exp\Big(b_1(t-t_0)\Big) + (b_1-\mu_1)\exp\Big(-b_1(t-t_0)\Big)\Big\}^{-(\nu+1)}} \tag{3.101}$$

for $t_0 < t_c$ and $t > t_c$:

$$z_{t_0} = \frac{(2b_1)^{\nu+1}\sigma}{\Big\{(M+m)\exp\Big(b_2(t-t_c)\Big) + (M-m)\exp\Big(-b_2(t-t_c)\Big)\Big\}^{-(\nu+1)}} \tag{3.102}$$

for $t_0 > t_c$ and $t > t_c$:

$$z_{t_0} = \frac{(2b_2)^{\nu+1}\sigma}{\Big\{(b_2+\mu_2)\exp\Big(b_2(t-t_0)\Big) + (b_2-\mu_2)\exp\Big(-b_2(t-t_0)\Big)\Big\}^{-(\nu+1)}} \tag{3.103}$$

where m and M are given by (3.94) and (3.95).

Since those expressions in (3.101)–(3.103) are rational in both t_0 and t, we can readily integrate them to give

for $t_0 < t_c$ and $t < t_c$:

$$z(t,t_0) = -\frac{\sigma}{b_1+\mu_1} + \frac{2b_1\sigma(b_1+\mu_1)^{-1}}{(b_1+\mu_1)\exp\Big(2b_1(t-t_0)\Big) + (b_1-\mu_1)} \tag{3.104}$$

for $t_0 > t_c$ and $t > t_c$:

$$z(t,t_0) = -\frac{\sigma}{b_2+\mu_2} + \frac{2b_2\sigma(b_2+\mu_2)^{-1}}{(b_2+\mu_2)\exp\Big(2b_2(t-t_0)\Big) + (b_2-\mu_2)} \tag{3.105}$$

for $t_0 < t_c$ and $t > t_c$:

$$\begin{aligned} z(t,t_0) = &-\frac{\sigma}{b_2+\mu_2} + \frac{2b_2\sigma(b_2+\mu_2)^{-1}}{(b_2+\mu_2)\exp\Big(2b_2(t-t_0)\Big) + (b_2-\mu_2)} \\ &+ \frac{8b_1b_2^2\sigma\Big(V(t)\Big)^{-1}}{V(t)\exp\Big(2b_1(t_c-t_0)\Big) + v(t)} - \frac{8b_1b_2^2\sigma\Big(V(t)\Big)^{-1}}{V(t)+v(t)}\,, \end{aligned} \tag{3.106}$$

where

$$b_1 = \mu_1\sqrt{\sigma} \qquad b_2 = \mu_2\sqrt{\sigma}$$

$$\begin{aligned} v(t) = {} & b_2(b_1-\mu_1)\left\{\exp\Big(b_2(t-t_c)\Big)+\exp\Big(-b_2(t-t_c)\Big)\right\} \\ & -b_1(b_1-\mu_1)\left\{\exp\Big(b_2(t-t_c)\Big)-\exp\Big(-b_2(t-t_c)\Big)\right\} \end{aligned} \tag{3.107}$$

$$\begin{aligned} V(t) = {} & b_2(b_1+\mu_1)\left\{\exp\Big(b_2(t-t_c)\Big)+\exp\Big(-b_2(t-t_c)\Big)\right\} \\ & +b_1(b_1+\mu_1)\left\{\exp\Big(b_2(t-t_c)\Big)-\exp\Big(-b_2(t-t_c)\Big)\right\} . \end{aligned} \tag{3.108}$$

Comparing equation (3.87) with (3.83), one notes that the flame position $D = -z$, corresponds to the characteristic curve. Thus we obtain the flame position D by solving for characteristic curve.

In figures 3.28 and 3.29, we show the response of flame to a sudden change in strain rate at time $t = 3$, as predicted by equation (3.106). As shown by Petrov and Ghoniem(1995), there is a delay for the flame to adjust to its new steady state position. Figure 3.28 considers the effect of doubling the strain rate, while in figure 3.29 the strain rate is suddenly reduced by half. The delay time is clearly seen to be larger in the latter case.

3.7 Inclusion of Transport and Viscous Effects

We now return to the problem of a flame in stagnation point flow with oscillating strain rate. Of interest here will be to determine the role of thermal diffusive effects on flame response. These effects are contained in the $O(\delta)$ terms shown in (3.26)–(3.31). The leading order system treated in section 3.3 was in fact Landau's original model. Here we retain thermal-diffusive effects as a perturbation, and from the system system (3.26)–(3.31), $O(\delta)$ corrections satisfy the following system:

$$G_{1zt} + (\nu+1)G_0G_{1zz} + (\nu+1)G_1G_{0zz} - 2G_{0z}G_{1z} = Pr(1+q)^2G_{0zzz} \tag{3.109}$$

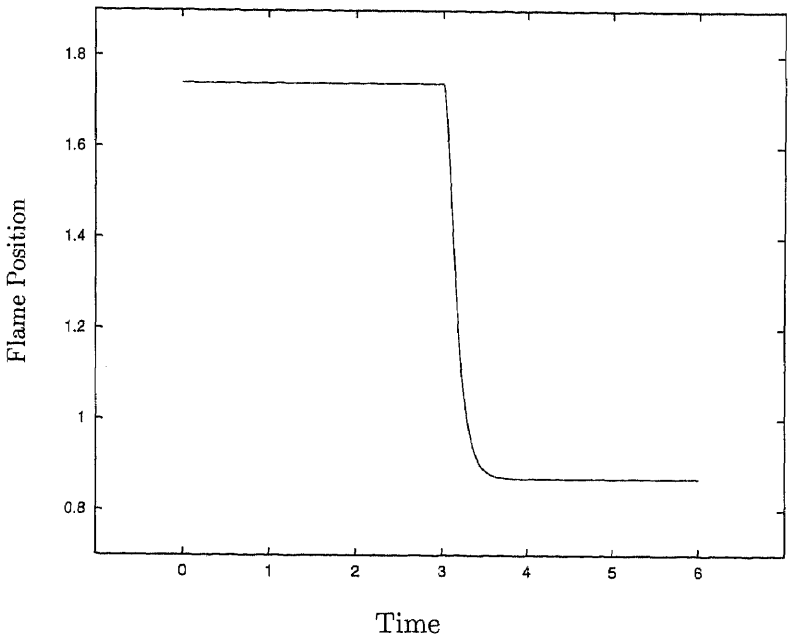

Figure 3.28 Flame response to sudden change in strain rate for $\mu_1 < \mu_2$ with $\sigma = 6$, $\mu_1 = 1$ and $\mu_2 = 2$

$$G_1(0,t) = \mu(1+q)(\alpha - q) \tag{3.110}$$

$$G_{1z}(0,t) = -q(Pr+1)(\mu_t + \mu^2) \tag{3.111}$$

$$G_{1zz}(0,t) = f(t) \tag{3.112}$$

$$D_{1t} = -(\nu+1)\Big(G_1(-D_0,t) - D_1 G_{0z}(-D_0,t)\Big) \tag{3.113}$$

$$D_{1t} + (\nu+1)(D_1 - a_1)\mu = -(\nu+1)\alpha\mu\ , \tag{3.114}$$

where $f(t)$ is given by

$$f(t) = \frac{q}{1+q}\Big((\nu+1)(\alpha-q)(\mu\mu_t + \mu^3) - (Pr+1)(\mu_{tt} + 4\mu\mu_t + 2\mu^3) - Pr\left(\mu_{tt} + 2\mu\mu_t + (1-\nu)(\mu\mu_t + \mu^3)\right)\Big)\ . \tag{3.115}$$

For a constant strain rate, $\mu = constant$, the system (3.109)–(3.114) possesses an exact solution as constructed by Eteng, Ludford and Matalon(1986) (see Appendix

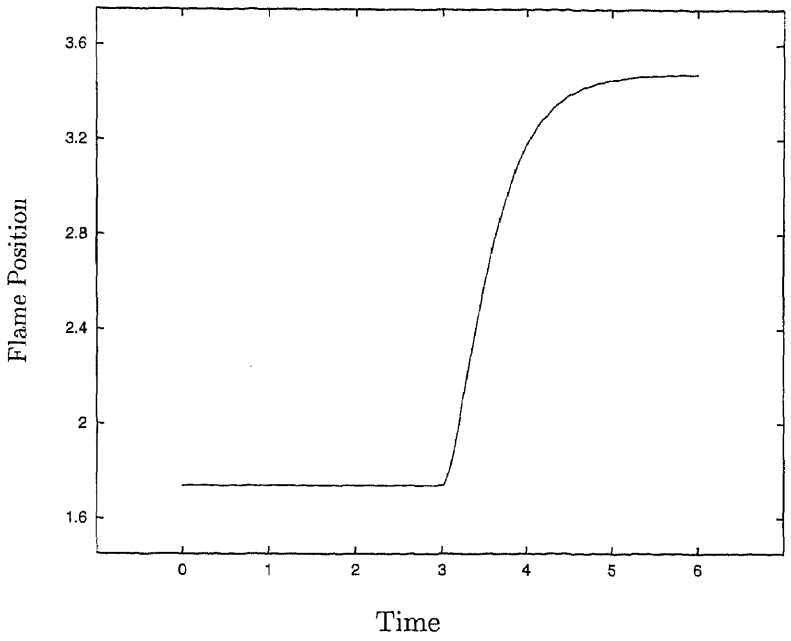

Figure 3.29 Flame response to sudden change in strain rate for $\mu_1 > \mu_2$ with $\sigma = 6$, $\mu_1 = 1$ and $\mu_2 = 0.5$

B); these results are listed here for completeness. For the two-dimensional case ($\nu = 0$), the solution G_1 and flame location D_1 are given by

$$G_1(z) = E\cos(kz) + F\sin(kz) + G_{1p}(z) \tag{3.116}$$

$$D_1 = \frac{1}{\mu\sigma}\left(\sqrt{\sigma - 1}\,F - E\right), \tag{3.117}$$

where

$$k = \frac{\mu\sqrt{\sigma - 1}}{\sigma} \tag{3.118}$$

and the particular solution $G_{1p}(z)$ is given by

$$\begin{aligned} G_{1p}(z) = &-\frac{C}{2k}(z + D_0)\cos(kz + kD_0) \\ &+ \frac{1}{2}kPr\sigma^2\sin(kz + kD_0)\ln\left(\tan\left(\frac{kz + kD_0}{2}\right)\right) \\ &- \frac{1}{2}k^2Pr\sigma^2(z + D_0)\cos(kz + kD_0)\ln\left(\tan\left(\frac{kz + kD_0}{2}\right)\right) \\ &+ \frac{1}{2}kPr\sigma^2\cos(kz + kD_0)\,. \end{aligned} \tag{3.119}$$

The constants C, E, F are:

$$C = \frac{\sqrt{\sigma-1}}{\sqrt{\sigma}}\Big(2\alpha - 2\sigma - 3Pr\Big)\mu^3 - \frac{Pr\mu^3(\sigma-1)^{3/2}}{2\sigma}\ln\left(\frac{\sqrt{\sigma}-1}{\sqrt{\sigma}+1}\right) \tag{3.120}$$

$$E = \mu\sigma(\alpha - \sigma + 1) - G_{1p}(0) \tag{3.121}$$

$$F = -\frac{1}{k}\Big((\sigma-1)(Pr+1)\mu^2 + G_{1pz}(0)\Big)\ . \tag{3.122}$$

For the axisymmetric case ($\nu = 1$), the solution G_1 and flame location D_1 are given by

$$G_1(z) = \frac{\sigma-1}{\sigma}\Big(\alpha - \sigma - Pr\Big)\mu^3 z^2 - (\sigma-1)(Pr+1)\mu^2 z + \sigma\mu(\alpha - \sigma + 1) \tag{3.123}$$

$$D_1 = -\frac{(\alpha-\sigma-Pr)(\sqrt{\sigma}-1) + (\sigma-1)(Pr+1) + (\alpha-\sigma+1)(\sqrt{\sigma}+1)}{1+(\sqrt{\sigma})^{-1}} \tag{3.124}$$

respectively. In both cases, the displacement a_1 follows from (3.114).

The flame speed correction term D_1 increases whenever we decrease Prandtl number Pr or ℓ_c, the deviation of Lewis number Le from unity.

For an unsteady strain rate, the system (3.109)–(3.114) must be solved numerically. We will use the exact same procedure as we did at leading order to solve the correction terms $G_1(z,t)$, $D_1(t)$ and $a_1(t)$. It is convenient to introduce the new dependent variables $\phi_0(z,t)$ and $\phi_1(z,t)$, given by

$$G_0(z,t) = -\frac{\sigma}{\nu+1} + \int_0^z \phi_0(\eta,t)\,d\eta \tag{3.125}$$

$$G_1(z,t) = \mu\sigma(\alpha - \sigma + 1) + \int_0^z \phi_1(\eta,t)\,d\eta\ , \tag{3.126}$$

such that equation (3.109) takes the form

$$\phi_{1t} + (\nu+1)G_0\phi_{1z} = \sigma^2 Pr\phi_{0zz} + 2\phi_0\phi_1 - (\nu+1)\phi_{0z}G_1\ . \tag{3.127}$$

We consider characteristic curves as determined from the equation

$$\frac{dz}{dt} = (\nu+1)G_0(z,t)\ , \tag{3.128}$$

and along each of these curves, ϕ_1 satisfies the equation

$$\frac{d\phi_1}{dt} = \sigma^2 Pr\phi_{0zz} + 2\phi_0\phi_1 - (\nu+1)\phi_{0z}G_1 \ . \tag{3.129}$$

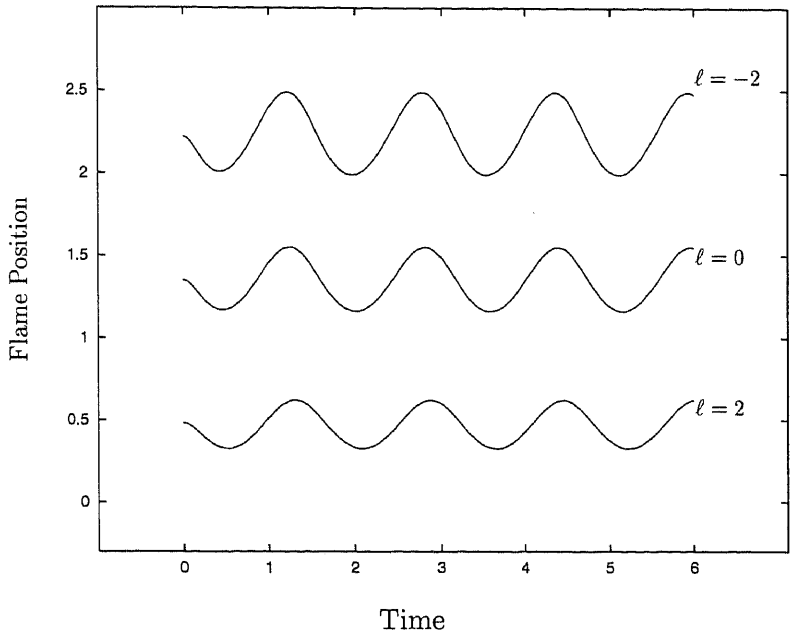

Figure 3.30 Flame position versus time for three different values of the deviation of Lewis number from unity, with $\sigma = 6$, $\omega = 4$, $A = 0.1$, $\delta = 0.05$ and $Pr = 0.7$

In figure 3.30, we plot the flame position $D \sim D_0 + \delta D_1$ as a function of time for three different values of the deviation of Lewis number ℓ from unity. Note that the flame locates itself further from the wall as Lewis number is decreased. The amplitude of the flame response is also seen to be larger at the smaller Lewis number. This is due to the fact that the flame encounters larger fluctuations in the normal velocity. Figure 3.31 shows that flame amplitude is an monotonic decreasing function of the deviation of Lewis number.

In figure 3.32, we plot flame position D as function of time for three different values of Prandtl number, and fixed $\ell = -1$. The flame is seen to position itself closer to the wall as the Prandtl number is increased. The same trend was predicted in the steady analysis of Eteng, Ludford and Matalon(1986). We also investigate the relationship between Prandtl number and flame oscillating amplitude, and this

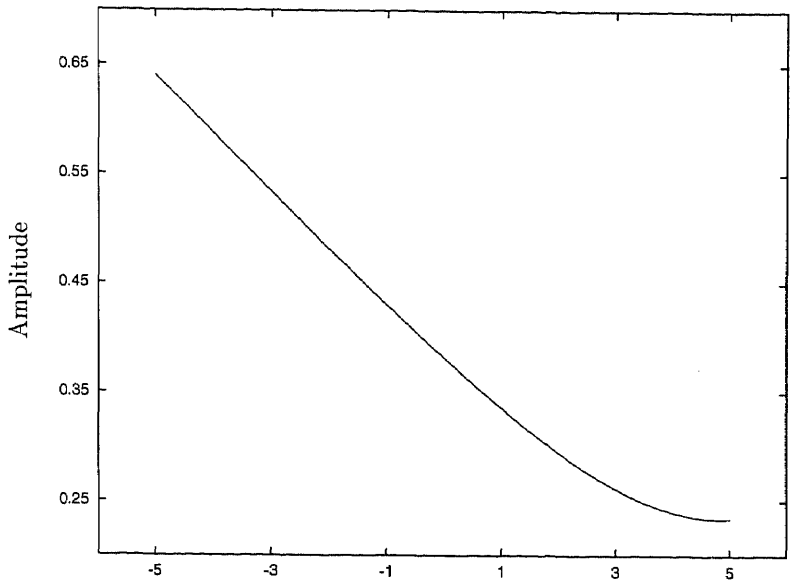

Figure 3.31 Flame oscillating amplitude versus the deviation of Lewis number from unity, with $\sigma = 6$, $\omega = 4$, $A = 0.1$, $\delta = 0.05$ and $Pr = 0.7$

relationship is sketched on figure 3.33 which states that the flame amplitude almost linearly depends on Prandtl number and the flame amplitude is a strict monotonic decreasing function of Prandtl number.

We now consider modifications to the high frequency flame response due to viscous effects. Recall that, at $O(1)$, the mean flame position was found to shift upstream of its steady state value. Here we find that viscosity tends to sfift the mean position back toward the wall. This is illustrated in figures 3.34 and 3.35. In figure 3.34, we plot flame position D as a function of time for high frequency, $\omega = 50$.

In figure 3.35, we plot the phase plane for flame position D with $\omega = 50$. The flame is seen to eventually relax to a periodic state, with mean position clearly closer to the wall.

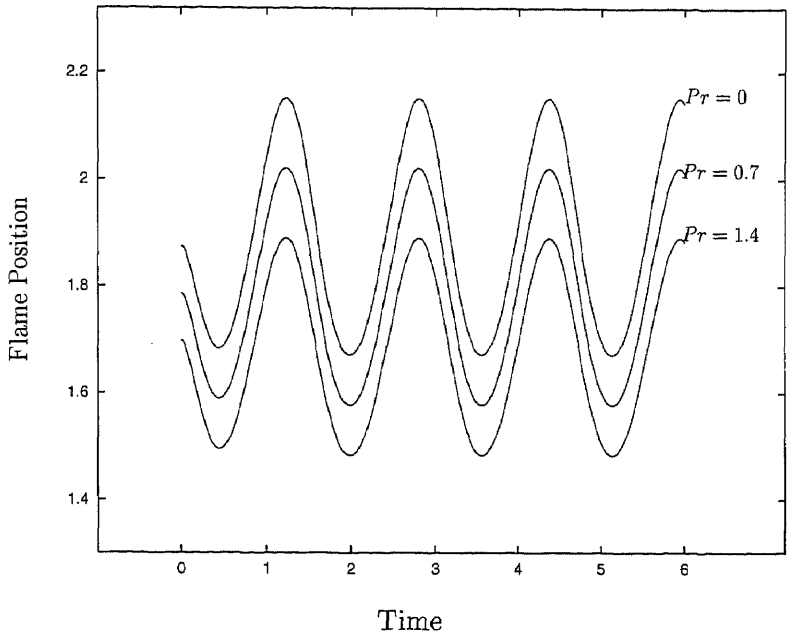

Figure 3.32 Flame position versus time for three different values of Prandtl number, with $\sigma = 6$, $\omega = 4$, $A = 0.1$, $\delta = 0.05$ and $\ell = -1$

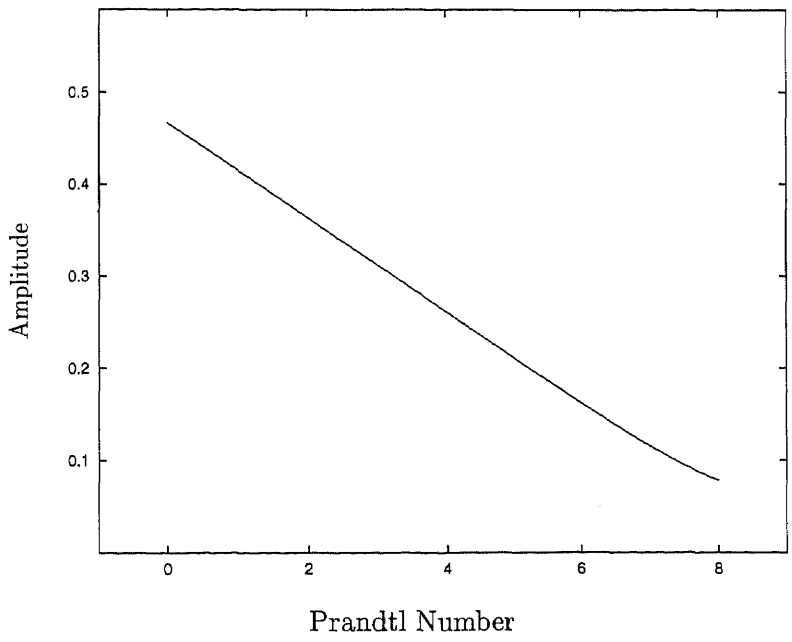

Figure 3.33 Flame oscillating amplitude versus Prandtl number, with $\sigma = 6$, $\omega = 4$, $A = 0.1$, $\delta = 0.05$ and $\ell = -1$

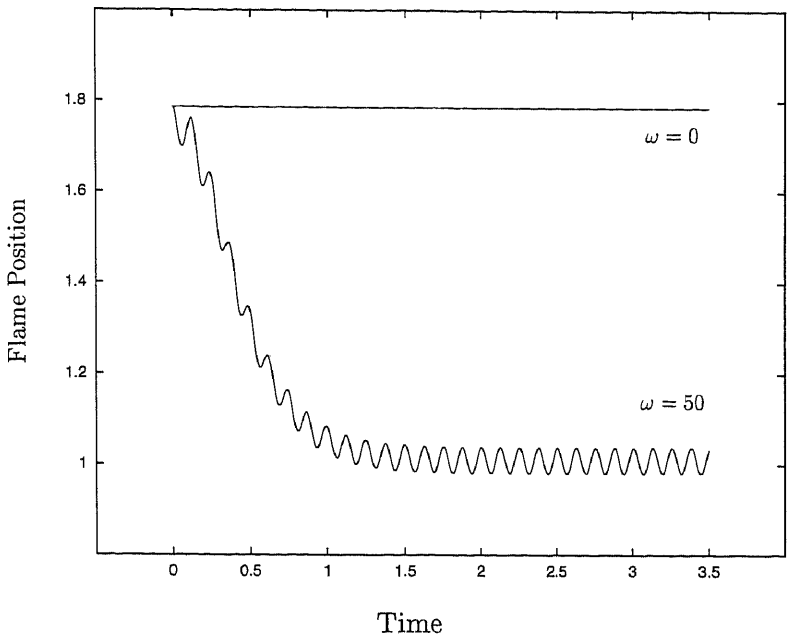

Figure 3.34 Flame position versus time for high frequency $\omega = 50$, with $\sigma = 6$, $A = 0.2$, $\delta = 0.05$, $\ell = -1$ and $Pr = 0.7$; the straight line represents the steady state solution ($\omega = 0$)

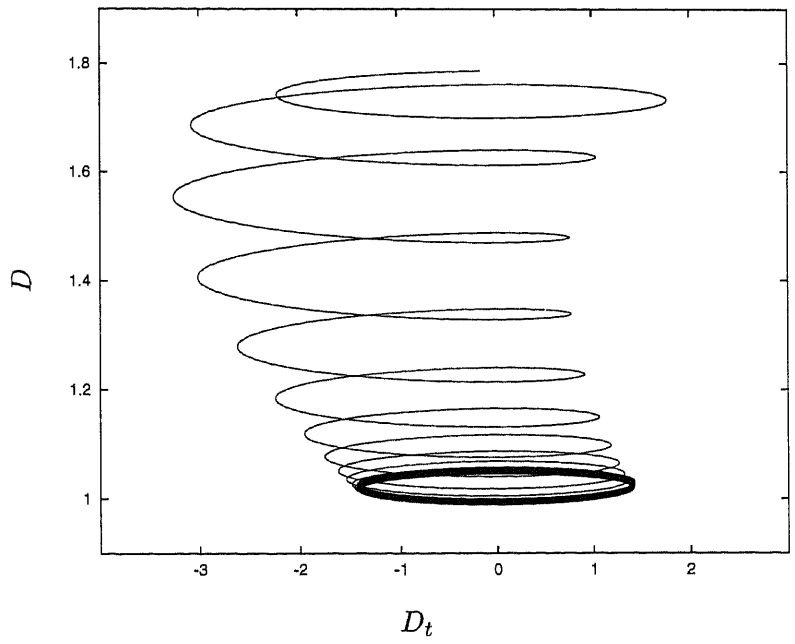

Figure 3.35 Phase plane of flame position D, with the imposed values $\sigma = 6$, $\omega = 50$, $A = 0.2$, $\delta = 0.05$, $\ell = -1$ and $Pr = 0.7$

CHAPTER 4

A NONLINEAR FLAME MODEL

4.1 Problem Description

In the previous chapters, the response of a premixed flame to a flow field with a time dependent strain rate was studied by using NEF models. In such models, the dependence of flame speed on stretch is linear and furthermore, variations in flame speed from its adiabatic value occur only as a perturbation. As such, NEF's are unable to capture nonlinear phenomena such as extinction. On the other hand, SVF models (see chapter one) do exhibit a nonlinear dependence of flame speed on stretch. These models have been used previously to study flame extinction in steady stagnation point flow cf. Kim and Matalon(1988). While these models are known to give correct qualitative predictions of steady flames, it is also well known that they can yield incorrect predictions of unsteady behavior such as instability cf. Buckmaster(1977). Part of the difficulty may be that the formulation of these models considers quasi-steady flame strutures, ignoring transient effects that take place on a time scale comparable to the one used to measure reaction-diffusion. In this chapter, we derive an equation for flame speed that allows for arbitray Lewis number Le and also consider the distinguished limit of SVF's ($\delta = \varepsilon$). However, we also allow for unsteadiness on the transient time scale such that the flame structure is unsteady. For simplicity, we specifically examine the stagnation point flow, although the analysis can readily be extended to arbitrary geometries. The configuration is sketched in figure 4.1.

The flow field is $\mathbf{V} = (U, V)$, where U and V denote the axial and transverse velocity components, respectively. The flame location is $x = D(t)$, and the dashed line at $x = a(t)$ is the flow displacement due to thermal expansion, as discussed earlier.

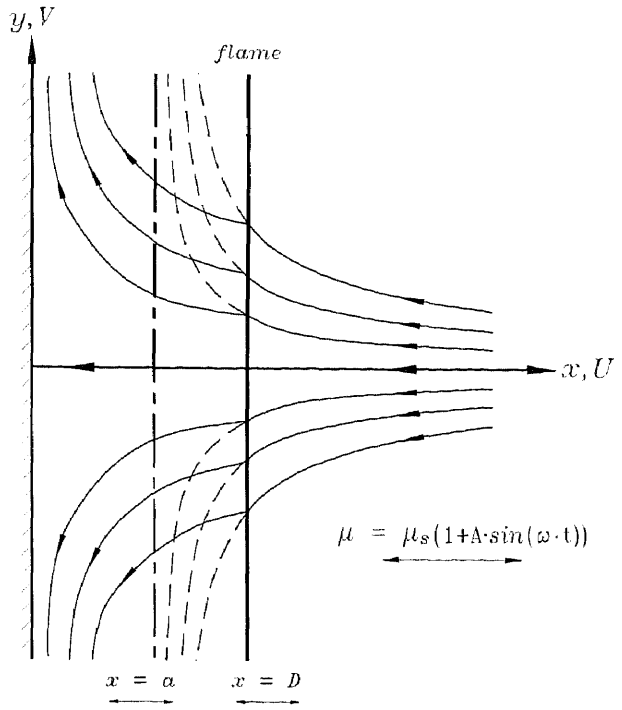

Figure 4.1 Flame in oscillating stagnation point flow

In previous SVF formulations, the flame structure was treated as quasi-steady since fluctuations are only permitted on the hydrodynamic time scale rather than the reaction and diffusion time scales. Here, I will introduce both a fast time τ and slow time t to be $t = \delta\tau$. Thus, $\partial_t \rightarrow \partial_t + \delta^{-1}\partial_\tau$, and the dependent variables ρ, T, Y, and $\mathbf{V}$ will depend on both t and τ

$$\rho = \rho(t, \tau, \mathbf{x}) \qquad T = T(t, \tau, \mathbf{x}) \tag{4.1}$$

$$Y = Y(t, \tau, \mathbf{x}) \qquad \mathbf{V} = \mathbf{V}(t, \tau, \mathbf{x}) \ , \tag{4.2}$$

and in addition, we assume there is a linear dependence between λ and T, such that $\lambda = T$. Thus, equations (2.10) – (2.18) now become

$$\rho T = 1 \tag{4.3}$$

$$\rho_t + \delta^{-1}\rho_\tau + \nabla \cdot (\rho \mathbf{V}) = 0 \tag{4.4}$$

$$\rho\Big(\mathbf{V}_t + \delta^{-1}\mathbf{V}_\tau + (\mathbf{V} \cdot \nabla)\mathbf{V}\Big) = -\nabla p + \delta Pr \nabla \cdot \sigma_{ij} \tag{4.5}$$

$$\rho\Big(T_t + \delta^{-1}T_\tau + (\mathbf{V}\cdot\nabla)T\Big) = \delta q\Omega + \delta\nabla\cdot(T\nabla T) \tag{4.6}$$

$$\rho\Big(Y_t + \delta^{-1}Y_\tau + (\mathbf{V}\cdot\nabla)Y\Big) = -\delta\Omega + \frac{\delta}{Le}\nabla\cdot(T\nabla Y)\ , \tag{4.7}$$

where

$$\sigma_{ij} = 2T\left(d_{ij} - \frac{1}{3}\nabla\cdot\mathbf{V}\right) \qquad d_{ij} = \frac{1}{2}\left(\frac{\partial u_i}{\partial x_j} + \frac{\partial u_j}{\partial x_i}\right)\ . \tag{4.8}$$

We now examine this system for the stagnation point flow geometry in the limit $\delta = \varepsilon \ll 1$. Our main objective is the derivation of a nonlinear flame speed equation.

4.2 Analysis

We call the thin flame region the flame zone whose nondimensional thickness is $\delta \ll 1$. Within this narrow region, there exists a thinner layer called the reaction zone where chemistry is confined. The nondimensional thickness of the reaction zone is $\varepsilon = (T_a^2/E) \ll 1$, where E is the activation energy and T_a is the adiabatic flame temperature. A schematic illustration of the flame and reaction zones is shown in Figure 4.2.

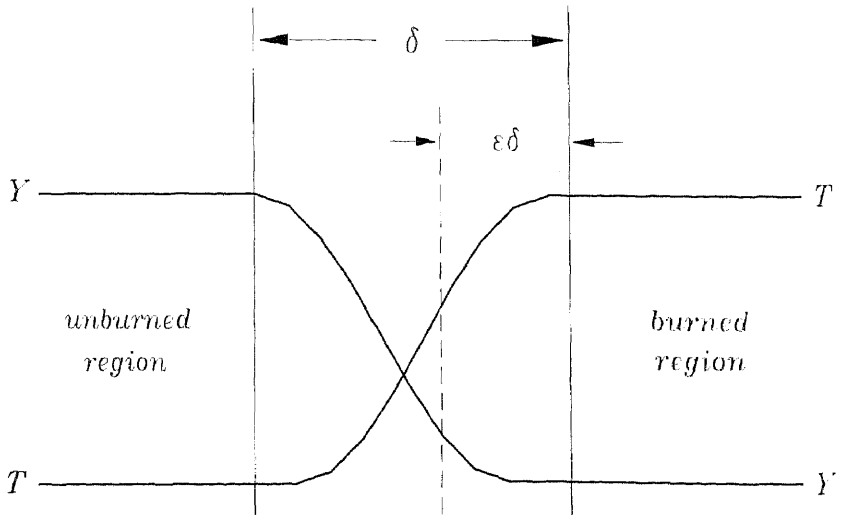

Figure 4.2 Reaction zone embeded in flame zone

Based on the parameters δ and ε, we have three regions to consider. These regions are an $O(1)$ hydrodynamic zone, an $O(\delta)$ flame zone and an $O(\varepsilon\delta)$ reaction zone. Although δ and ε are independent parameters, we consider the distinguished limit $\delta = \varepsilon$, similar to previous SVF formulations.

We restrict our attention to a planar flame in oscillating stagnation point flow, and thus, it is convenient to introduce a new coordinate system attached to the flame front

$$\xi = x - f(t,\tau) \ , \tag{4.9}$$

so that

$$\partial_x \longrightarrow \partial_\xi \qquad\qquad \partial_y \longrightarrow \partial_y \tag{4.10}$$

$$\partial_t \longrightarrow \partial_t - f_t\partial_\xi \qquad\qquad \partial_\tau \longrightarrow \partial_\tau - f_\tau\partial_\xi \ . \tag{4.11}$$

Upon making this coordinate transformation, the continuity equation becomes

$$\rho_t - f_t\rho_\xi + \delta^{-1}\left(\rho_\tau - f_\tau\rho_\xi\right) + \left(\rho u\right)_\xi + \left(\rho v\right)_y = 0 \ . \tag{4.12}$$

It is convenient to define

$$s = u - f_t - \delta^{-1}f_\tau \ , \tag{4.13}$$

where s is the flame speed. We consider weak stretch, so that the amplitude of the rapid fluctuating front is small, $O(\delta)$. Therefore we can write

$$f(t,\tau) = f_{slow}(t) + \delta f_{fast}(t,\tau) \ , \tag{4.14}$$

thus s becomes

$$s = u - \frac{\partial f_{slow}}{\partial t} - \frac{\partial f_{fast}}{\partial \tau} - \delta\frac{\partial f_{fast}}{\partial t} \ . \tag{4.15}$$

The continuity equation now becomes

$$\rho_t + \delta^{-1}\rho_\tau + \left(\rho s\right)_\xi + \left(\rho v\right)_y = 0 \tag{4.16}$$

and similarly, we can rewrite energy, mass fraction, and momentum equations in terms of new coordinate system as

$$\begin{aligned}&\rho T_t + \delta^{-1}\rho T_\tau + (\rho s)T_\xi + \rho v T_y \\ &\quad = q\delta\Omega + \delta\left(TT_{\xi\xi} + TT_{yy} + T_\xi^2 + T_y^2\right)\end{aligned} \tag{4.17}$$

$$\begin{aligned}&\rho Y_t + \delta^{-1}\rho Y_\tau + (\rho s)Y_\xi + \rho v Y_y \\ &\quad = -\delta\Omega + \frac{\delta}{Le}\Big(TY_{\xi\xi} + TY_{yy} + T_\xi Y_\xi + T_y Y_y\Big)\end{aligned} \tag{4.18}$$

$$\begin{aligned}&\rho u_t + \delta^{-1}\rho u_\tau + (\rho s)u_\xi + \rho v u_y \\ &\quad = -p_\xi + \delta PrT\left(\frac{4}{3}u_{\xi\xi} + u_{yy} + \frac{1}{3}v_{\xi y}\right) \\ &\quad + \delta Pr\left(\frac{4}{3}T_\xi u_\xi + T_y u_y + T_y v_\xi - \frac{2}{3}T_\xi v_y\right)\end{aligned} \tag{4.19}$$

$$\begin{aligned}&\rho v_t + \delta^{-1}\rho v_\tau + (\rho s)v_\xi + \rho v v_y \\ &\quad = -p_y + \delta PrT\left(v_{\xi\xi} + \frac{4}{3}u_{yy} + \frac{1}{3}u_{\xi y}\right) \\ &\quad + \delta Pr\left(T_\xi v_\xi + \frac{4}{3}T_y v_y + T_\xi u_y - \frac{2}{3}T_y u_\xi\right)\ .\end{aligned} \tag{4.20}$$

From (4.19) and (4.20), we see that, to balance fluctuations in the velocity field $\mathbf{V} = (u, v)$, we must rescale the pressure as

$$p = \delta^{-1}P\ . \tag{4.21}$$

Equation (4.19) and (4.20) now become

$$\begin{aligned}&\rho u_t + \delta^{-1}\rho u_\tau + (\rho s)u_\xi + \rho v u_y \\ &\quad = -\delta^{-1}P_\xi + \delta PrT\left(\frac{4}{3}u_{\xi\xi} + u_{yy} + \frac{1}{3}v_{\xi y}\right) \\ &\quad + \delta Pr\left(\frac{4}{3}T_\xi u_\xi + T_y u_y + T_y v_\xi - \frac{2}{3}T_\xi v_y\right)\end{aligned} \tag{4.22}$$

$$\begin{aligned}
&\rho v_t + \delta^{-1}\rho v_\tau + (\rho s)v_\xi + \rho v v_y \\
&\quad = -\delta^{-1}P_y + \delta PrT\left(v_{\xi\xi} + \frac{4}{3}u_{yy} + \frac{1}{3}u_{\xi y}\right) \\
&\quad + \delta Pr\left(T_\xi v_\xi + \frac{4}{3}T_y v_y + T_\xi u_y - \frac{2}{3}T_y u_\xi\right) . \qquad (4.23)
\end{aligned}$$

In order to avoid dealing with the reaction rate term Ω, it is convenient for us to define a new enthalpy variable H, which is a linear combination of T and Y, that is

$$H = T + qY \ , \qquad (4.24)$$

thus an equation for H is gotten upon adding (4.17) to (4.18), yielding

$$\begin{aligned}
&\rho H_t + \delta^{-1}\rho H_\tau + (\rho s)H_\xi + \rho v H_y \\
&\quad = +\frac{\delta}{Le}\Big(TH_{\xi\xi} + T_\xi H_\xi + TH_{yy} + T_y H_y\Big) \\
&\quad + \frac{\delta(Le-1)}{Le}\Big(TT_{\xi\xi} + T_\xi^2 + TT_{yy} + T_y^2\Big) . \qquad (4.25)
\end{aligned}$$

Equation (4.25) will now replace the equation for the mass fraction (4.18) in the ensuing analysis.

We now consider the limit $\delta \to 0$, and analysis of the various regions results in the derived flame speed equation. To analyze the flame zone, we introduce the density-weighted coordinate

$$\eta = \int_0^{\xi/\delta} \rho(\xi', \bar{y}, \bar{t}, \bar{\tau})\, d\xi' \qquad (4.26)$$

$$\bar{y} = y \qquad \bar{t} = t \qquad \bar{\tau} = \tau \ , \qquad (4.27)$$

so that

$$\partial_\xi \longrightarrow \delta^{-1}\rho\partial_\eta \qquad (4.28)$$

$$\partial_{\bar{y}} \longrightarrow \partial_y + \left(\int_0^{\xi/\delta} \rho_{\bar{y}}\, d\xi'\right)\partial_\eta \qquad (4.29)$$

$$\partial_{\bar{t}} \longrightarrow \partial_t + \left(\int_0^{\xi/\delta} \rho_{\bar{t}}\, d\xi' \right) \partial_\eta \tag{4.30}$$

$$\partial_{\bar{\tau}} \longrightarrow \partial_\tau + \left(\int_0^{\xi/\delta} \rho_{\bar{\tau}}\, d\xi' \right) \partial_\eta \ , \tag{4.31}$$

and we define the mass burning rate $\hat{m}$ as

$$\hat{m}(\eta, y, t, \tau) = \rho(\eta, y, t, \tau) \cdot s(\eta, y, t, \tau) \ . \tag{4.32}$$

The above governing equations take the form

$$\begin{aligned} &T_\tau + mT_\eta - u_\eta \\ &\quad = \delta \left(-T_t + T^2(\rho v)_y + T^2(\rho v)_\eta \int_0^{\xi/\delta} \rho_{\bar{y}}\, d\xi' + T_\eta \int_0^{\xi/\delta} (\rho v)_{\bar{y}}\, d\xi' \right) \end{aligned} \tag{4.33}$$

$$\begin{aligned} &T_\tau + mT_\eta - T_{\eta\eta} \\ &\quad = \delta^2 qT\Omega + \delta \left(-T_t + T_\eta \int_0^{\xi/\delta} (\rho v)_{\bar{y}}\, d\xi' - v\Big(T_y + T_\eta \int_0^{\xi/\delta} \rho_{\bar{y}}\, d\xi' \Big) \right) \end{aligned} \tag{4.34}$$

$$\begin{aligned} &H_\tau + mH_\eta - \frac{1}{Le} H_{\eta\eta} - \frac{(Le-1)}{Le} T_{\eta\eta} \\ &\quad = \delta \left(-H_t + H_\eta \int_0^{\xi/\delta} (\rho v)_{\bar{y}}\, d\xi' - v\Big(H_y + H_\eta \int_0^{\xi/\delta} \rho_{\bar{y}}\, d\xi' \Big) \right) \end{aligned} \tag{4.35}$$

$$u_\tau + mu_\eta - \frac{4}{3} Pr\, u_{\eta\eta} + \frac{P_\eta}{\delta} = O(\delta) \tag{4.36}$$

$$v_\tau + mv_\eta - Pr\, v_{\eta\eta} + P_y = O(\delta) \tag{4.37}$$

where

$$m = \hat{m}(\eta = 0, y, t, \tau) \ . \tag{4.38}$$

The first step to analyze (4.33) to (4.37) is to resolve the reaction zone. This requires dealing with the nonlinear reaction rate term in equation (4.34). We employ the method of matched asymptotic expressions to relate all variables across this zone.

In reaction zone, the reactant is consumed, so mass fraction is an $O(\delta)$ quantity. We introduce a stretched reaction zone variable, ζ,

$$Y = \delta\check{y} \qquad \eta = \delta\zeta \qquad \partial_\eta \longrightarrow \delta^{-1}\partial_\zeta \tag{4.39}$$

and expand the variables T and H as follows:

$$T = C(y,t,\tau) + \delta\theta_0(\zeta,y,t,\tau) + \delta^2\theta_1(\zeta,y,t,\tau) + O(\delta^3) \tag{4.40}$$

$$H = C(y,t,\tau) + \delta h_0(\zeta,y,t,\tau) + \delta^2 h_1(\zeta,y,t,\tau) + O(\delta^3)\ . \tag{4.41}$$

Note that to leading order in the reaction zone, both T and H are the same constant independent of ζ. This follows from (4.24) since $Y = O(\delta)$. To recall that $Y \equiv 0$ when the reactant is totally consumed, this means

$$H \equiv T \qquad\qquad \text{for all } \zeta > 0\ . \tag{4.42}$$

In the reaction zone, the equations for T and H are

$$\delta m T_\zeta - T_{\zeta\zeta} = \delta^4 q T\Omega + O(\delta^2) \tag{4.43}$$

$$\delta m H_\zeta - \frac{1}{Le}H_{\zeta\zeta} - \frac{(Le-1)}{Le}T_{\zeta\zeta} = O(\delta^2)\ , \tag{4.44}$$

and upon inserting (4.40)–(4.41) into (4.44), we get

$$h_{0\zeta\zeta} + (Le-1)\theta_{0\zeta\zeta} = 0 \tag{4.45}$$

$$h_{1\zeta\zeta} + (Le-1)\theta_{1\zeta\zeta} = mLeh_{0\zeta}\ . \tag{4.46}$$

We can now integrate (4.45) twice and (4.46) once respectively, to get

$$h_0 + (Le-1)\theta_0 = C_{01}\zeta + C_{02} \tag{4.47}$$

$$h_{1\zeta} + (Le-1)\theta_{1\zeta} = mLeh_0 + C_1\ , \tag{4.48}$$

where C_{01}, C_{02}, and C_1 are integration constants. The solutions we construct here must be matched to solutions in the outer flame zone.

The expansions for those outer solutions T and H are given by

$$T_{out} = T_0 + \delta T_1 + \delta^2 T_2 + O(\delta^3) \tag{4.49}$$

$$H_{out} = H_0 + \delta H_1 + \delta^2 H_2 + O(\delta^3) \ , \tag{4.50}$$

and expressing these in terms of the inner variable, ζ, yields $\eta = \delta\zeta$, then T_{out} and H_{out} become

$$\begin{aligned} T_{out}(\delta\zeta) &= T_0(0) + \delta\Big(T_1(0) + \zeta T_{0\eta}(0)\Big) \\ &\quad + \delta^2\left(T_2(0) + \zeta T_{1\eta}(0) + \frac{1}{2}\zeta^2 T_{0\eta\eta}(0)\right) + O(\delta^3) \end{aligned} \tag{4.51}$$

$$\begin{aligned} H_{out}(\delta\zeta) &= H_0(0) + \delta\Big(H_1(0) + \zeta H_{0\eta}(0)\Big) \\ &\quad + \delta^2\left(H_2(0) + \zeta H_{1\eta}(0) + \frac{1}{2}\zeta^2 H_{0\eta\eta}(0)\right) + O(\delta^3) \ . \end{aligned} \tag{4.52}$$

Employing the method of matched asymptotics, we equate (4.51) and (4.52) with (4.40), (4.41), (4.47) and (4.48) in the limit $\zeta \to \infty$, to get

$$T_0(0^-) = T_0(0^+) = H_0(0^-) = H_0(0^+) = C(y,t,\tau) \tag{4.53}$$

$$H_0(0^-) + (Le-1)T_0(0^-) = H_0(0^+) + (Le-1)T_0(0^+) = C_{02} \tag{4.54}$$

$$H_{0\eta}(0^-) + (Le-1)T_{0\eta}(0^-) = H_{0\eta}(0^+) + (Le-1)T_{0\eta}(0^+) = C_{01} \tag{4.55}$$

$$\begin{aligned} &H_{1\eta} + (Le-1)T_{1\eta} - mLeH_1 \\ &\quad = mLe\zeta H_{0\eta} - \zeta H_{0\eta\eta} - (Le-1)\zeta T_{0\eta\eta} + C_1 \ . \end{aligned} \tag{4.56}$$

Since in the flame zone, to leading order, T and H satisfy

$$H_{0\tau} + mH_{0\eta} - \frac{1}{Le}H_{0\eta\eta} - \frac{(Le-1)}{Le}T_{0\eta\eta} = 0 \ , \tag{4.57}$$

then (4.56) can be written

$$H_{1\eta} + (Le-1)T_{1\eta} - mLeH_1 + \zeta LeH_{0\tau} = C_1 \ . \tag{4.58}$$

To summarize, we can express the above jump conditions as

$$\Big[T_0(0)\Big] = \Big[H_0(0)\Big] = 0 \tag{4.59}$$

$$\Big[H_{0\eta}(0)\Big] + (Le-1)\Big[T_{0\eta}(0)\Big] = 0 \tag{4.60}$$

$$\Big[H_{1\eta}(0)\Big] + (Le-1)\Big[T_{1\eta}(0)\Big] - mLe\Big[H_1(0)\Big] = 0 \ , \tag{4.61}$$

where the jump operator $[\cdot]$ is defined as

$$\Big[\phi(x=a)\Big] = \phi(a^+) - \phi(a^-) \ . \tag{4.62}$$

A final condition is needed to determine flame speed. This follows from analysis of (4.43). To leading order, diffusion and reaction balance to give

$$-\theta_{0\zeta\zeta} = q\check{y}\bar{\Lambda}\exp(\theta_0) \ , \tag{4.63}$$

where

$$\bar{\Lambda} = \delta^4\tilde{\Lambda} \qquad \tilde{\Lambda} = \delta^{-2}\Lambda\exp(-T_a^2/\varepsilon) \ , \tag{4.64}$$

and $\check{y}$ denotes the local mass fraction perturbation, which is given by

$$q\check{y} = h_0 - \theta_0 \ . \tag{4.65}$$

Therefore (4.63) becomes

$$-\theta_{0\zeta\zeta} = \bar{\Lambda}(h_0 - \theta_0)\exp(\theta_0) \ . \tag{4.66}$$

We can express h_0 explicitly in terms of θ_0 by using (4.47), and thus obtain a single ODE for θ_0. Since $Y \equiv 0 \ \ \forall\zeta > 0$, it follows from (4.54) and (4.55) that

$$C_{01} = LeT_{0\eta}(0^+) \qquad\qquad C_{02} = LeT_1(0^+) \ , \tag{4.67}$$

and thus (4.47) can be rewritten into

$$h_0 - \theta_0 = LeT_{0\eta}(0^+)\zeta + LeT_1(0^+) - Le\theta_0 \ . \tag{4.68}$$

Inserting (4.68) into (4.66), now gives the ODE

$$-\theta_{0\zeta\zeta} = Le\bar{\Lambda}\left(T_{0\eta}(0^+)\zeta + T_1(0^+) - \theta_0\right)\exp(\theta_0) \ . \tag{4.69}$$

Equation (4.69) can be written in the canonical form of Liñán(1974). We first introduce the new variable

$$\psi = T_{0\eta}(0^+)\zeta + T_1(0^+) - \theta_0 \ , \tag{4.70}$$

so that (4.69) becomes

$$\psi_{\zeta\zeta} = Le\bar{\Lambda}\psi\exp\left(T_{0\eta}(0^+)\zeta + T_1(0^+) - \psi\right) \ , \tag{4.71}$$

and ψ must satisfy matching conditions which follow from (4.70) as

$$\psi_\zeta = T_{0\zeta}(0^+) - \theta_{0\zeta} = \begin{cases} 0 & \zeta \to +\infty \\ T_{0\eta}(0^+) - T_{0\eta}(0^-) & \zeta \to -\infty \end{cases} \ .$$

In order to utilize the results of Liñán(1974), we set

$$\zeta = a\chi \qquad\qquad \psi(\zeta) = \psi(\chi) \ , \tag{4.72}$$

and it is easy to find that when

$$a = -\frac{1}{\left(T_{0\eta}(0^+) - T_{0\eta}(0^-)\right)} = -\frac{1}{\left[T_{0\eta}(0)\right]} > 0 \ , \tag{4.73}$$

then the matching conditions simplify to

$$\psi_\chi = \begin{cases} 0 & \chi \to +\infty \\ -1 & \chi \to -\infty \end{cases} \ .$$

The equation (4.71) becomes

$$\psi_{\chi\chi} = \breve{\Lambda}\psi\exp(-\psi - \tilde{m}\chi) \ , \tag{4.74}$$

where

$$\breve{\Lambda} = Le\bar{\Lambda}a^2 \exp\left(T_1(0^+)\right) \qquad \tilde{m} = -aT_{0\eta}(0^+) \ , \tag{4.75}$$

and then the results of Liñán(1974) suggest that the eigenvalue, $\breve{\Lambda}$ has the approximation form

$$\breve{\Lambda} = Le\bar{\Lambda}a^2 \exp\left(T_1(0^+)\right) = \frac{1}{2}\left(1 - 1.344\tilde{m} + 0.6307\tilde{m}^2\right) \ . \tag{4.76}$$

Recall that the adiabatic flame speed is unity, and thus $Le\bar{\Lambda} = q^2/2$. (4.76) now gives the downstream temperature perturbation

$$T_1(0^+) = \ln\left(q^{-2}\Big[T_{0\eta}(0)\Big]^2 - 1.344q^{-2}T_{0\eta}(0^+)\Big[T_{0\eta}(0)\Big] + 0.6307q^{-2}T_{0\eta}^2(0^+)\right) \ . \tag{4.77}$$

The final condition, as follows from Liñán's analysis, is that T_1 is continuous across the reaction zone. To demonstrate this, we consider the matching condition from above:

$$\psi = \begin{cases} D_1 & \chi \to +\infty \\ -\chi + D_2 & \chi \to -\infty \end{cases} \ ,$$

and we change back to the ζ coordinate, to get

$$\psi = T_{0\eta}(0^+)\zeta + T_1(0^+) - \theta_0 = -\frac{\zeta}{a} + D_2 \qquad \zeta \to -\infty \tag{4.78}$$

$$\psi = T_{0\eta}(0^+)\zeta + T_1(0^+) - T_{0\eta}(0^-)\zeta - T_1(0^-) = -\frac{\zeta}{a} + D_2 \qquad \zeta \to -\infty \ . \tag{4.79}$$

From above, it follows that

$$\Big[T_{0\eta}(0)\Big] = -\frac{1}{a} \qquad \Big[T_1(0)\Big] = D_2 \ . \tag{4.80}$$

We shift the χ coordinate in (4.74), and let

$$\chi = \varrho + B \ , \tag{4.81}$$

so that (4.74) becomes

$$\psi_{\varrho\varrho} = \breve{\Lambda}\psi \exp(-\psi - \tilde{m}\varrho - \tilde{m}B) \ . \tag{4.82}$$

We follow Liñán and choose B to satisfy

$$\breve{\Lambda}\exp(-\tilde{m}B) = \frac{1}{2}\ , \tag{4.83}$$

and from (4.76), it follows that

$$B = \frac{1}{\tilde{m}}\ln\left(1 - 1.344\tilde{m} + 0.6307\tilde{m}^2\right)\ , \tag{4.84}$$

and our system is now identical to Liñán's, i.e.

$$2\psi_{\varrho\varrho} = \psi\exp(-\psi - \tilde{m}\varrho) \tag{4.85}$$

$$\psi_\varrho = \begin{cases} 0 & \varrho \to +\infty \\ -1 & \varrho \to -\infty \end{cases}\ .$$

From the results of Liñán(1974), we found that

$$\psi = -\varrho - B = -\chi \qquad \text{as } \chi \to \infty\ , \tag{4.86}$$

so that

$$\left[T_1(0)\right] = D_2 = 0\ . \tag{4.87}$$

These jump conditions can now be applied to find solutions in the outer flame zone.

4.3 Flame Response and Extinction

Solutions in the outer region are sought in the form of power series expansion in δ, i.e.

$$\rho = \rho_0 + \delta\rho_1 + \delta^2\rho_2 + O(\delta^3) \tag{4.88}$$

$$T = T_0 + \delta T_1 + \delta^2 T_2 + O(\delta^3) \tag{4.89}$$

$$H = H_0 + \delta H_1 + \delta^2 H_2 + O(\delta^3) \tag{4.90}$$

$$u = u_0 + \delta u_1 + \delta^2 u_2 + O(\delta^3) \tag{4.91}$$

$$v = v_0 + \delta v_1 + \delta^2 v_2 + O(\delta^3) \tag{4.92}$$

$$P = P_0 + \delta P_1 + \delta^2 P_2 + O(\delta^3) \ . \tag{4.93}$$

These expansions are inserted into equations (4.33)–(4.37) and solutions are sought that satisfy the jump conditions

$$\Big[T_0(0)\Big] = \Big[H_0(0)\Big] = 0 \tag{4.94}$$

$$\Big[H_{0\eta}(0)\Big] + (Le-1)\Big[T_{0\eta}(0)\Big] = 0 \tag{4.95}$$

$$\Big[T_1(0)\Big] = \Big[H_1(0)\Big] = 0 \tag{4.96}$$

$$\Big[H_{1\eta}(0)\Big] + (Le-1)\Big[T_{1\eta}(0)\Big] = 0 \ , \tag{4.97}$$

and the boundary conditions

$$T_0(-\infty) = 1 \qquad T_0(\infty) = 1+q \qquad T_j(-\infty) = T_j(\infty) = 0 \tag{4.98}$$

$$H_0(-\infty) = 1+q \qquad H_0(\infty) = 1+q \qquad H_j(-\infty) = H_j(\infty) = 0 \tag{4.99}$$

$$T_1(0^+) = \ln\left(q^{-2}\Big[T_{0\eta}(0)\Big]^2 - 1.344q^{-2}T_{0\eta}(0^+)\Big[T_{0\eta}(0)\Big] + 0.6307q^{-2}T_{0\eta}^2(0^+)\right) \tag{4.100}$$

where

$$m = \hat{m}(\eta = 0, y, t, \tau) \qquad \text{and} \qquad j = 1, 2, 3, \cdots \ . \tag{4.101}$$

Suppose that we introduce a time harmonic unsteady perturbation into the fresh flow field, and it has a small amplitude $A(\ll 1)$. Based on this assumption, we can further expand the above variables as

$$m = m^0 + Am^1 \exp(i\omega\tau) + O(A^2) \tag{4.102}$$

$$\rho_j = \rho_j^0 + A\rho_j^1 \exp(i\omega\tau) + O(A^2) \tag{4.103}$$

$$T_j = T_j^0 + AT_j^1 \exp(i\omega\tau) + O(A^2) \tag{4.104}$$

$$H_j = H_j^0 + AH_j^1 \exp(i\omega\tau) + O(A^2) \tag{4.105}$$

$$u_j = u_j^0 + Au_j^1 \exp(i\omega\tau) + O(A^2) \tag{4.106}$$

$$v_j = v_j^0 + A v_j^1 \exp(i\omega\tau) + O(A^2) \tag{4.107}$$

$$P_j = P_j^0 + A P_j^1 \exp(i\omega\tau) + O(A^2) \tag{4.108}$$

where $j = 0, 1, 2, 3, \cdots$.

We consider first the leading order solutions in δ. The $O(A^0)$ subsystem for the transport variables is

$$m^0 T_{0\eta}^0 - T_{0\eta\eta}^0 = 0 \tag{4.109}$$

$$m^0 H_{0\eta}^0 - \frac{1}{Le} H_{0\eta\eta}^0 - \frac{(Le-1)}{Le} T_{0\eta\eta}^0 = 0 \tag{4.110}$$

$$\left[T_0^0(0)\right] = \left[H_0^0(0)\right] = 0 \tag{4.111}$$

$$\left[H_{0\eta}^0(0)\right] + (Le-1)\left[T_{0\eta}^0(0)\right] = 0 \tag{4.112}$$

$$T_0^0(-\infty) = 1 \qquad T_0^0(\infty) = 1 + q \tag{4.113}$$

$$H_0^0(-\infty) = 1 + q \qquad H_0^0(\infty) = 1 + q\,, \tag{4.114}$$

whose solutions are

$$T_0^0 = \begin{cases} 1 + q\exp(m^0\eta) & \eta < 0 \\ 1 + q & \eta > 0 \end{cases}$$

$$H_0^0 = \begin{cases} 1 + q + q\exp(m^0\eta) - q\exp(Le\, m^0\eta) & \eta < 0 \\ 1 + q & \eta > 0 \end{cases}.$$

At $O(A)$, we have the system

$$i\omega T_0^1 + m^0 T_{0\eta}^1 + m^1 T_{0\eta}^0 - T_{0\eta\eta}^1 = 0 \tag{4.115}$$

$$i\omega H_0^1 + m^0 H_{0\eta}^1 + m^1 H_{0\eta}^0 - \frac{1}{Le} H_{0\eta\eta}^1 - \frac{(Le-1)}{Le} T_{0\eta\eta}^1 = 0 \tag{4.116}$$

$$\left[T_0^1(0)\right] = \left[H_0^1(0)\right] = 0 \tag{4.117}$$

$$\left[H_{0\eta}^1(0)\right] + (Le-1)\left[T_{0\eta}^1(0)\right] = 0 \tag{4.118}$$

$$T_0^1(-\infty) = 0 \qquad T_0^1(\infty) = 0 \tag{4.119}$$

$$H_0^1(-\infty) = 0 \qquad H_0^1(\infty) = 0 \ , \tag{4.120}$$

whose solutions are readily found to be

$$T_0^1 = \begin{cases} \left(a_0^1 \exp(D_+\eta) - d_0^1 \exp(m^0\eta)\right) & \eta < 0 \\ b_0^1 \exp(D_-\eta) & \eta > 0 \end{cases}$$

$$H_0^1 = \begin{cases} \Big(- d_0^1 \exp(m^0\eta) + Le\, d_0^1 \exp(Le\, m^0\eta) \\ + a_0^1 \exp(D_+\eta) + c_0^1 \exp(E_+\eta)\Big) & \eta < 0 \\ b_0^1 \exp(D_-\eta) & \eta > 0 \end{cases} ,$$

where

$$D_\pm = \frac{m^0 \pm \sqrt{(m^0)^2 + 4i\omega}}{2} \tag{4.121}$$

$$E_\pm = \frac{Le\, m^0 \pm \sqrt{(Le\, m^0)^2 + 4Le\, i\omega}}{2} \tag{4.122}$$

$$d_0^1 = \frac{qm^0m^1}{i\omega} \qquad c_0^1 = -\frac{Le\, qm^0m^1}{i\omega} \tag{4.123}$$

$$b_0^1 = \frac{qm^0m^1(E_+ - Le\, m^0 - D_+ + m^0)}{i\omega(D_+ - D_-)} \tag{4.124}$$

$$a_0^1 = \frac{qm^0m^1(E_+ - Le\, m^0 - D_+ + m^0)}{i\omega(D_+ - D_-)} + \frac{qm^0m^1}{i\omega} \ . \tag{4.125}$$

We now turn to the fluid equations. From (4.36), it follows that the leading order pressure term P_0 is independent of η. Matching P_0 with the outer solution in the hydrdynamic zone, reveals that P_0^0 is independent of y, that is $P_{0y}^0 = 0$. Then the solution for (4.37) is

$$v_0 = v_0^0 + Av_0^1 \exp(i\omega\tau) + O(A^2) \ , \tag{4.126}$$

where v_0^0 and v_0^1 are independent of η. And the leading order transversal velocity u_0 can be easily found from (4.33) and (4.34), and given by

$$u_0 = T_{0\eta} + C \ , \tag{4.127}$$

where C is integration constant.

To solve the $O(\delta)$ system, we first have to deal with the integrals in (4.33), (4.34) and (4.35). Since

$$\eta = \int_0^{\xi/\delta} \rho(\xi', \bar{y}, \bar{t}, \bar{\tau})\, d\xi' \ , \tag{4.128}$$

it follows

$$\frac{d\eta}{d\xi} = \frac{\rho}{\delta} \sim \frac{\rho_0}{\delta} + O(\delta) \ ,$$

and thus

$$\begin{aligned} \frac{\xi}{\delta} = \eta + \frac{q}{m^0}\Big(\exp(m^0\eta) - 1\Big) + A\left(\frac{a_0^1}{D_+}\Big(\exp(D_+\eta) - 1\Big)\right. \\ \left. -\frac{d_0^1}{m^0}\Big(\exp(m^0\eta) - 1\Big)\right)\exp(i\omega\tau) \qquad \eta < 0 \end{aligned} \tag{4.129}$$

$$\frac{\xi}{\delta} = (1+q)\eta + A\frac{b_0^1}{D_-}\Big(\exp(D_-\eta) - 1\Big)\exp(i\omega\tau) \qquad \eta > 0 \ . \tag{4.130}$$

From (4.128) to know that η is a function of old coordinate $\bar{y}$, then differentiate (4.130) with respect to $\bar{y}$ to get

$$\eta_{\bar{y}} = -\frac{A\left(\frac{b_0^1}{D_-}\right)_{\bar{y}}\Big(\exp(D_-\eta) - 1\Big)\exp(i\omega\tau)}{1 + q + A\left(\frac{b_0^1}{D_-}\right)D_{-\bar{y}}\,\eta\exp(D_-\eta)\exp(i\omega\tau)} \ . \tag{4.131}$$

Since we only consider planar flame case and the fresh flow field is potential, as well as the density ρ is a function of only η. And by the definition of mass burning rate m, to know that m^0 and m^1 are independent of $\bar{y}$, which means

$$\left(\frac{b_0^1}{D_-}\right)_{\bar{y}} = 0 \ ,$$

thus we have proven that $\eta_{\bar{y}} = 0$ when $\eta > 0$. In the same way, we can prove $\eta_{\bar{y}} = 0$ when $\eta < 0$ if we differentiate (4.129) with respect to $\bar{y}$.

From (4.29), we know that the partial derivative between the old variable $\bar{y}$ and new variable y is

$$\partial_{\bar{y}} \longrightarrow \partial_y + \eta_{\bar{y}} \cdot \partial_\eta \ , \tag{4.132}$$

and since $\eta_{\bar{y}} = 0$, it follows

$$\partial_{\bar{y}} \longrightarrow \partial_y \ . \tag{4.133}$$

To evaluate the remaining integrals, we will interchange the limits of integration from old variable ξ/δ to new variable η. From (4.128) it follows that

$$\xi' \in \left(0\ ,\ \frac{\xi}{\delta}\right) \qquad \text{as} \qquad \eta \in \left(0\ ,\ \int_0^{\xi/\delta} \rho(\xi', \bar{y}, \bar{t}, \bar{\tau})\, d\xi'\right)\ , \tag{4.134}$$

and also we know

$$\frac{d\eta}{\rho} = \frac{d\xi}{\delta}\ . \tag{4.135}$$

We can now evaluate the following integrals

$$\int_0^{\xi/\delta} \Big(\rho_0 v_0\Big)_{\bar{y}}\, d\xi' = \int_0^{\eta} \frac{1}{\rho}\Big(\rho_0 v_0\Big)_y\, d\eta' = \eta\, v_{0y} + O(\delta) \tag{4.136}$$

$$\int_0^{\xi/\delta} \rho_{0\bar{y}}\, d\xi' = \int_0^{\eta} \frac{\rho_{0y}}{\rho}\, d\eta' = 0\ . \tag{4.137}$$

We now turn to the $O(\delta)$ system for the transport variables. Expanding T_1, H_1 in power series expansions in A, we have at $O(A^0)$:

$$m^0 T^0_{1\eta} - T^0_{1\eta\eta} = \eta T^0_{0\eta} v^0_{0y} \tag{4.138}$$

$$m^0 H^0_{1\eta} - \frac{1}{Le} H^0_{1\eta\eta} - \frac{(Le-1)}{Le} T^0_{1\eta\eta} = \eta H^0_{0\eta} v^0_{0y} \tag{4.139}$$

$$\Big[T^0_1(0)\Big] = \Big[H^0_1(0)\Big] = 0 \tag{4.140}$$

$$\Big[H^0_{1\eta}(0)\Big] + (Le-1)\Big[T^0_{1\eta}(0)\Big] = 0 \tag{4.141}$$

$$T^0_1(-\infty) = 0 \qquad T^0_1(\infty) = 0 \tag{4.142}$$

$$H^0_1(-\infty) = 0 \qquad H^0_1(\infty) = 0\ , \tag{4.143}$$

whose solutions are

$$T^0_1 = \begin{cases} \left(-\frac{q v^0_{0y}}{2}\eta^2 + \frac{q v^0_{0y}}{m^0}\eta + a^0_1\right)\exp(m^0\eta) & \eta < 0 \\ b^0_1 & \eta > 0 \end{cases}$$

$$H_1^0 = \begin{cases} \left(-\frac{qv_{0y}^0}{2}\eta^2 + \frac{qv_{0y}^0}{m^0}\eta + a_1^0\right)\exp(m^0\eta) \\ + \left(\frac{Le\,qv_{0y}^0}{2}\eta^2 - \frac{qv_{0y}^0}{m^0}\eta\right)\exp(Le\,m^0\eta) & \eta < 0 \\ b_1^0 & \eta > 0 \end{cases}$$

where

$$a_1^0 = b_1^0 = \frac{(1-Le)qv_{0y}^0}{Le(m^0)^2}\ . \tag{4.144}$$

The $O(A^1)\cdot O(\delta^1)$ subsystem is

$$i\omega T_1^1 + m^0 T_{1\eta}^1 + m^1 T_{1\eta}^0 - T_{1\eta\eta}^1 = \eta v_{0y}^0 T_{0\eta}^1 + \eta v_{0y}^1 T_{0\eta}^0 \tag{4.145}$$

$$i\omega H_1^1 + m^0 H_{1\eta}^1 + m^1 H_{1\eta}^0 - \frac{1}{Le}H_{1\eta\eta}^1 - \frac{(Le-1)}{Le}T_{1\eta\eta}^1 = \eta v_{0y}^0 H_{0\eta}^1 + \eta v_{0y}^1 H_{0\eta}^0 \tag{4.146}$$

$$\left[T_1^1(0)\right] = \left[H_1^1(0)\right] = 0 \tag{4.147}$$

$$\left[H_{1\eta}^1(0)\right] + (Le-1)\left[T_{1\eta}^1(0)\right] = 0 \tag{4.148}$$

$$T_1^1(-\infty) = 0 \qquad T_1^1(\infty) = 0 \tag{4.149}$$

$$H_1^1(-\infty) = 0 \qquad H_1^1(\infty) = 0\ . \tag{4.150}$$

For convenience, we rewrite (4.145) and (4.146) as

$$i\omega T_1^1 + m^0 T_{1\eta}^1 - T_{1\eta\eta}^1 = T_{right} \tag{4.151}$$

$$i\omega H_1^1 + m^0 H_{1\eta}^1 - \frac{1}{Le}H_{1\eta\eta}^1 - \frac{(Le-1)}{Le}T_{1\eta\eta}^1 = H_{right} \tag{4.152}$$

where

$$T_{right} = -m^1 T_{1\eta}^0 + \eta v_{0y}^0 T_{0\eta}^1 + \eta v_{0y}^1 T_{0\eta}^0 \tag{4.153}$$

$$H_{right} = -m^1 H_{1\eta}^0 + \eta v_{0y}^0 H_{0\eta}^1 + \eta v_{0y}^1 H_{0\eta}^0\ . \tag{4.154}$$

We now substract (4.151) from (4.152) to get

$$i\omega(H-T)_1^1 + m^0(H-T)_{1\eta}^1 - \frac{1}{Le}(H-T)_{1\eta\eta}^1 = (H-T)_{right}\ . \tag{4.155}$$

We solve (4.151) and (4.155) by using integrating factors

$$\left(\left(a_1^+ T_1^1 + b_1^+ T_{1\eta}^1\right)\exp(c_1^+\eta)\right)_\eta = T_{right}^+ \exp(c_1^+\eta) \tag{4.156}$$

$$\left(\left(a_1^- T_1^1 + b_1^- T_{1\eta}^1\right)\exp(c_1^-\eta)\right)_\eta = T_{right}^- \exp(c_1^-\eta) \tag{4.157}$$

$$\left(\left(a_2^-(H-T)_1^1 + b_2^-(H-T)_{1\eta}^1\right)\exp(c_2^-\eta)\right)_\eta = (H-T)_{right}^- \exp(c_2^-\eta) \tag{4.158}$$

where super indecies '+' and '−' imply the regions $\eta > 0$ and $\eta < 0$ respectively. And also the coefficients a, b and c satisfy

$$\begin{cases} a_1^\pm c_1^\pm = i\omega \\ a_1^\pm + b_1^\pm c_1^\pm = m^0 \\ b_1^\pm = -1 \end{cases} \qquad \begin{cases} a_2^\pm c_2^\pm = i\omega \\ a_2^\pm + b_2^\pm c_2^\pm = m^0 \\ b_2^\pm = -1/Le \end{cases}$$

$$c_1^\pm = \frac{-m^0 \mp \sqrt{(m^0)^2 + 4i\omega}}{2} \qquad c_2^\pm = \frac{-Le\, m^0 \mp \sqrt{(Le\, m^0)^2 + 4Le\, i\omega}}{2}\,.$$

We integrate (4.156) from 0^+ to $+\infty$; (4.157) and (4.158) from $-\infty$ to 0^-, to get

$$a_1^+ T_1^1(0^+) + b_1^+ T_{1\eta}^1(0^+) = \int_{+\infty}^{0^+} T_{right}^+ \exp(c_1^+\eta)\, d\eta' \tag{4.159}$$

$$a_1^- T_1^1(0^-) + b_1^- T_{1\eta}^1(0^-) = \int_{-\infty}^{0^-} T_{right}^- \exp(c_1^-\eta)\, d\eta' \tag{4.160}$$

$$a_2^-(H-T)_1^1(0^-) + b_2^-(H-T)_{1\eta}^1(0^-) = \int_{-\infty}^{0^-} (H-T)_{right}^- \exp(c_2^-\eta)\, d\eta'\,. \tag{4.161}$$

Note that all the RHS of above equations (4.159), (4.160) and (4.161) are known. Now we can solve for $T_1^1(0^+)$ from (4.159), (4.160) and (4.161). Since $b_1^\pm = -1$, $b_2^\pm = -1/Le$ and $T_1^1(0^+) = T_1^1(0^-) = H_1^1(0^+) = H_1^1(0^-)$ by jump condition (4.147), and recall that $H \equiv T$ and $H_\eta \equiv T_\eta$ in burned region $\eta > 0$. It then follows that

$$T_1^1(0^+) = \frac{1}{\Gamma}\left(\frac{1}{D_+} - \frac{Le}{E_+}\right)\left\{\frac{q(m^0)^2 v_{0y}^1}{i\omega} + qm^0 m^1 v_{0y}^0\left(\frac{1}{\Gamma^2} + \frac{1}{i\omega} - \frac{1}{Le(m^0)^2} - \frac{4D_+^2E_+^2 - Le(m^0)^2 D_+E_+}{i\omega\Gamma^2\Gamma_{Le}^2}\right)\right\} \tag{4.162}$$

where

$$\Gamma = \sqrt{(m^0)^2 + 4i\omega} \qquad \Gamma_{Le} = \sqrt{(Le\, m^0)^2 + 4Le\, i\omega}$$

$$D_+ = \frac{m^0 + \sqrt{(m^0)^2 + 4i\omega}}{2} \qquad E_+ = \frac{Le\, m^0 + \sqrt{(Le\, m^0)^2 + 4Le\, i\omega}}{2}.$$

4.4 Results and Discussions

The flame speed equation is now gotten by equating (4.100) and (4.162)

$$T_1(0^+) = \ln\left(q^{-2}\Big[T_{0\eta}(0)\Big]^2 - 1.344q^{-2}T_{0\eta}(0^+)\Big[T_{0\eta}(0)\Big] + 0.6307q^{-2}T_{0\eta}^2(0^+)\right) \quad (4.163)$$

with

$$T_1^0(0^+) = \frac{(1-Le)qv_{0y}^0}{Le(m^0)^2}$$

$$T_1^1(0^+) = \frac{1}{\Gamma}\left(\frac{1}{D_+} - \frac{Le}{E_+}\right)\left\{\frac{q(m^0)^2v_{0y}^1}{i\omega} + qm^0m^1v_{0y}^0\left(\frac{1}{\Gamma^2} + \frac{1}{i\omega} - \frac{1}{Le(m^0)^2} - \frac{4D_+^2E_+^2 - Le(m^0)^2D_+E_+}{i\omega\Gamma^2\Gamma_{Le}^2}\right)\right\} \quad (4.164)$$

$$d_0^1 = \frac{qm^0m^1}{i\omega} \qquad a_0^1 = b_0^1 + d_0^1$$

$$b_0^1 = \frac{qm^0m^1(E_+ - Le\, m^0 - D_+ + m^0)}{i\omega(D_+ - D_-)}$$

$$\Gamma = \sqrt{(m^0)^2 + 4i\omega} \qquad \Gamma_{Le} = \sqrt{(Le\, m^0)^2 + 4Le\, i\omega}$$

$$D_\pm = \frac{m^0 \pm \sqrt{(m^0)^2 + 4i\omega}}{2} \qquad E_\pm = \frac{Le\, m^0 \pm \sqrt{(Le\, m^0)^2 + 4Le\, i\omega}}{2}$$

and

$$T_i = T_i^0 + AT_i^1\exp(i\omega\tau) + O(A^2) \qquad i = 0, 1$$

$$T_0^0 = \begin{cases} 1 + q\exp(m^0\eta) & \eta < 0 \\ 1 + q & \eta > 0 \end{cases}$$

$$T_0^1 = \begin{cases} \left(a_0^1\exp(D_+\eta) - d_0^1\exp(m^0\eta)\right) & \eta < 0 \\ b_0^1\exp(D_-\eta) & \eta > 0 \end{cases}.$$

We first expand (4.163) into power series in A. The leading order $O(A^0)$ term is

$$(m^0)^2 \cdot \ln\left((m^0)^2\right) = \frac{(1-Le)}{Le} q v_{0y}^0 \tag{4.165}$$

where, for the stagnation point geometry studied here, v_{0y}^0 is constant. Therefore (4.165) takes the form of previous steady flame structure analyses given by Buckmaster(1977). It is well known that this equation captures flame extinction properties when Lewis number $Le > 1$. On the other hand, when $Le < 1$, (4.165) predicts that flame speed is a monotonic increasing function of imposed flow strain rate. Typical plots of flame speed as function of qv_{0y}^0 for different Lewis number $Le > 1$ and $Le < 1$ are shown in figure 4.3 and figure 4.4, respectively. In figure 4.3, we note that flame extinction occurs when the scaled strain rate qv_{0y}^0 exceeds the critical value $\frac{Le}{e(Le-1)}$.

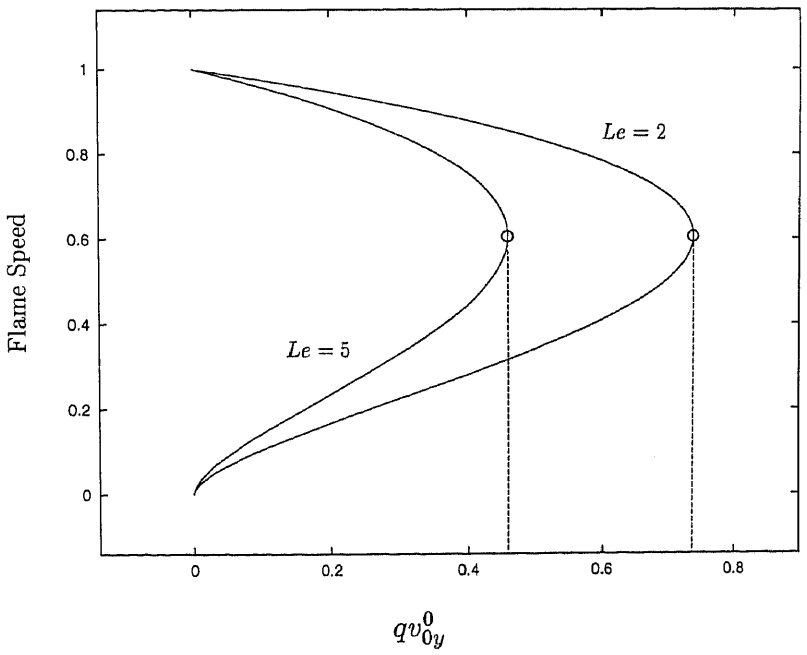

Figure 4.3 Steady flame speed as function of the scaled strain rate qv_{0y}^0 for two different values of Lewis number Le, and flame extinction happens when the scaled strain rate qv_{0y}^0 exceeds the critical value $\frac{Le}{e(Le-1)}$ when $Le > 1$

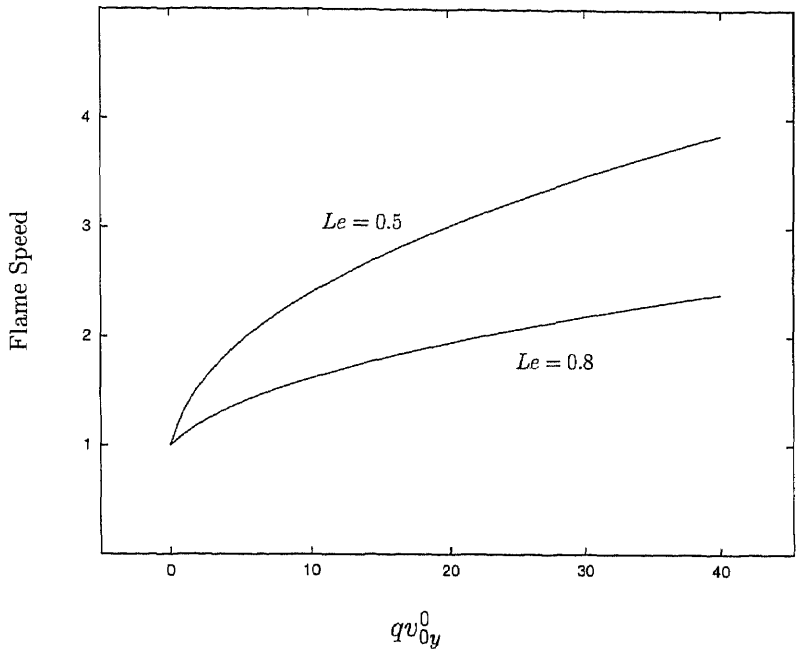

Figure 4.4 Steady flame speed as function of the scaled strain rate qv_{0y}^0 for two different values of Lewis number Le, and there is no flame extinction happenning when $Le < 1$

To assess unsteady effects, we now consider the $O(A)$ term. From (4.163) we have

$$T_1^1(0^+) = \frac{2\left[T_{0\eta}^1(0)\right] - 1.344T_{0\eta}^1(0^+)}{\left[T_{0\eta}^0(0)\right]} . \tag{4.166}$$

Equating (4.166) to (4.164) yields the following expression for m^1

$$m^1 = \frac{q\varsigma(m^0)^2 v_{0y}^1}{-0.656\tilde{b}_0^1 D_- + 2\tilde{a}_0^1 D_+ - 2m^0 - q\varsigma\varpi m^0 v_{0y}^0} , \tag{4.167}$$

where

$$\tilde{b}_0^1 = \frac{E_+ - Le\, m^0 - D_+ + m^0}{D_+ - D_-} \qquad \tilde{a}_0^1 = \tilde{b}_0^1 + 1 \qquad \varsigma = \frac{1}{\Gamma}\left(\frac{1}{D_+} - \frac{Le}{E_+}\right)$$

$$\varpi = \frac{i\omega}{\Gamma^2} + 1 - \frac{i\omega}{Le(m^0)^2} - \frac{4D_+^2E_+^2 - Le(m^0)^2 D_+ E_+}{\Gamma^2\Gamma_{Le}^2} .$$

We first examine the two limiting cases $\omega \to 0$ and $\omega \to \infty$ in (4.167), to get

$$m^1 \to \left(\frac{2Le(m^0)^4 \ln(m^0)}{0.656(Le-1) + 2(\sqrt{Le}+1)^2}\right)\frac{1}{(i\omega)^{3/2}} \quad \text{as} \quad \omega \to \infty \tag{4.168}$$

$$m^1 \to \frac{m^0 \ln(m^0)}{1 + 2\ln(m^0)} \quad \text{as} \quad \omega \to 0 \,. \tag{4.169}$$

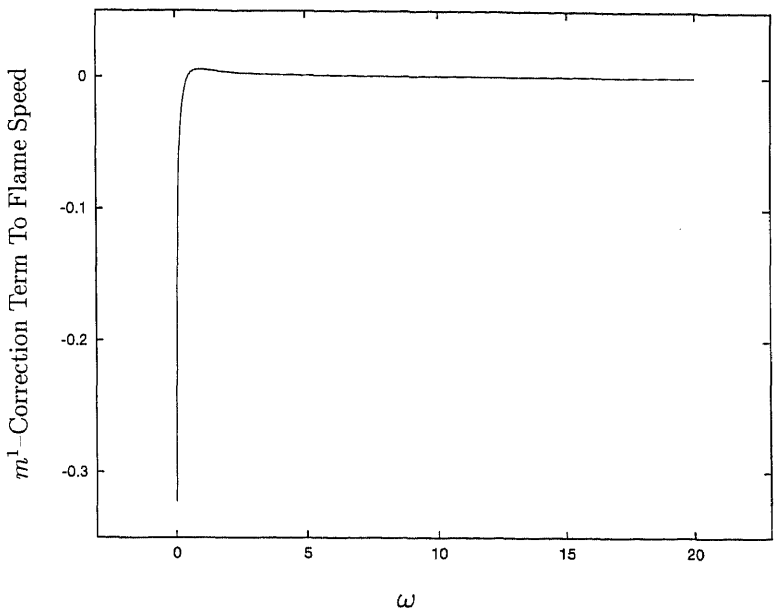

Figure 4.5 The real part of m^1 versus frequency ω for fixed scaled strain rate $qv^0_{0y} = \frac{2Le(m^0)^2\ln(m^0)}{1-Le}$ with the $Le = 2$ and $m^0 = 0.8$

It follows that the amplitude of m^1 diminishes at high frequency, and the burning rate becomes 135° out of phase with imposed oscillation. In figure 4.5, we plot the real part of m^1 as a function of frequency ω with fixed leading order flame speed $m^0 = 0.8$. In fact, for any given value of m^0, the profile of the real part of m^1 as function of frequency ω with fixed leading order flame speed m^0 is similar to that shown in figure 4.5. When ω is small, the system is quasi-steady and m^1 responds instantaneously. There is no phase lag and m^1 approaches the real value, given by (4.169). When ω is large, both real and imaginary parts of m^1 approach zero, and the phase lag becomes more noticeable. This agrees with previous studies cf. Im, Bechtold and Law(1996).

From (4.168), we note that, no matter what value the Lewis number takes (greater or less than unity), when frequency ω becomes large, the magnitude of m^1

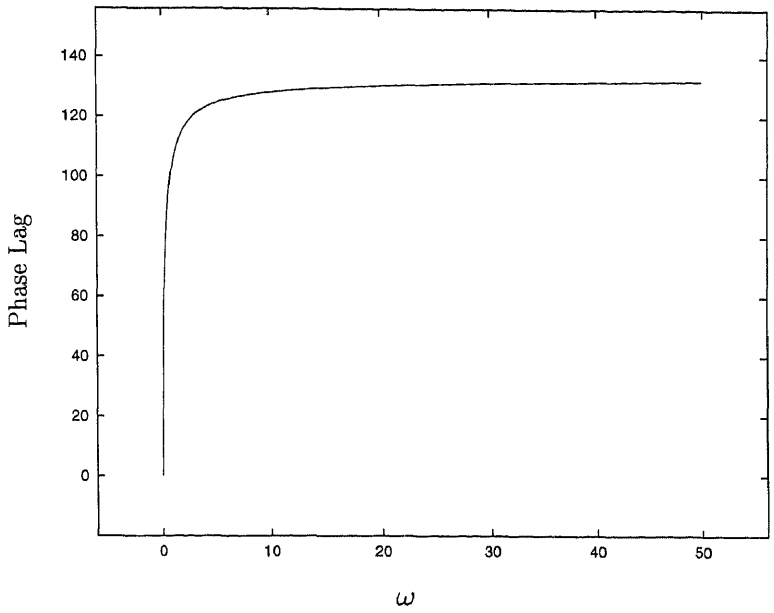

Figure 4.6 Phase lag of flame relative to the incoming flow as a function of frequency ω for the entire range of Lewis number Le

approaches zero, while the phase lag between flame and imposed oscillation becomes 135° out of phase. In figure 4.6, we plot phase lag between flame and imposed oscillation as function of frequency ω, for any Lewis number. The graph shows that the phase lag is a monotonic increasing function of ω. This result agrees with that of Petrov and Ghoniem(1995), who found that for high frequency oscillating strains, and over the entire range of Lewis number and flame temperature, the phase lag is of order of 140°.

In figures (4.7)–(4.12) we plot the real part of m^1 as function of scaled strain rate with fixed Lewis number, $Le = 2$, for different values of frequency ω. Our attention will focus on $Le > 1$, in which case, flame extinction happens. Figure 4.7 shows that for small frequency, m^1 becomes infinite when the strain rate approaches the steady state extinction point, i.e. the strain rate for which $m^0 = \frac{1}{\sqrt{e}}$. This is consistent with the expression (4.169). At high frequencies, m^1 achieves a finite

value, suggesting that extiction can be delayed at high frequency. This agrees with the result reported by Im, Bechtold and Law(1996).

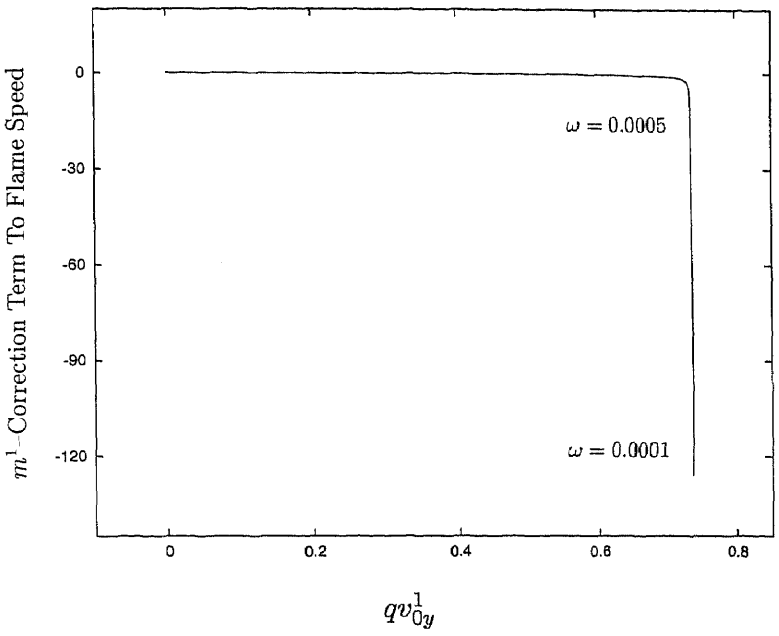

Figure 4.7 The real part of m^1 versus scaled strain rate qv^1_{0y} for two different values of frequency ω with fixed Lewis number $Le = 2$

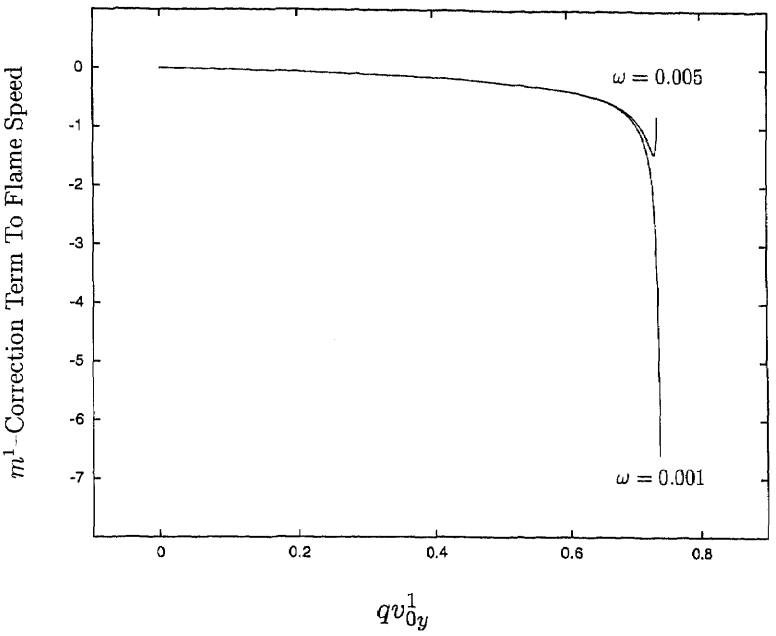

Figure 4.8 The real part of m^1 versus scaled strain rate qv_{0y}^1 for two different values of frequency ω with fixed Lewis number $Le = 2$

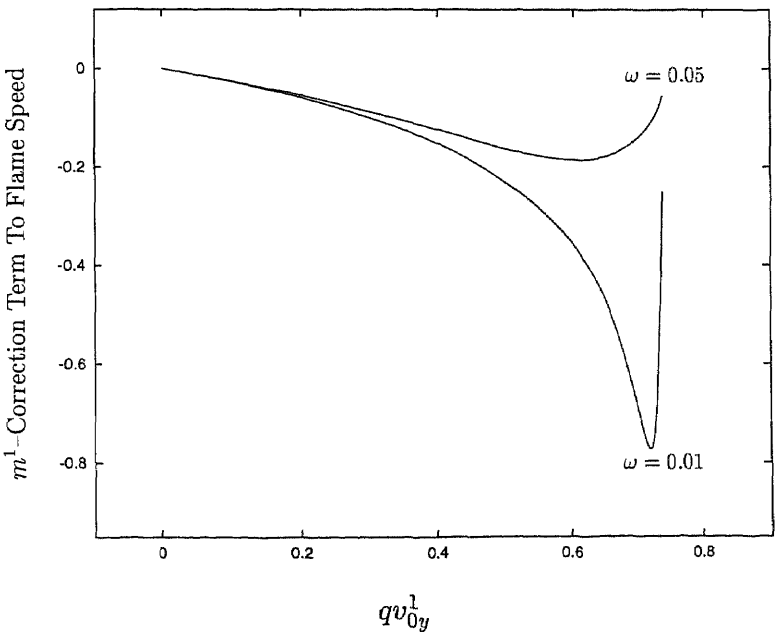

Figure 4.9 The real part of m^1 versus scaled strain rate qv_{0y}^1 for two different values of frequency ω with fixed Lewis number $Le = 2$

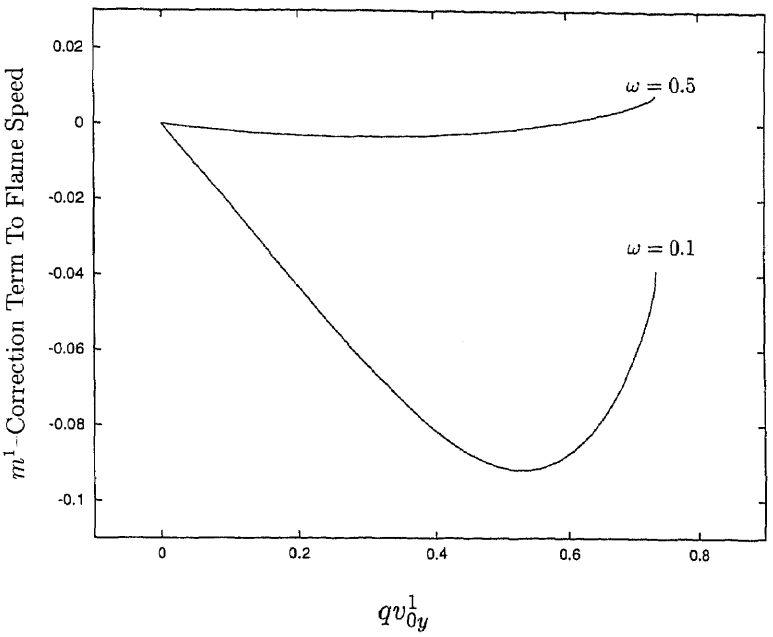

Figure 4.10 The real part of m^1 versus scaled strain rate qv_{0y}^1 for two different values of frequency ω with fixed Lewis number $Le = 2$

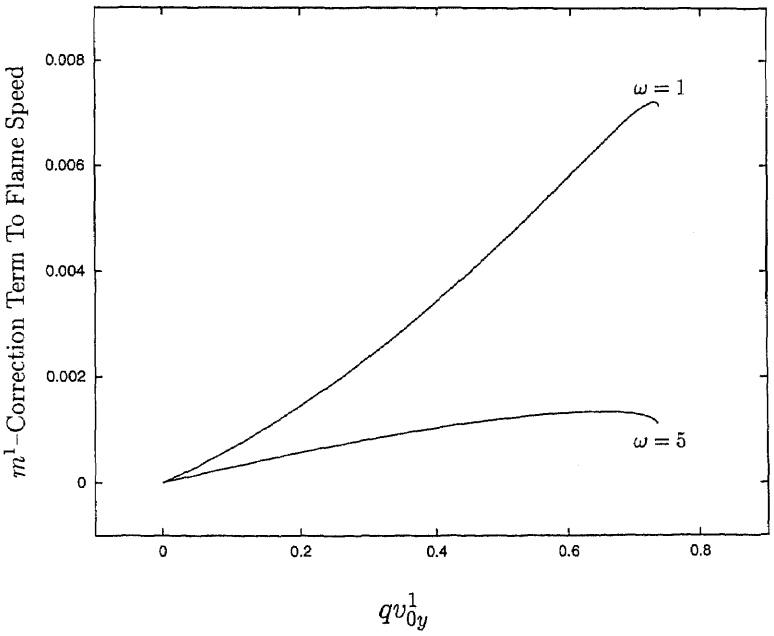

Figure 4.11 The real part of m^1 versus scaled strain rate qv_{0y}^1 for two different values of frequency ω with fixed Lewis number $Le = 2$

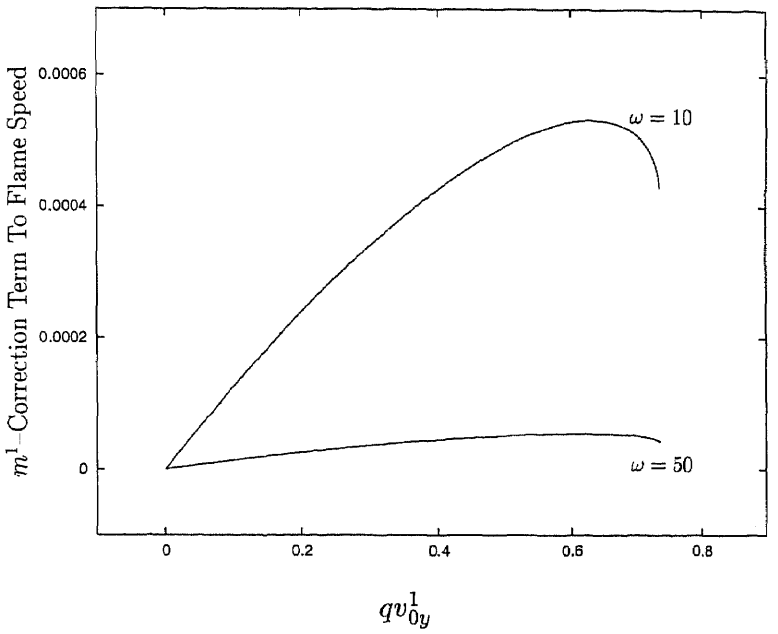

Figure 4.12 The real part of m^1 versus scaled strain rate qv_{0y}^1 for two different values of frequency ω with fixed Lewis number $Le = 2$

CHAPTER 5

CONCLUSIONS

In this work, we have used a combination of numerical techniques and matched asymptotics to investigate the response of premixed flames to time-dependent strained flow fields for both near equidiffusional flames and slowly varying flames. Due to the potential application to turbulent combustion modeling, our main interest was to analyze flame-flow interactions in a simple unsteady strained flow, namely the oscillating stagnation point flow.

For near equidiffusional flames, this study complements the work of Im, Bechtold and Law(1996) in several ways. First, we extend the range of strain rates by considering weak strain so that the flame resides outside the viscous boundary layer. Second, our analysis is not limited to small amplitude perturbations from the mean steady state, and thus nonlinear effects can be captured. Finally, our analysis accounts for the full interaction between the flame and the flow field, and thus we focus on hydrodynamic effects. Our predictions regarding flame response are found to be in agreement with previous studies of Saitoh and Otsuka(1976); and Im, Bechtold and Law(1996). We also obtain the following results that are attributed to hydrodynamic effects: (a) the mean flame position is shifted upstream from the steady state location, (b) a region of reverse flow temporarily appears immediately ahead of the flame even though the magnitude of the imposed oscillations is smaller than the mean strain rate, and (c) there is a maximum amplitude of oscillation beyond which the flame fails to exist. These results are most pronounced at high frequencies and agree with the asymptotic solution constructed in that regime.

Viscous and transport effects on near equidiffusional flame response to incoming flow were also examined. The flame was found to shift closer to the stagnation plane

with an increase in either Lewis number or Prandtl number. The viscous effects become more noticeable at high frequency.

A nonlinear flame speed equation for SVFs was also derived by exploring the unsteady flame structure caused by the imposed unsteadiness. This flame speed model demonstrates the importance of Lewis number, which causes flame extinction. This model predicts that flame extinction can be delayed when the strain rate oscillates about the static extinction point, which is in agreement with the results reported by Im, Bechtold and Law(1996). It also predicts that the phase lag between flame and incoming flow becomes 135° no matter what value the Lewis number takes when the imposed frequency become large enough. This result is in agreement with that of Petrov and Ghoniem(1995).

APPENDIX A

THE DERIVATION OF CONSERVATION CONDITIONS FOR SYSTEMS (3.2)-(3.7)

Jump conditions (3.5)-(3.7) imply the boundary conditions of stream function $\Psi(x,y,t) = y^{\nu+1}H(x,t)$ in the burned region, therefore a detailed analysis is needed.

The flame stretch κ defined in (3.8) takes value; $\kappa = (\nu+1)\mu$, and (3.5) implies that

$$U(D^-,t) = D_t - (1+q) + \delta\sigma(\nu+1)(\alpha-q)\mu\,, \tag{A.1}$$

which implies

$$H(D^-,t) = \frac{D_t}{\nu+1} - \frac{1+q}{\nu+1} + \delta(1+q)(\alpha-q)\mu\,. \tag{A.2}$$

On the RHS of (3.6), only leading order term of $[\nabla \times \mathbf{V}]$ is needed. To get $[\nabla \times \mathbf{V}_0]$, we apply the jump operator $[\cdot]$ to the leading order term of y-momentum equation, which yields

$$\Big[\rho V_{0t}\Big] + \Big[\rho U_0 V_{0x}\Big] + \Big[\rho V_0 V_{0y}\Big] = -\Big[p_{0y}\Big]\,. \tag{A.3}$$

Because $[p_0]$ is independent of y, and also $[p_{0y}] = \partial_y([p_0])$, then (A.3) becomes

$$\Big[\rho V_{0t}\Big] + \Big[\rho U_0 V_{0x}\Big] + \Big[\rho V_0 V_{0y}\Big] = 0\,. \tag{A.4}$$

By the definition of jump

$$\Big[S\Big] = \int_{D_-}^{D^+} S_x(x',y,t)dx'\,, \tag{A.5}$$

and also

$$\frac{d}{dt}\Big[S\Big] = \int_{D_-}^{D^+} S_{xt}dx' + D_t S_x^+ - D_t S_x^- = \Big[S_t\Big] + D_t\Big[S_x\Big]\,, \tag{A.6}$$

we can find that

$$\begin{aligned}\Big[\rho V_{0t}\Big] &= \rho^+\Big[V_{0t}\Big] + V_{0t}^-\Big[\rho\Big] = \rho^+\left(\frac{d}{dt}\Big[V_0\Big] - D_{0t}\Big[V_{0x}\Big]\right) + V_{0t}^-\Big[\rho\Big] \\ &= -\frac{q\mu_t}{1+q}y - \frac{D_{0t}}{1+q}\Big[V_{0x}\Big]\end{aligned} \tag{A.7}$$

$$\left[\rho U_0 V_{0x}\right] = (\rho U_0)^+ \left[V_{0x}\right] + V_{0x}^- \left[\rho U_0\right] = \left(\frac{D_{0t}}{1+q} - 1\right)\left[V_{0x}\right] \tag{A.8}$$

$$\left[\rho V_0 V_{0y}\right] = (\rho V_0)^+ \left[V_{0y}\right] + V_{0y}^- \left[\rho V_0\right] = -\frac{q}{1+q}\mu^2 y \ . \tag{A.9}$$

As we know that

$$\left[\nabla \times \mathbf{V_0}\right] = \left[V_{0x}\right] - \left[U_{0y}\right] = \left[V_{0x}\right] \ . \tag{A.10}$$

By using (A.4), (A.7), (A.8) and (A.9), we can simplify (A.10)

$$\left[\nabla \times \mathbf{V_0}\right] = -\frac{q}{1+q}(\mu_t + \mu^2)y \tag{A.11}$$

$$H_{0xx}(D^-, t) = \frac{q}{1+q}(\mu_t + \mu^2) \ . \tag{A.12}$$

In order to find $\mathbf{n} \times \tau^- \cdot \mathbf{n}$, we first evaluate τ^-, which is

$$\tau^- = \tau \mid_{x=D^+} \approx \begin{pmatrix} 2U_x & U_y + V_x \\ U_y + V_x & 2V_y \end{pmatrix} = \begin{pmatrix} -2(\nu+1)\mu & 0 \\ 0 & 2\mu \end{pmatrix}$$

thus, it is easy to verify $\mathbf{n} \times \tau^- \cdot \mathbf{n} = 0$, and finally

$$\left[\mathbf{V} \times \mathbf{n}\right] = \delta q(Pr+1)(\mu_t + \mu^2)y \tag{A.13}$$

$$V(D^-, t) = \mu y + \delta q(Pr+1)(\mu_t + \mu^2)y \tag{A.14}$$

$$H_x(D^-, t) = -\mu - \delta q(Pr+1)(\mu_t + \mu^2) \ . \tag{A.15}$$

I claim that both $[p]$ and the leading order term $[\mathbf{n} \cdot p_0]$ in (3.7) are independent of y. To prove it, let's apply the jump operator $[\cdot]$ to the leading order x-momentum equation

$$\left[\mathbf{n} \cdot \nabla p_0\right] = \left[p_{0x}\right] = -\left[\rho U_{0t}\right] - \left[\rho U_0 U_{0x}\right] - \left[\rho V_0 U_{0y}\right] \ , \tag{A.16}$$

and also apply jump operator $[\cdot]$ to the leading order continuity equation, which yields

$$\left[U_{0x}\right] = -\frac{1}{y^\nu}\left[\frac{\partial(y^\nu V_0)}{\partial y}\right] = -(\nu+1) \ , \tag{A.17}$$

this is because V_0 is continuous, i.e. $V_0^+ = V_0^- = \mu y$.

We evaluate (A.16) term by term

$$\Big[\rho U_{0t}\Big] = \rho^+\Big[U_{0t}\Big] + U_{0t}^-\Big[\rho\Big] = U_{0t}^-\Big[\rho\Big] + \frac{d}{dt}\Big[V_0\Big] - D_{0t}\Big[U_{0x}\Big] \tag{A.18}$$

$$\Big[\rho U_0 U_{0x}\Big] = \rho^+ U_0^+\Big[U_{0x}\Big] + U_{0x}^-\Big[\rho U_0\Big] \tag{A.19}$$

$$\Big[\rho V_0 U_{0y}\Big] = \rho^+ V_0 \partial_y\Big(\Big[U_0\Big]\Big) + V_0 U_{0y}^-\Big[\rho\Big] = 0\,, \tag{A.20}$$

since $[U_0]$ and U_0^- are independent of y. Every term above is independent of y, thus we have proved that $[p_{0x}]$ is y-independent. It is obvious that $[p]$ is y-independent also.

Before we evaluate the total vorticity $[\nabla \times \mathbf{V}]$ produced along flame surface, we need to find out $[V_{0xx}]$ first. Upon doing this, we differentiate the leading order y-momentum equation and apply jump operator $[\cdot]$ to it, to get

$$\Big[\rho V_{0xt}\Big] + \Big[\rho U_0 V_{0xx}\Big] + \Big[\rho U_{0x} V_{0x}\Big] + \Big[\rho V_0 V_{0xy}\Big] + \Big[\rho V_{0x} V_{0y}\Big] = -\Big[p_{0xy}\Big] \tag{A.21}$$

where

$$\Big[p_{0xy}\Big] = \frac{\partial}{\partial y}\Big[p_{0x}\Big] = 0 \tag{A.22}$$

$$\begin{aligned}\Big[\rho V_{0xt}\Big] &= \rho^+\Big[V_{0xt}\Big] + V_{0xt}^-\Big[\rho\Big] = \rho^+\left(\frac{d}{dt}\Big[V_{0x}\Big] - D_{0t}[V_{0xx}]\Big]\right) \\ &= -\frac{D_{0t}}{1+q}\Big[V_{0xx}\Big] - \frac{q}{(1+q)^2}(\mu_{tt} + 2\mu\mu_t)y\end{aligned} \tag{A.23}$$

$$\begin{aligned}\Big[\rho U_{0x} V_{0x}\Big] &= (\rho U_{0x})^+\Big[V_{0x}\Big] + V_{0x}^-\Big[\rho U_{0x}\Big] \\ &= -\rho^+\left(\frac{1}{y^\nu}\frac{\partial(y^\nu V_0)}{\partial y}\right)^+\Big[V_{0x}\Big] = \frac{q\mu(1+\nu)}{(1+q)^2}(\mu_t + \mu^2)y\end{aligned} \tag{A.24}$$

$$\Big[\rho U_0 V_{0xx}\Big] = (\rho U_0)^+\Big[V_{0xx}\Big] + V_{0xx}^-\Big[\rho U_0\Big] = \frac{D_{0t} - 1 - q}{1+q}\Big[V_{0xx}\Big] \tag{A.25}$$

$$\Big[\rho V_{0x} V_{0y}\Big] = (\rho V_{0y})^+\Big[V_{0x}\Big] + V_{0x}\Big[\rho V_{0y}\Big] = -\frac{q\mu}{(1+q)^2}(\mu_t + \mu^2)y \tag{A.26}$$

$$\Big[\rho V_0 V_{0xy}\Big] = (\rho V_0)^+\Big[V_{0xy}\Big] + V_{0xy}^-\Big[\rho V_0\Big] = -\frac{q\mu}{(1+q)^2}(\mu_t + \mu^2)y \ . \tag{A.27}$$

We plug these terms into (A.21) and solve for

$$\Big[V_{0xx}\Big] = -\frac{q}{(1+q)^2}\left(\mu_{tt} + 2\mu\mu_t + (1-\nu)(\mu\mu_t + \mu^3)\right) y \ , \tag{A.28}$$

which gives

$$H_{0xxx}(D^-, t) = \frac{q}{(1+q)^2}\left(\mu_{tt} + 2\mu\mu_t + (1-\nu)(\mu\mu_t + \mu^3)\right) \ . \tag{A.29}$$

Back to $[\nabla \times \mathbf{V}]$ consideration, we apply jump operator $[\cdot]$ to y-momentum equation, and recall that V_0 is continuous acrossing flame surface, to get

$$\Big[\rho V_t\Big] + \Big[\rho U V_x\Big] + \Big[\rho V V_y\Big] = -\Big[p_y\Big] + \Big[\frac{\delta Pr}{\rho} V_{0xx}\Big] \tag{A.30}$$

where

$$\begin{aligned}\Big[\rho V_t\Big] &= \rho^+\Big[V_t\Big] + V_t^-\Big[\rho\Big] = \rho^+\left(\frac{d}{dt}\Big[V\Big] - D_t\Big[V_x\Big]\right) + V_t^-\Big[\rho\Big] \\ &= -\frac{1}{1+q}\Big(q\mu_t y + D_t\Big[V_x\Big] - \delta q(Pr+1)(\mu_{tt} + 2\mu\mu_t)y\Big)\end{aligned} \tag{A.31}$$

$$\Big[\rho U V_x\Big] = (\rho U)^+\Big[V_x\Big] + V_x^-\Big[\rho U\Big] = \left(\frac{D_t}{1+q} - 1 + \delta\mu(\alpha - q)(\nu+1)\right)\Big[V_x\Big] \tag{A.32}$$

$$\Big[\rho V V_y\Big] = (\rho V)^+\Big[V_y\Big] + V_y^-\Big[\rho V\Big] = \frac{q\mu}{1+q}\Big(-\mu + \delta(2Pr+2)(\mu_t + \mu^2)\Big)y \tag{A.33}$$

$$\Big[p_y\Big] = \frac{\partial}{\partial y}\Big[p\Big] = 0 \tag{A.34}$$

$$\begin{aligned}\Big[\frac{\delta Pr V_{0xx}}{\rho}\Big] &= \frac{\delta Pr}{\rho^+\rho^-}\Big(\rho^-\Big[V_{0xx}\Big] - V_{0xx}^-\Big[\rho\Big]\Big) \\ &= -\frac{\delta q Pr}{1+q}\Big(\mu_{tt} + 2\mu\mu_t + (1-\nu)(\mu\mu_t + \mu^3)\Big)y \ .\end{aligned} \tag{A.35}$$

By using the definition of vorticity $\varpi = \frac{\partial V}{\partial x} - \frac{\partial U}{\partial y}$ and using (A.30)–(A.35), we can easily find the jump of vorticity, which is given by

$$\Big[\varpi\Big] = \Big[V_x\Big] - \Big[U_y\Big] = \Big[V_x\Big] = -yH_{xx}(D^-, t) \ . \tag{A.36}$$

In (A.31), solving for $[V_x]$ to get

$$H_{xx}(D^-,t) = \frac{q\Big(\mu_t + \mu^2 - \delta(Pr+1)(\mu_{tt} + 4\mu\mu_t + 2\mu^3)\Big)}{(1+q)\Big(1 - \delta\mu(\alpha - q)(1+\nu)\Big)}$$
$$- \frac{\delta q Pr\Big(\mu_{tt} + 2\mu\mu_t + (1-\nu)(\mu\mu_t + \mu^3)\Big)}{(1+q)\Big(1 - \delta\mu(\alpha - q)(1+\nu)\Big)} . \tag{A.37}$$

After all above analysis, we have obtained the complete set of boundary conditions, which are

$$H(D^-,t) = \frac{D_t}{\nu+1} - \frac{1+q}{\nu+1} + \delta(1+q)(\alpha - q)\mu \tag{A.38}$$

$$H_x(D^-,t) = -\mu - \delta q(Pr+1)(\mu_t + \mu^2) \tag{A.39}$$

$$H_{xx}(D^-,t) = \frac{q}{1+q}(\mu_t + \mu^2) + \delta f(t) \tag{A.40}$$

$$H_{xxx}(D^-,t) = \frac{q}{(1+q)^2}\Big(\mu_{tt} + 2\mu\mu_t + (1-\nu)(\mu\mu_t + \mu^3)\Big) , \tag{A.41}$$

where

$$f(t) = \frac{q}{1+q}\Big((\nu+1)(\alpha - q)(\mu\mu_t + \mu^3) - (Pr+1)(\mu_{tt} + 4\mu\mu_t + 2\mu^3)$$
$$- Pr\left(\mu_{tt} + 2\mu\mu_t + (1-\nu)(\mu\mu_t + \mu^3)\right)\Big) . \tag{A.42}$$

APPENDIX B

SOLUTIONS OF SYSTEMS (3.26)–(3.31) WITH CONSTANT STRAIN RATE

For constant strain rate μ, the solution for system (3.26)–(3.31) will independent of time t, therefore, it can be rewritten into

$$(\nu+1)GG_{zz} - G_z^2 = -(1+q)\mu^2 + \delta Pr\sigma^2 G_{zzz} \tag{B.1}$$

$$G(-D) = 0 \tag{B.2}$$

$$G(0) = -\frac{\sigma}{\nu+1} + \delta\mu\sigma(\alpha - \sigma + 1) \tag{B.3}$$

$$G_z(0) = -\mu - \delta(\sigma-1)(Pr+1)\mu^2 \tag{B.4}$$

$$G_{zz}(0) = \frac{\sigma-1}{\sigma}\mu^2 + \delta\frac{\sigma-1}{\sigma}\Big((\nu+1)(\alpha-\sigma+1) - 2(Pr+1) - Pr(1-\nu)\Big)\mu^3 \tag{B.5}$$

Since the nondimensional flame thickness δ is small, so we can expand variables $G(z)$ and D into power series of δ

$$G(z) \sim G_0(z) + \delta G_1(z) + \delta^2 G_2(z) + \cdots \tag{B.6}$$

$$D \sim D_0 + \delta D_1 + \delta^2 D_2 + \cdots . \tag{B.7}$$

The leading order $O(1)$ terms of system (B.1)–(B.5) for two-dimensional case ($\nu = 0$) are

$$G_0 G_{0zz} - G_{0z}^2 = -\sigma\mu^2 \tag{B.8}$$

$$G_0(-D_0) = 0 \qquad G_0(0) = -\sigma \tag{B.9}$$

$$G_{0z}(0) = -\mu \qquad G_{0zz}(0) = \frac{\sigma-1}{\sigma}\mu^2 . \tag{B.10}$$

We differentiate (B.8) with respect to z, to get

$$\frac{G_{0zzz}}{G_{0zz}} = \frac{G_{0z}}{G_0} \qquad G_{0zz} = cG_0 , \tag{B.11}$$

where c is integration constant, which can be determined by using the boundary conditions

$$G_0(0) = -\sigma \qquad G_{0zz}(0) = \frac{\sigma - 1}{\sigma}\mu^2 \ , \tag{B.12}$$

thus c takes value $c = -(\sigma - 1)\mu^2/\sigma^2$. Therefore the general solution takes the form

$$G_0(z) = a\sin(kz) + b\cos(kz) \ , \tag{B.13}$$

where a and b can be determined by using the boundary conditions and the condition $G_0(-D_0) = 0$, and $G_0(z)$ is given by

$$G_0(z) = -\frac{\sigma^{3/2}}{\sqrt{\sigma - 1}}\sin\left(\frac{\mu\sqrt{\sigma - 1}}{\sigma}\left(z + \frac{\sigma}{\mu\sqrt{\sigma - 1}}\arctan(\sqrt{\sigma - 1})\right)\right) \tag{B.14}$$

with

$$D_0 = \frac{\sigma}{\mu\sqrt{\sigma - 1}}\arctan\left(\sqrt{\sigma - 1}\right) \ . \tag{B.15}$$

The $O(\delta)$ term of system (B.1)–(B.5) for two-dimensional case ($\nu = 0$) are

$$G_0 G_{1zz} + G_1 G_{0zz} - 2G_{0z}G_{1z} = Pr\sigma^2 G_{0zzz} \tag{B.16}$$

$$D_1 = \frac{G_1(-D_0)}{G_{0z}(-D_0)} \qquad G_1(0) = \mu\sigma(\alpha - \sigma + 1) \tag{B.17}$$

$$G_{1z}(0) = -(\sigma - 1)(Pr + 1)\mu^2 \qquad G_{1zz}(0) = \frac{\sigma - 1}{\sigma}\Big(\alpha - \sigma - 3Pr - 1\Big)\mu^3 \ . \tag{B.18}$$

In order to simplify equation (B.14), we make following substitution

$$A = -\frac{\sigma^{3/2}}{\sqrt{\sigma - 1}} \qquad k = \frac{\mu\sqrt{\sigma - 1}}{\sigma} \ , \tag{B.19}$$

and plug $G_0(z)$ into (B.16), after some simplification to get

$$\Big(G_{1zz} + k^2 G_1\Big)_z - k\cot(kz + kD_0)\Big(G_{1zz} + k^2 G_1\Big) = Pr\sigma^2 k^4 \ . \tag{B.20}$$

We multiply (B.20) by integral factor and integrate it once

$$G_{1zz} + k^2 G_1 = C\sin(kz + kD_0) + Pr\sigma^2 k^3 \sin(kz + kD_0)\ln\left(\tan\left(\frac{kz + kD_0}{2}\right)\right) \tag{B.21}$$

the integral constant C can be determined by boundary conditions, which is given

$$C = \frac{\sqrt{\sigma-1}}{\sqrt{\sigma}}\Big(2\alpha - 2\sigma - 3Pr\Big)\mu^3 - \frac{Pr\mu^3(\sigma-1)^{3/2}}{2\sigma}\ln\left(\frac{\sqrt{\sigma}-1}{\sqrt{\sigma}+1}\right) . \qquad (B.22)$$

It is easy to find out the particular solution, which is

$$\begin{aligned} G_{1p}(z) = &-\frac{C}{2k}(z+D_0)\cos(kz+kD_0) \\ &+ \frac{1}{2}kPr\sigma^2\sin(kz+kD_0)\ln\left(\tan\left(\frac{kz+kD_0}{2}\right)\right) \\ &- \frac{1}{2}k^2Pr\sigma^2(z+D_0)\cos(kz+kD_0)\ln\left(\tan\left(\frac{kz+kD_0}{2}\right)\right) \\ &+ \frac{1}{2}kPr\sigma^2\cos(kz+kD_0)\int_0^{k(z+D_0)}\eta\csc(\eta)\,d\eta\,, \end{aligned} \qquad (B.23)$$

thus the general solution $G_1(z)$ is given by

$$G_1(z) = E\cos(kz) + F\sin(kz) + G_{1p}(z)\,, \qquad (B.24)$$

where E and F are determined by boundary conditions

$$E = \mu\sigma(\alpha - \sigma + 1) - G_{1p}(0) \qquad (B.25)$$

$$F = \frac{1}{k}\Big(-(\sigma-1)(Pr+1)\mu^2 - G_{1pz}(0)\Big) \qquad (B.26)$$

$$D_1 = \frac{G_1(-D_0)}{G_{0z}(-D_0)} = -\frac{1}{\mu\sigma}\Big(-\sqrt{\sigma-1}F + E\Big)\,. \qquad (B.27)$$

The leading order $O(1)$ terms of system (B.1)-(B.5) for two-dimensional case ($\nu = 1$) are

$$2G_0G_{0zz} - G_{0z}^2 = -\sigma\mu^2 \qquad (B.28)$$

$$G_0(-D_0) = 0 \qquad G_0(0) = -\frac{\sigma}{2} \qquad (B.29)$$

$$G_{0z}(0) = -\mu \qquad G_{0zz}(0) = \frac{\sigma-1}{\sigma}\mu^2\,. \qquad (B.30)$$

We look for solution which takes following form

$$G_0(z) = az^2 + bz + c\,, \qquad (B.31)$$

and plug (B.31) into (B.28) and utilizing the boundary conditions to get

$$G_0(z) = \frac{\sigma - 1}{2\sigma}\mu^2 z^2 - \mu z - \frac{\sigma}{2} \tag{B.32}$$

$$D_0 = \frac{\sigma}{\mu(1 + \sqrt{\sigma})} \, . \tag{B.33}$$

The $O(\delta)$ term of system (B.1)–(B.5) for two-dimensional case ($\nu = 1$) are

$$G_0 G_{1zz} + G_1 G_{0zz} - G_{0z} G_{1z} = \frac{1}{2} Pr\sigma^2 G_{0zzz} \tag{B.34}$$

$$D_1 = \frac{G_1(-D_0)}{G_{0z}(-D_0)} \qquad G_1(0) = \mu\sigma(\alpha - \sigma + 1) \tag{B.35}$$

$$G_{1z}(0) = -(\sigma - 1)(Pr + 1)\mu^2 \qquad G_{1zz}(0) = \frac{2(\sigma - 1)}{\sigma}\Big(\alpha - \sigma - Pr\Big)\mu^3 \, . \tag{B.36}$$

We look for solution which takes following form

$$G_0(z) = az^2 + bz + c \tag{B.37}$$

and plug (B.37) into (B.35) and utilizing the boundary conditions to get

$$G_1(z) = \frac{\sigma - 1}{\sigma}\Big(\alpha - \sigma - Pr\Big)\mu^3 z^2 - (\sigma - 1)(Pr + 1)\mu^2 z + \mu\sigma(\alpha - \sigma + 1) \tag{B.38}$$

$$D_1 = -\frac{(\alpha - \sigma - Pr)(\sqrt{\sigma} - 1) + (\sigma - 1)(Pr + 1) + (\alpha - \sigma + 1)(\sqrt{\sigma} + 1)}{1 + (\sqrt{\sigma})^{-1}} \, . \tag{B.39}$$

REFERENCES

1. Landau, L. D. 1944, On the theory of slow combustion. *Acta Physicochimica URSS* **19:** P77

2. Markstein, G. H. 1951, Experimental and theoretical studies of flame front stability. *Journal of Aerosol Science* **18:** P199

3. Bush, W. B. and Fendell, F. E. 1970, Asymptotic analysis of the structure of a steady planar detonation. *Combustion Science and Technology* **1:** P421

4. Williams, F. A. 1971, Theory of combustion in laminar flows. *Annual Review of Fluid Mechanics* **3:** P171

5. Liñán, A. 1974, The asymptotic structure of counterflow diffusion flames for large activation energies. *Acta Astronautica* **1:** P1007

6. Sivashinsky, G. I. 1976, On a distorted flame front as a hydrodynamic discontinuity. *Acta Astronautica* **3:** P889

7. Saitoh, T. and Otsuka, Y. 1976, Unsteady behavior of diffusion flames and premixed flames for counter flow geometry. *Combustion Science and Technology* **12:** P135

8. Buckmaster, J. D. 1977, Slowly varying laminar flames. *Combustion and Flame* **28:** P225

9. Smith, G. D. 1978, *Numerical solution of partial differential equations: finite difference methods.* Clarendon Press, Oxford

10. Matkowsky, B. J. and Sivashinsky, G. I. 1979, An asymptotic derivation of two models in flame theory associate with the constant density approximation. *SIAM Journal of Applied Mathematics* **37:** P686

11. Clavin, P. and Williams, F. A. 1982, Effects of molecular diffusion and thermal expansion of the structure and dynamics of premixed flames in turbulent flows of large scale and low intensity. *Journal of Fluid Mechanics* **116:** P251

12. Pelce, P. and Clavin, P. 1982, Influence of hydrodynamics and diffusion upon the stability limits of laminar premixed flame. *Journal of Fluid Mechanics* **124:** P219

13. Matalon, M. and Matkowsky, B. J. 1982, Flames as gasdynamic discontinuities. *Journal of Fluid Mechanics* **124:** P239

14. Libby, P. A. and Williams, F. A. 1982, Structure of laminar flamelets in premixed turbulent flames. *Combustion and Flame* **44:** P287

15. Buckmaster, J. D. and Ludford, G. S. S. 1982, *Theory of Laminar Flames.* Cambridge University Press, Cambridge

16. Matalon, M. 1983, On flame stretch. *Combustion Science and Technology* **31:** P169

17. Buckmaster, J. D. and Ludford, G. S. S. 1983, *Lectures on Mathematical Combustion.* SIAM. Philadelphia, Pennsylvania

18. Wu, C. K. and Law, C. K. 1984, On the determination of laminar flame speeds from stretched flames. *Twentieth Symposium (International) on Combustion* P1941. The Combustion Institute, Pittsburgh

19. Williams, F. A. 1985, *Combustion Theory,* 2nd Edition. Benjamin Cummings. Menlo Park, California

20. Eteng, E., Ludford, G. S. S. and Matalon, M. 1986, Displacement effect of a flame in a stagnation-point flow. *Physics of Fluids* **29:** P2172

21. Peters, N. 1986, Laminar flamelet concepts in turbulent combustion. *Twenty-first Symposium (International) on Combustion* P1231. The Combustion Institute, Pittsburgh

22. Kim, Y. D. and Matalon, M. 1988, Propagation and extinction of a flame in a stagnation-point flow. *Combustion and Flame* **73:** P303

23. Clavin, P., Pelce, P. and He, L. 1990, One-dimensional vibratory instability of planar flames propagating in tubes. *Journal of Fluid Mechanics* **216:** P299

24. Stahl, G. and Warnatz, J. 1991, Numerical investigation of time-dependent properties and extinction of strained methane- and propane-air flamelets. *Combustion and Flame* **85:** P285

25. Jackson, T. L. and Matalon, M. 1993, Stability of a premixed flame in stagnation-point flow against general disturbances. *Combustion Science and Technology* **90:** P385

26. Egolfopoulos, F. N. 1994, Dynamics and structure of unsteady strained laminar premixed flames. *Twenty-fifth Symposium (International) on Combustion* P1365. The Combustion Institute, Pittsburgh

27. Joulin, G. 1994, On the response of premixed flames to time-dependent stretch and curvature. *Combustion Science and Technology* **97:** P219

28. Petrov, C. A. and Ghoniem, A. F. 1995, The transient response of strained laminar-premixed flames. *Combustion and Flame* **102:** P401

29. Im, H. G., Bechtold, J. K. and Law, C. K. 1995, Counterflow diffusion flames with unsteady strain rates. *Combustion Science and Technology* **106:** P345

30. Im, H. G., Bechtold, J. K. and Law, C. K. 1996, Response of counterflow premixed flames to oscillating strain rates. *Combustion and Flame* **105:** P358

31. Huang, Z., Bechtold, J. K. and Matalon, M. 1997, A premixed flame in oscillating stagnation point flow: hydrodynamic effects. *ESCI Fall Technical Meeting.* Hartford, Connecticut

32. Huang, Z., Bechtold, J. K. and Matalon, M. 1998, Weakly stretched premixed flames in oscillating flows. *Combustion Theory and Modeling* **2:** P115

33. Bechtold, J. K. and Matalon, M. 1998, Hydrodynamic model of near-stoichiometric flames with variable transport properties. *To appear*